THE UNIVERSITY OF CALGARY

Prediction of Electrophoretic Mobilities in Capillary Zone Electrophoresis

by

Shilin Fu

A THESIS

SUBMITTED TO THE FACULTY OF GRADUATE STUDIES

IN PARTIAL FULFILMENT OF THE REQUIREMENTS FOR THE

DEGREE OF MASTER OF SCIENCE

DEPARTMENT OF CHEMISTRY

CALGARY, ALBERTA

JANUARY, 1998

Abstract

Capillary electrophoresis separates ions based on their mobilities. The electrophoretic mobility of a molecule results from the balancing of two forces: the electrostatic attraction between the solute charge and the applied electric field; and the resistive drag due to friction between the moving analyte and the solvent. In order to predict the solute behavior before separation, numerous factors must be considered. These include molecular size and shape, hydration and solvent structure effects. The size, shape and other physicochemical parameters were determined using molecular modeling. However, these could not accurately reflect the friction.

Dielectric friction in addition to the hydrodynamic friction must be considered for the absolute mobility prediction. This results in excellent agreement between the predicted absolute mobilities and literature or experimentally obtained mobilities for the three major classes of analytes investigated (monoamines, aliphatic carboxylates and sulfonates).

Acknowledgments

I would like to thank my supervisor Dr. Charles A. Lucy for his guidance. Every step of my progress is through his support, and encouragement. He give me guidance not only on research but also on all aspects of my academic life.

Thanks are expressed to my supervisor committee member, Dr. Viola I. Birss, for giving me suggestions on this research project and reviewing my annual progress.

I would like to thank Dr. A. Scott Hinman for discussions on data analysis.

My thanks are also extended to all past and present students in Dr. Lucy's group for their support, help and collaboration, particularly Ken Yeung, Liwen Ye, Dr. Quanji Wu, Wayne Rae, Dongmei Li, Jinglan Yan, and Yusuf Muombwa.

I would like to acknowledge the financial support from the Department of Chemistry, the University of Calgary, and the Natural Sciences and Engineering Research Council of Canada.

Table of Contents

List of Tables

List of Figures

List of Abbreviations

CE	Capillary Electrophoresis
CITP	Capillary Isotachophoresis
CMC	Critical Micelle Concentration
CZE	Capillary Zone Electrophoresis
EOF	Electroosmotic Flow
kV	Kilovolts
MEKC	Micellar Electrokinetic Chromatography
MMP™	Molecular Modeling Pro™
nS	nanosiemens
UV	Ultraviolet

CHAPTER 1 INTRODUCTION

1.1 PRINCIPLES OF CAPILLARY ELECTROPHORESIS SEPARATIONS

Capillary Electrophoresis (CE) has become an important separation technique in analytical chemistry. This technique has been used to separate analytes ranging from small inorganic and organic ions to macromolecular species such as DNA and proteins. Capillary zone electrophoresis (CZE) separates ions based on their mobilities (μ):

$$\mu = \frac{q}{f} \qquad 1\text{-}1$$

where q is the electrical charge on the molecule and f is the frictional coefficient. The mobility differences of analytes result in the migration velocity differences under a given electric field strength. Therefore, charged species can be separated using capillary zone electrophoresis as long as their mobilities are not exactly the same. For a given running buffer, the mobility of an ion is a constant, which is characteristic of that ion. The mobility of an ion is determined by the balancing of two forces:

$$\mu \propto \frac{F_E}{f} \qquad 1\text{-}2$$

The first force is the electric force (driving force, F_E), which is the attraction force resulting from the applied electric field and the charge on the molecule:

$$F_E = qE \qquad 1\text{-}3$$

where E is the electric field strength (V/cm). This force can be considered as a constant for all monocharged molecules at infinite dilution investigated in this project. The second

force is the frictional drag force (f) between the moving ion and the running buffer medium, which is much more important for the prediction of analyte mobilities.

The general configuration of a capillary electrophoresis separation system is shown below:

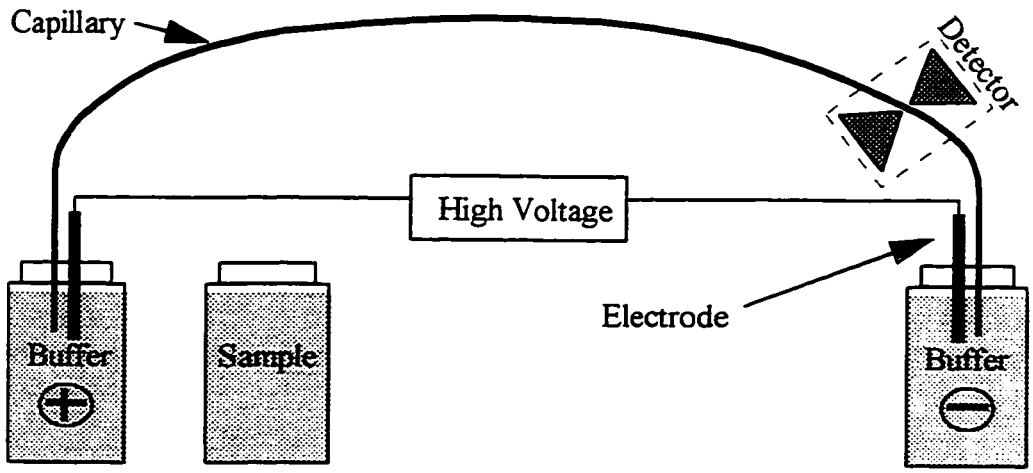

Figure 1.1 Schematic diagram of a capillary electrophoresis separation system

The capillary used is usually made of fused silica with a polyimide coating. Typically, the inner diameter (I.D.) of the capillary ranges from 25 to 75 μm, and the length of the capillary from 30 to 110 cm. In comparison with the traditional slab-gel electrophoresis, the resistance of the narrow-bore capillary is much higher, which allows the application of very high electric fields during the separation (100 to 500 V/cm) without problems due to Joule heating. This is becuase the narrow-bore capillary allows very efficient heat dissipation. In turn, the use of high electric field results in fast separation of analytes

and high efficiency. There are three main steps for a CE separation. First, the sample solution is loaded at the inlet end (anode for cations, and cathode for anions) of the capillary by either hydrodynamic (pressure) or electrokinetic injection. Second, after replacing the buffer vial, separation of analytes in the running buffer begins by applying the high voltage across the capillary. Finally, optical detection such as ultraviolet (UV) or conductivity detection is made at or near the outlet end of the capillary.

1.2 DEFINITION OF MOBILITIES

1.2.1 ELECTROOSMOTIC FLOW (EOF) "MOBILITY"

Different mobility concepts are widely used in the area of capillary electrophoresis. Before describing each concept, a special phenomenon, electroosmotic flow (EOF), needs to be addressed. Electroosmotic flow can be defined as the bulk flow of the running buffer solution in the capillary under an applied electric field [1]. Thus the running buffer is "pumped" continuously through the capillary during the separation. Although electroosmotic flow was first observed in 1808 by Reuss [2], a comprehensive theoretical treatment of this phenomenon in a narrow cylindrical capillary was not given until the 1965 work of Rice and Whitehead [3]. The issue of electroosmotic flow in modern capillary zone electrophoresis was first discussed by Jorgenson and Lukacs [4] in 1981. Most commonly, fused silica capillaries are used in CE. Under aqueous conditions, the silanol groups (SiOH) on the fused silica surface dissociate to form SiO^-:

$$SiOH \rightleftharpoons SiO^- + H^+ \qquad 1\text{-}4$$

The negative charges (SiO^-) on the inner capillary wall are the origin of electroosmotic flow. They cause the formation of an electrical double layer at the wall-solution interface. The mobile portion of the cationic counter-ions in the diffuse portion of the double layer migrate toward the cathode under the application of an electric field. This counter-ion migration is the driving force of electroosmotic flow. The double layer formation and EOF generation can be schematically illustrated in the following diagram:

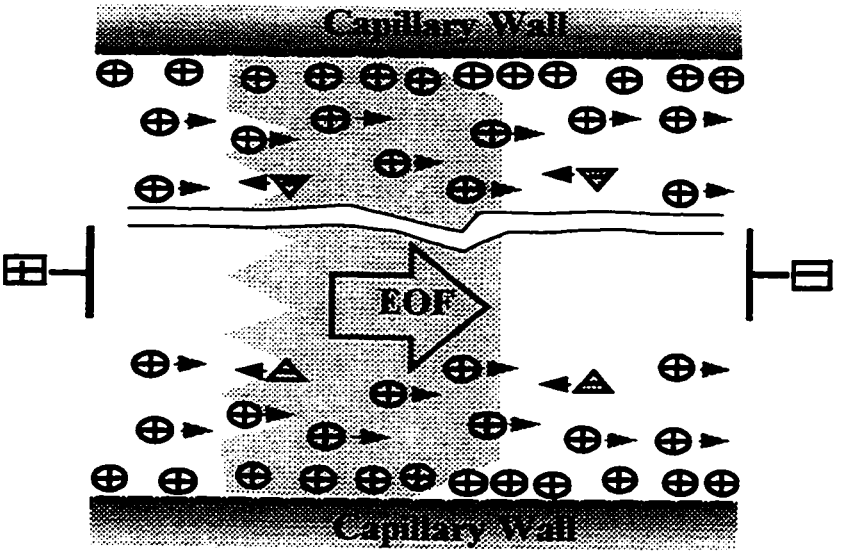

Figure 1.2 Schematic diagram of electrical double layer at the capillary wall and the flat profile of the EOF.

The formation of an electrical double layer creates a potential difference very close to the capillary wall, which is known as the zeta potential (ζ). The magnitude of electroosmotic flow can be expressed in terms of mobility by [1]:

$$\mu_{eof} = \frac{\varepsilon\zeta}{4\pi\eta} \qquad 1\text{-}5$$

where μ_{eof} is the electroosmotic flow "mobility", ε is the dielectric constant of the solution, ζ is the zeta potential, and η is the viscosity of the solution. The surface charge on the inner capillary wall is the main factor determining the zeta potential. The relationship between the zeta potential and the surface charge density is given by [5]:

$$\zeta = \exp(-\kappa x)(2kT/e)Sinh^{-1}(\sigma_{Si}\sqrt{500\pi/\varepsilon RC_i T}) \qquad 1\text{-}6$$

where κ is the inverse of the double layer thickness, x is the thickness of the counter-ion layer, k is the Boltzmann constant, T is the absolute temperature, e is the electric charge, σ_{Si} is the charge density on the fused silica surface, ε is the dielectric constant of the buffer, R is the molar gas constant, and C_i is the electrolyte concentration. It can be seen that the higher the surface charge density, the higher the zeta potential and the electroosmotic flow. Because the pH of the solution influences the ionization of silanol groups, and in turn the surface charge density, the magnitude of electroosmotic flow varies with the pH of the running buffer solution. The surface charge density is related to the running buffer pH by the following equation [6]:

$$\sigma_{Si} = \nu/(1+([H^+]/K_a)) \qquad 1\text{-}7$$

where ν is the total of both the ionized and protonated surface silanol group concentrations, and K_a is the dissociation constant of the silanol group. It can be seen that the higher the pH (or the lower the $[H^+]$) , the higher the capillary surface charge density, and thus the faster the EOF. In addition to the pH, the ionic strength of the buffer

solution is another major factor determining the zeta potential. The relationship between the ionic strength and the thickness of the double layer is given by [5]:

$$\kappa^{-1} = \left(\frac{\varepsilon_0 \varepsilon k T}{2e^2 I} \right)^{1/2} \qquad 1\text{-}8$$

where ε_0 is the permitivity of vacuum, and I is the ionic strength of the buffer solution. From Equation 1-8, it can be seen that increased ionic strength causes a decrease in the double layer thickness (κ^{-1}), the zeta potential and the electroosmotic flow [5][7]. Since the driving force of EOF is uniformly distributed along the capillary wall, the flat flow profile, which is indicated in Figure 1.2, is the distinct feature of EOF in comparison with the parabolic flow profile usually observed in pressure-driven systems. The flat EOF profile does not broaden the analyte zones. Therefore very high efficiency (sharp peaks) and resolution result in CZE. The velocity or "mobility" of electrophoretic flow can be determined very conveniently by adding neutral marker molecules into the sample solution. Neutral molecules will migrate at the same speed as EOF. Thus:

$$\mu_{eof} = \frac{L_t L_d}{V t_{eof}} \qquad 1\text{-}9$$

where L_t is the total capillary length, L_d is capillary length to the detector, V is the applied voltage, and t_{eof} is the migration time of the neutral EOF marker.

1.2.2 ELECTROPHORETIC MOBILITY

1.2.2.1 DEFINITION OF ELECTROPHORETIC MOBILITY

The concept of electrophoretic mobility, often called mobility of an analyte, was

addressed in Section 1.1 (Equation 1-1). Although the electrophoretic mobility is a constant for a given buffer solution, and so does not depend on the electric field strength, the velocity of each ion does vary with the electric field according to the following equation:

$$\upsilon = \mu E \qquad 1\text{-}10$$

where υ is the ion velocity, μ is the electrophoretic mobility of the ion, and E is the applied electric field strength.

1.2.2.2 FACTORS DETERMINING THE ELECTROPHORETIC MOBILITY

Many factors significantly affect the electrophoretic mobility of an analyte. These include pH, solvent, and the ionic strength of the solution. Some of the most important factors will be discussed below.

pH of the Buffer Solution Electrophoretic mobility adjustment by controlling the pH of the running buffer solution has been widely employed to separate analytes in capillary zone electrophoresis (CZE). For example, the observed electrophoretic mobility (μ_{obs}) of a weak acid (HA) is given by [8]:

$$\mu_{obs} = \mu_{A^-} \frac{K_a}{[H^+] + K_a} \qquad 1\text{-}11$$

where μ_{obs} is the observed mobility of a weak acid at a given pH, μ_{A^-} is the mobility of the anionic form of the acid, and K_a is the acid dissociation constant. It can be seen that even if the anion form of two weak acids had exactly the same mobility, they could still be separated by adjusting the buffer pH if their K_a values are different. For weak acids,

increased pH results in a higher degree of ionization (dissociation), thus a higher percentage of the anion in the solution and a larger observed mobility.

Solvent For small ions moving in the electric field, electrophoretic mobility is governed by Equation 1-1. The frictional force (f) is mainly from the viscous drag between the moving ions and the solvent. Solvent change results in the variation of viscosity (η), and thus the electrophoretic mobilities of solutes. It was reported that solvent change results in significant changes in the electrophoretic mobility and the separation order of 11 inorganic anions [9]. The mobility changes are believed to result from the changes in solvation of the ions.

Ionic Strength The influence of ionic strength on the electrophoretic mobility is very important in capillary zone electrophoresis. It was observed that the electrophoretic mobility of an ion decreases with increase of ionic strength of the buffer solution [10][11]. Some empirical correlations between the electrophoretic mobility and ionic strength have been proposed [12][13]. Theoretically, according to the Debye-Hückel-Onsager limiting law [14], the electrophoretic mobility varies linearly with the square root of ionic strength. It was found that this limiting law is only effective up to 0.01 M ionic strength [14][15][16]. For ionic strength ranges up to 0.1 M, the extended form of the Debye-Hückel-Onsager equation gives a much better linear relationship between the electrophoretic mobility and the running buffer ionic strength. A more thorough discussion of this issue is given in Section 3.2.3.4.

1.2.3 APPARENT MOBILITY

In capillary zone electrophoresis, the apparent mobility (μ_{app}) of an ion moving in the same direction as the EOF can be defined as the addition of electrophoretic mobility (μ) and EOF "mobility" (μ_{eof}):

$$\mu_{app} = \mu_{eof} + \mu \qquad 1\text{-}12$$

Apparent mobility can be calculated using the following equation:

$$\mu_{app} = \frac{L_t L_d}{V t_m} \qquad 1\text{-}13$$

where t_m is the migration time of the analyte, which can be obtained from the electropherogram of analytes (Figures 3.4 and 5.2). Rearrangement of Equation 1-12 gives a convenient expression for calculating the electrophoretic mobility:

$$\mu = \mu_{app} - \mu_{eof} = \frac{L_t L_d}{V}\left(\frac{1}{t_m} - \frac{1}{t_{eof}}\right) \qquad 1\text{-}14$$

1.2.4 ABSOLUTE MOBILITY

Absolute mobility (μ_0) is the electrophoretic mobility of an ion at infinite dilution (zero ionic strength). Although absolute mobility is a characteristic constant for a given ion, factors such as molecular size (ionic radius, molecular weight) [17][18] , shape [19], charge and charge distribution [20][21][22][23] are the intrinsic properties determining its magnitude. Traditionally, absolute mobilities of solutes were determined experimentally using conductivity [24][25][26] , capillary isotachophoresis (CITP) [27][28] or capillary

zone electrophoresis methods [12][10][11][16]. However, it is very time-consuming to measure the absolute mobilities experimentally.

1.3 PREDICTION OF ABSOLUTE MOBILITY

1.3.1 THEORETICAL MODELS

1.3.1.1 SPHERICAL MODEL

Since the mobility of an analyte is the most important parameter determining its separation in capillary electrophoresis, many efforts have been made to predict the electrophoretic mobility. The classical model based on hydrodynamic theories is the Hückel model, which is a modified Stokes-Einstein equation. Einstein derived in 1905 the relationship between the diffusion coefficient in infinitely dilute solution ($D°$) and the friction coefficient (f) of a particle. This is given by:

$$D° = kT/f \qquad 1\text{-}15$$

where k is the Boltzmann's constant and T is the absolute temperature [29]. In general, the friction coefficient (f) in Equation 1-15 is unknown. However, in 1856, Stokes [30] derived that the friction coefficient of a spherical particle moving in a continuous medium is governed by:

$$f = 6\pi\eta r \qquad 1\text{-}16$$

where η is the viscosity of the continuous fluid and r is the radius of the spherical particle.

Einstein assumed that Equation 1-16 can also be applied to spherical molecules. The diffusion coefficient is then expressed as:

$$D^0 = \frac{kT}{6\pi\eta r} \qquad 1\text{-}17$$

Equation 1-17 is known as Stokes-Einstein equation. In capillary electrophoresis, since the absolute mobility (μ_0) of a charged molecule and its diffusion coefficient has the following relationship:

$$\mu_0 = \frac{q}{kT} D^0 \qquad 1\text{-}18$$

therefore, the absolute mobility (μ_0) of an ion is given by:

$$\mu_0 = \frac{q}{6\pi\eta r} \qquad 1\text{-}19$$

Theoretical electrokinetic treatment of a charged particle by Hückel also gave the same expression. Therefore, Equation 1-19 is known as the Hückel equation in capillary electrophoresis [31].

1.3.1.2 ELLIPSOIDAL MODEL

The Hückel equation was derived for large spherical analytes only. Obviously, most molecules are not spherical. In 1936, Perrin [19] derived the friction coefficient for ellipsoidal molecules, which is given by:

$$f = 6\pi\eta r(f / f_0) \qquad 1\text{-}20$$

where f_0 is the friction coefficient of a sphere, and f is the friction coefficient of an ellipsoid of the same volume. The friction ratio can be obtained using the axial ratio of the ellipsoid [32] (Section 2.4.2). Thus, the absolute mobility of molecules is given by

$$\mu_0 = \frac{q}{6\pi\eta r(f / f_0)} \qquad 1\text{-}21$$

1.3.1.3 APPLICATION OF THEORETICAL MODELS TO ELECTROPHORETIC MOBILITY

The validity of Equation 1-21 has been widely investigated in electrophoresis [33][34][35][36][37]. Unfortunately, it was found that Equation 1-21 can not be applied universally to all classes of molecules. Although this equation has been verified for molecules which are significantly larger than the solvent molecules [33], it fails when the solute molecules and the solvent molecules are of comparable size. Various empirical corrections to the Hückel law have been made to make it applicable to the systems investigated. For small organic solutes in aqueous solution (radii = 3-6 Å), Edward [34][35] suggested that the numerical factor in the denominator should be 5 instead of 6. Robinson and Stokes [36] have used the mobilities of quaternary amines to estimate the correction factor. They demonstrated that no correction is needed for molecules with radii above 5.8 Å, but for smaller molecules, the correction factor varied with the molecular size. By investigating the extensive experimental data available, Spernol [37] showed that the correction factor (Δ) and the radius ratio (r_L/r) of the solvent (r_L) to the

solute (r) have the following relationship:

$$\Delta = (1 + r_L^2/r^2)^{-1} \qquad 1\text{-}22$$

From Equation 1-22, it can be seen that the correction factor is equal to 0.5 if the sizes of solute and solvent molecules are about the same ($r_L = r$). Therefore, the numerical factor in Equation 1-21 should be around 3 ($6\times\Delta=3$).

1.3.1.4 MODELS INCLUDING DIELECTRIC FRICTION

The above discussion demonstrated that corrections must be performed in order to use Equation 1-21 to predict the absolute mobilities of small ions. Further, for very small ions (< 1.5 Å), the mobility is actually inversely related to the crystallographic radii. This paradoxical behavior is believed to result from mobility depending upon another frictional term in addition to the hydrodynamic friction incorporated in the Hückel equation:

$$f = f_H + f_D \qquad 1\text{-}23$$

where f_H is the hydrodynamic friction and f_D is the dielectric friction. Dielectric friction results from the interaction between the moving ion and the adjacent solvent dipoles. As an ion migrates through the solvent it causes the adjacent solvent dipoles to orient. After passage of the ion, the solvent dipoles relax to their random orientation. However this relaxation takes a finite period of time (0.82×10^{-11} s in water at 25 °C [21]), and so imposes a retarding force on the migrating ion. Hubbard and Onsager [22][21] have provided the most thorough theoretical treatment of this effect. For continuum (stick) media, they showed that the friction coefficient of an ion can be expressed as:

$$f = 6\pi\eta r + (\frac{17}{280})\frac{\tau_D e^2}{r^3}(\frac{\varepsilon_0 - \varepsilon_\infty}{\varepsilon_0^2}) \qquad 1\text{-}24$$

where e is the ion charge, η is the solvent viscosity, ε_0 and ε_∞ are the low (zero) and high frequency (infinite) dielectric constants of the solvent, τ_D is the Debye dielectric relaxation time of the pure solvent, and r is the ionic radius. It is expected that substituting Equation 1-24 into Equation 1-1 should give a more accurate prediction of the absolute mobilities of small ions. However, this combination has not been highly successful at *a priori* prediction of mobilities in aqueous solution [21][23]. Nonetheless, it helps illustrate that the prediction of mobility is much more complex than solely the hydrodynamic drag predicted in the Hückel (Equation 1-19) or Perrin (1-21) models.

1.3.2 EMPIRICAL MODELS

Due to the complexity of the absolute mobility prediction of small ions, numerous empirical models have been developed for the different classes of molecules investigated. Some of the models widely adopted in capillary electrophoresis are discussed below.

1.3.2.1 OFFORD'S MODEL

In 1966, Offord [18] developed a very simple equation for the calculation of peptide absolute mobilities in paper electrophoresis. The relationship between the absolute mobility and the molecular weight is given by:

$$\mu_0 = \frac{KZ}{W^{2/3}} \qquad 1\text{-}25$$

where K is a constant, Z is the charge on the molecule, and W is the molecular weight. In this model, Offord suggested that the mobility might be a function of the surface area of the molecule. He supposes that the ionic atmosphere is oppositely charged and solvated. The movement of the ionic atmosphere causes a backwards flow of solvent in the immediate vicinity of the migrating molecule. The frictional force may then be considered to arise from the shear across a small element of liquid close to the migrating ion, which would be some function of the surface area. The molecular surface area was approximated by the (molecular weight)$^{2/3}$ to yield Equation 1-25. Equation 1-25 was successfully applied to the prediction of peptide absolute mobilities, except for peptides containing histidine and cysteic acid [18]. Equation 1-25 was also effective for capillary zone electrophoresis separation of peptides [38][39], although not quite universally so [40]. However, Offord did note that this expression did not include *"the possible contribution of the ionic atmosphere to the effective mass, and factors due to shape"* [18]. Indeed, in a study of the mobilities of monosubstituted alkyl pyridines [41], both the Hückel (Equation 1-19)and Offord (Equation 1-25) equations accurately modeled the effect of increasing alkyl chain length, but failed to distinguish between positional isomers.

1.3.2.2 COMPTON'S MODEL

In 1991, Compton [42] proposed a semi-empirical model to predict the electrophoretic mobility of proteins in free solution:

$$\mu = \frac{K_1 q}{K_2 W^{1/3} + K_3 I^{1/2} W^{2/3}} \qquad 1\text{-}26$$

where K_1, K_2 and K_3 are constants, q is the charge on the molecule, W is the molecular weight, and I is the ionic strength. This equation was derived from the Debye-Hückel-Henry equation [42] by expressing the size of protein using molecular weight rather than molecular radius. From Equation 1-26, it can be seen that at zero ionic strength the absolute mobilities of very large molecules (proteins) can be expressed as:

$$\mu_0 = \frac{K_1 q}{K_2 W^{1/3}} \qquad 1\text{-}27$$

Although both Equation 1-25 and 1-27 use molecular weight to reflect molecular size, the power dependences of the molecular weight are totally different. This power difference may have resulted from the molecular size difference, which indicates that for molecules smaller than the proteins, the power dependence is significantly different from that predicted from Hückel's model.

1.3.2.3 GROSSMAN'S MODEL

In 1989, Grossman *et al.* [43] developed an empirical model to predict the electrophoretic mobilities of peptides using the number of amino acids in the polypeptide chain (n) as the parameter to reflect the peptide size:

$$\mu = \frac{5.23 \times 10^{-4} \ln(q+1)}{n^{0.43}} \qquad 1\text{-}28$$

where q is the charge on the peptide. They initially treated the peptide molecule as a classical polymer in solution for which the mobility is inversely related to the radius of gyration. The radius of gyration is given by the root-mean-square of the end-to-end distance of the peptide, which is proportional to $n^{0.5}$. However, fitting to experimental

mobilities for peptides varying in length from 3 to 38 amino acids yielded a power dependence of 0.43, as shown in Equation 1-28. The constant 5.23×10^{-4} was experimentally determined using 20 mM monosodium citrate buffer solution at pH 2.50. Therefore it probably should vary with the concentration and composition of the buffer solution used. However, for a given solvent condition the general form of Equation 1-28 would remain valid. Note, Equation 1-28 omits the constant term initially reported by Grossman *et al*, because a subsequent informal *errata* [44] indicated that the constant was an experimental artifact.

Equation 1-28 has been used to predict the electrophoretic mobility of protein molecules [43]. Unfortunately, it was found that the predicted mobilities were consistently lower than the experimentally measured mobilities. It was suggested that this was due to the conformation of the protein, which are more tightly folded than peptides.

1.4 OBJECTIVE AND SCOPE OF THIS PROJECT

The absolute mobility (intrinsic mobility) of an ion is of fundamental importance in capillary electrophoresis. Knowledge of the absolute mobility of a solute would aid in prediction of its behavior before separation and the identification of unknown peaks. However, traditionally, the absolute mobility can only be determined experimentally which is very time consuming. This limits our ability to *a priori* predict whether capillary zone electrophoresis is appropriate for a given application or identify an unknown peak within the electropherogram. The purpose of this research project is to develop empirical expressions for the prediction of absolute mobilities, and to determine the underlying

factors that govern these mobilities. Herein, molecular modeling is used to determine the size, shape and other physicochemical parameters employed to generate the absolute mobility prediction models. This work deals with the prediction of the absolute mobilities of monocharged small organic cations and anions. We aimed to investigate the behavior of three main kinds of analytes, which were amines, aliphatic carboxylates and sulfonates. Independent tests are performed to evaluate the predictability of the proposed empirical models.

1.5 REFERENCES

1. Li, S. F. Y. *Capillary electrophoresis: Principles, practice and applications*; Elsevier: Amsterdam, Netherlands, 1993; pp 14-17.
2. Burgreen, D.; Nakache, F. R. *J. Phys. Chem.* **1964**, *68*, 1084-1091.
3. Rice, C. L.; Whitehead, R. *J. Phys. Chem.* **1965**, *69*, 4017-4024.
4. Jorgenson, J. W.; Lukacs, K. D. *Anal. Chem.* **1981**, *53*, 1298-1302.
5. Lucy, C. A.; Underhill, R. S. *Anal. Chem.* **1966**, *68*, 300-305.
6. Hayes, M. A.; Kheterpal, I.; Ewing, A. G. *Anal. Chem.* **1993**, *65*, 27.
7. Van Orman, B. B.; Liversidge, G. G.; McIntyre, G. L.; Olefirowicz; Ewing, A. G. *J. Microcolumn Sep.* **1990**, *2*, 176-180.
8. Smith, S. C.; Khaledi, M. G. *Anal. Chem.* **1993**, *65*, 193-198.
9. Salimi-Moosavi, H.; Cassidy, R. M. *Anal. Chem.* **1995**, *67*, 1067-1073.
10. Nashabeh, W.; Rassi, Z. E. *J. Chromatogr.* **1990**, *514*, 57-64.

11. Bruin, G. J. M.; Chang, J. P.; Kuhlman, R. H.; Zegers, K.; Kraak, J. C.; Poppe, H. *J. Chromatogr.* **1989**, *471*, 429-436.

12. Friedl, W.; Reijenga, J. C.; Kenndler, E. *J. Chromatogr.* **1995**, *709*, 163-170.

13. Cao, C.-X. *J. Chromatogr.* **1997**, *771*, 374-378.

14. Erdey-Grúz, T. *Transport Phenomena in Aqueous Solutions*; Halsted Press: New York, 1974; 294-326.

15. Edward, J. T. Crawford, R. *J. Chromatogr.* **1958**, *1*, 449-456.

16. Tiselius, A.; Svensson, H. *Trans. Faraday Soc.* **1940**, *36*, 16-22.

17. Compton, B. J.; O'Grady, E. A. *Anal. Chem.* **1991**, *63*, 2597-2602.

18. Offord, R. E. *Nature* **1966**, *211*, 591-593.

19. Perrin, F. *J. Phys. Radium* **1936**, *7*, 1.

20. Hubbard, J. B. *J. Chem. Phys.* **1978**, *68*, 1649-1664.

21. Evans, D. F.; Tominaga, T.; Hubbard, J. B.; Wolynes, P. G. *J. Phys. Chem.* **1979**, *83*, 2669-2677.

22. Hubbard, J.; Onsager, L. *J. Chem. Phys.* **1977**, *67*, 4850-4857.

23. Kay, R. *Pure & Appl. Chem.* **1991**, *63*, 1393-1399.

24. Jones, J. H.; Spuhler, F. J.; Felsing, W. A. *J. Am. Chem. Soc.* **1942**, *64*, 965.

25. Kuhn, D. W.; Kraus, C. A. *J. Am. Chem. Soc.* **1950**, *72*, *3676.*

26. Jandik, P.; Bonn, G. *Capillary Electrophoresis of Small Molecules and Ions*; VCH: New York, 1993; p. 15.

27. Hirokawa, T.; Kiso, Y. *J. Chromatogr.* **1982**, *252*, 33-36.

28. Beckers, J. L.; Everaerts, F. M. *J. Chromatogr.* **1989**, *470*, 277-287.

29. Edward, J. T. *J. Chem. Education* **1970**, *47*, 261-270.

30. Stokes, G. *Tran. Cambridge Phil. Soc.* **1856**, *9*, 5.

31. Hiemenz, P. C. *Principles of Colloid and Surface Chemistry*, 2nd edition; Marcel Dekker: New York, 1986; p. 747.

32. Eisenberg, D.; Crothers, D. *Physical Chemistry with the Application to the Life Sciences;* Benjamin/Cummings: Menlo Park, CA, 1979; pp 718-724.

33. Cheng, P. V.; Schachman, H. K. *J. Polumer Sci.* **1955**, *16*, 19.

34. Edward, J. T. *Scient. Proc., R. D. S.* **1957**, *27*, 273.

35. Edward, J. T. *Scient. Proc., R. D. S.* **1957**, *27*, 287.

36. Robinson, R. A.; Stokes, R. H. *Electrolyte Solutions*, 2nd Ed.; Butterworth Scientific Publications: London, 1959. pp 123-126.

37. Spernol, A. *J. Phys. Chem.* **1956**, *60*, 703.

38. Adamson, N.; Riley, P. F.; Reynolds, E. C. *J. Chromatogr.* **1993**, 391-396.

39. Kašicka, V.; Prusík, Z.; Mudra, P.; Štepánek, J. *J. chromarogr. A.* **1995**, *709*, 31.

40. Gaus, H.-J.; Beck-Sickinger, A. G.; Bayer, E. *Anal. Chem.* **1993**, *65*, 1399.

41. Rowe, R. C.; Wren, S. A. C.; McKillop, A. G. *Electrophoresis* **1994**, *15*, 635.

42. Compton, B. J. *J. Chromatogr.* **1991**, *559*, 357-366.

43. Grossman, P. D.; Colburn, J. C.; Lauer, H. H. *Anal. Biochem.* **1989**, *179*, 28-33.

44. Grossman, P. D. *Capillary Electrophoresis: Theory and Practice*, Grossman, P.D.; Colburn, J. C., Eds.; Academic Press: San Diego, 1992. Ch. 4.

CHAPTER 2 MOLECULAR MODELING

2.1 INTRODUCTION

Molecular modeling has become more and more important in chemistry. It has been employed to select the stationary phase in liquid chromatography [1], to study the selectivity of extracting Cs^+ with Calix-Crowns [2] and enantiomer separation in gas chromatography [3], to give only a few examples. Many molecular physicochemical properties such as molecular volume, surface area, shape index, solubility parameters, dipole moment, and mean waters of hydration can be estimated using molecular modeling software. Some of the popular commercially available molecular modeling programs are HyperChem (Autodesk, Inc.), Molecular Modeling Pro™ (WindowChem), and Insight II (Biosym Technologies).

Molecular Modeling Pro™ can be installed on most personal computers and over 70 physicochemical properties can be calculated including molecular volume, molecular length, width and depth, which are the important parameters to determine molecular shape. Therefore, in this study, most of the physicochemical parameters were obtained using Molecular Modeling Pro™ (Version 1.44, WindowChem Software, Fairfield, CA). This software is a 3-dimensional chemical structure drawing program and physicochemical property estimation program. All molecular mechanics/dynamics calculations are performed using classical mechanical forcefields. Quantum mechanics calculations employ several semi-empirical molecular orbital methods (CNDO, MINDO3, and MNDO). Molecular Modeling Pro™ requires a 80386 or better CPU with 3.8 megabytes of RAM

or more, and runs faster and smoother on faster 80486 or Pentium computers. In our laboratory, this software was installed on a 75-MHz Pentium microcomputer. Molecular volumes obtained from Insight II, a higher level molecular modeling software which employs the CFF91 forcefield for molecular mechanics calculations and *ab initio* for quantum mechanics calculations, are also included in this study. Insight II molecular modeling software was installed on an IBM RS/6000 work station. The operating system used was AIX 3.2.

2.2 DRAWING MOLECULES

2.2.1 MOLECULAR MODELING PRO™ (MMP™) [4]

Molecules can be constructed very easily with a mouse and the pulldown menus. The main screen of Molecular Modeling Pro™ is shown below:

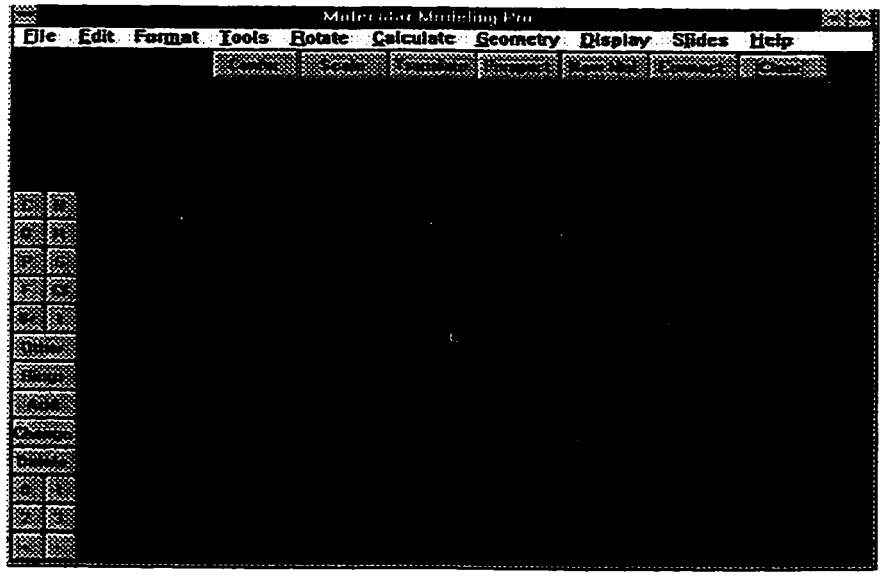

Figure 2.1 The main screen of Molecular Modeling Pro™.

The procedures for drawing molecules are as follows:

1. Select the atom type button desired from the left side of the main screen. The default atom type is carbon (**C**). For atoms other than hydrogen (**H**), carbon (**C**), nitrogen (**N**), oxygen (**O**), phosphorus (**P**), sulfur (**S**), fluorine (**F**), chlorine (**Cl**), bromine (**Br**) and iodine (**I**), the "**Other**" button needs to be selected and the periodic table will appear on the screen. Any atom type can then be selected using the left button on the mouse.

2. Click anywhere on the black screen, the selected atom appears in the center of the screen.

3. To add the second atom, just select the correct bond type from the toolbar at the bottom left of the screen. "**1**" is a single bond, "**2**" a double bond, and "**3**" a triple bond. Then click the mouse on the atom symbol (letter) of the first atom if the atom type need not to be changed. Otherwise, the atom type and bond type of the second atom have to be selected before clicking on the first atom. Now the molecule will appear as a line, with atoms at either end. The atom type is indicated by color instead of the element symbol.

4. Repeat step 3 to add more atoms by clicking on the atom (end of lines or angle vertices).

5. To delete atoms, the "**Delete**" button at the left side of the screen must be selected before clicking on the atoms to delete.

6. To add a ring to the molecule, click on the "**Rings**" button at the left side of the screen and select a ring system from the list that appears. When the list disappears, click

on the atom in the previously drawn molecule that should be connected to the ring first, then click on the ring atom to connect to the previously drawn molecule.

7. Formal charge can be added to a particular atom by selecting the "+" or "-" button at the left bottom of the main screen and then clicking on the corresponding atom of the molecule.

8. To add the correct number of hydrogens to the molecule, just quickly double click on the "**H**" button, a message "**add hydrogens to all atoms?**" will appear on the screen. Select "**yes**" to add hydrogens.

2.2.2 INSIGHT II

The procedures of drawing molecules using Insight II are as follows:

1. Choose Builder under the **Module** menu.

2. Select the element type from the **Mol Builder** pulldown.

3. Move the cursor to the desired place on the screen. Press the left button on the mouse and draw a line, and then click the left and right buttons consecutively.

4. Select another type of atom, and repeat step 3.

5. Repeat step 4 and 3 until the desired molecule is constructed.

6. Formal charge can be added to a particular atom by clicking the "**Atom**" button from the upper tool bar, and selecting "**Charge**" from the pulldown. Then select "**Formal Charge**" from the **Charge** pulldown and type in the charge number (with + or - sign). Select the atom to which the charge will be added. Finally, select "**Execute**" to complete the charge addition.

7. Select the "**2D → 3D**" button from the **Mol Builder** pulldowns to convert the constructed molecule from 2 dimensions to 3 dimensions. Hydrogen atoms will be added to the molecule automatically.

2.3 OPTIMIZATION (MINIMIZATION) OF MOLECULAR GEOMETRY

2.3.1 MOLECULAR MODELING PRO™ (MMP™)

In this study, all molecules were drawn in the "extended form" because this conformation usually represents the lowest energy state [5]. After construction of the desired molecule, optimization of molecular geometry must be performed before calculating any molecular physicochemical parameters. The strain energy of the constructed molecule can be minimized with the "**Minimize**" function under the "**Geometry**" menu. Complicated molecules can take a time long (≥120 minutes) to minimize their strain energy. To reduce the minimization time, all initial minimization steps were performed in the absence of hydrogen atoms. The overall minimization took from 5 min for ammonium (the smallest molecule investigated) to about 2 hours for octadecyltributylammonium (the biggest molecule studied). The optimization of molecular geometry in Molecular Modeling Pro™ and other molecular modeling softwares is based on the **local minimization** of molecular strain energy, not the **global minimization** (molecule as a whole). That is, the minimization optimizes the strain in each bond individually, rather than for the molecule as a whole.

The minimization procedures are:

1. Place the molecule in the absence of hydrogens in a reasonable conformation before minimization ("extended form" in this work).

2. Select the "**Minimize**" button under the Geometry menu. Then set the minimizer level to "**make extreme changes**" and click the "**Done**" button. After the molecular energy reaches the local minimum, the minimizer quits and displays the strain of the molecule on the screen.

3. Repeat step 2 successively using minimizer levels of "**make large changes**"; "**make moderate changes**"; and finally "**refine**".

4. Double click on the "**H**" button on the left side of the screen to add hydrogens to the molecule.

5. Do the minimization once more at the "**refine**" level.

After the minimization, the molecule can be saved as a Macromodel file for subsequent calculation of the physicochemical parameters.

2.3.2 INSIGHT II

After the constructed molecule is converted from 2 dimensions to 3 dimensions, minimization (optimization) is performed by selecting the "**Optimize**" button from the **Mol Builder** menu.

2.4 CALCULATION OF MOLECULAR PHYSICOCHEMICAL PARAMETERS

2.4.1 MOLECULAR VOLUME AND SURFACE AREA

2.4.1.1 MOLECULAR MODELING PRO™ (MMP™)

After minimization, many molecular parameters can be calculated very easily using the "**Calculate**" menu. Molecular Van der Waals volumes in cubic angstroms ($Å^3$) can be calculated by selecting "**Molecular volume/density**" under the **Calculate** menu.

Molecules can be pictured as being enclosed by a Van der Waals surface, which is spherical about each atom. This surface limits the approach of other molecules at ordinary temperature. The molecular Van der Waals volume is then defined as the volume enclosed by the Van der Waals surface. In Molecular Modeling Pro™, molecular volume is calculated by excluding the overlap volumes from the total volume obtained by summing volumes for the individual atoms of the molecules. This is done by using the Van der Waals increments of A. Bondi [6], which allow for atomic volume variation due to the functionality of the atom. The Van der Waals increments of some common atoms or groups are listed in Table 2.1.

Table 2.1 Van der Waals increments for atoms or functional groups*.

Atom or Group	Increment (Å^3)	Atom or Group	Increment (Å^3)
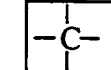	5.6		11.3
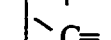	8.1		10.1
	11.6		17.9
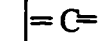	13.4		20.1
 (attached to C)[a]	5.7		7.2
 (attached to C)[b]	5.3		4.6
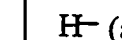 (attached to N)	5.2		
 (attached to N^+)	2.3		6.7
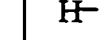 (attached to O)	7.2		11.0
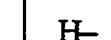	9.9		17.2
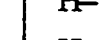	19.8		14.8
	24.5		27.9
	32.8		6.2

* Table adapted from reference [8], [a] Alkane, alkene, or alkyne, [b] Aromatic

Due to the local minimization of all molecular modeling softwares, the calculated molecular volumes using Molecular Modeling Pro™ were not quite reproducible. For molecules which were constructed and minimized in exactly the same way, the relative standard deviation for molecular volume varied from 0.04% to 0.3%. Indeed, even high level molecular modeling software such as Insight II (Version 95.0.2, Biosym Technologies, San Diego, CA) gave about the same uncertainty in molecular volume. Version 1.44 of Molecular Modeling Pro™ was chosen because, after minimization, it gave the conformations of molecules in the most extended form, which

matched those obtained using Insight II, while the newest version of Molecular Modeling Pro (version 2.11) did not give the conformations we expected. Using Version 2.11, after mimimization, the aliphatic chains were not in the most extended form. Furthermore, the calculated molecular volumes were slightly lower than those calculated using Version 1.44. For the nine molecules listed in Table 3.1, the molecular Van der Waals volumes obtained from Version 2.11 were about 1.7 percent lower than those from Version 1.44.

The surface area of molecule was given along with the molecular volume. It was calculated by summing the surface area of atomic spheres of Van der Waals radius minus the overlaps.

2.4.1.2 INSIGHT II [7]

Molecular Van der Waals volumes in cubic angstroms ($Å^3$) can also be determined using Insight II (Version 95.0.2, Biosym Technologies, San Diego, CA). Molecular volume is created by first constructing a grid that spans the molecule (Figure 2.2). Then the volume within the Van der Waals surface (grid points lie within it) of the molecule is calculated.

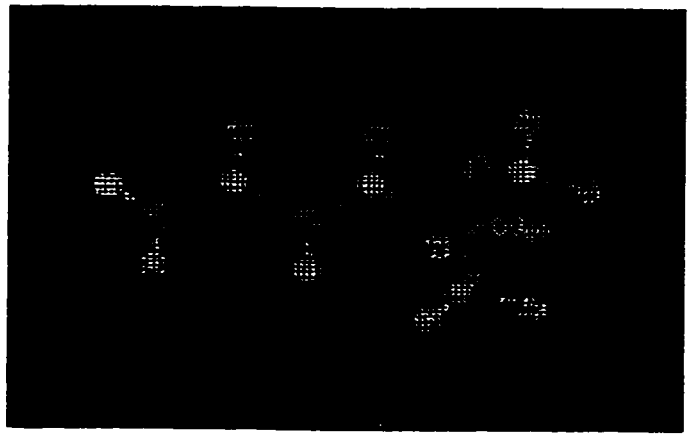

Figure 2.2 A grid that spans around a molecule (Insight II).

The procedures for determining molecular volume are as follows:

1. Select **Search-Compare** from the **Module** menu, then click the **Volume** to open the volume pulldown.

2. Use **Grid-Setup** to set specifications for the calculation of molecular volumes. The following parameters must be specified before the calculation of molecular volume:

Grid Style: Grid Style is set to "Enclosure", which allows Insight II to automatically determine the extent of grid needed to enclose the molecule.

Border Space: This parameter specifies the thickness of the border (in angstroms) that is added around the grid. The default value is set to 0.6 Å. Less than 0.5% relative errors were observed if the Border Space was set to less than 0.6 Å, but much larger errors resulted if the Border Space was set to greater than the default value. In general, the larger the Border Space, the smaller the calculated molecular Van der Waals volume.

Grid Step: Grid Step specifies the grid resolution (in angstroms). Smaller values give higher resolution. However, for the algorithm to function properly, the Grid Step is usually set to one half of the Border Space.

3. Select **Create** from the **Volume** pulldown to calculate the molecular volume. Two parameters (**VDW Scale** and **VDW Increment**) determining the relative volume size must be specified before the creation of molecular volume. **VDW Scale** (Van der Waals Scale) is the number that each atom's Van der Waals radius is multiplied by and should be set to 1.00. **VDW Increment** is the number in angstroms that is added to each atom's Van der Waals radius and should be set to 0.00 to calculate the unadjusted molecular volume. Finally, select the name of the molecule from the operand list and the molecular Van der Waals volume will be calculated within a few seconds.

It was found that the volumes calculated using Insight II were systematically lower than those calculated using classical mechanics (Molecular Modeling Pro™). For nine molecules, the Van der Waals volumes calculated using both programs are listed in Table 2.2.

Table 2.2 Molecular volumes from literature, MMP™, and Insight II.

Molecules	Van der Waals Volume (Å^3)					$V_{MMP}/V_{In.}$
	Literature*	MMP	Error%	Insight	Error%	
Methane	28.4	27.4	-3.5	22.4	-21	1.23
Ethane	45.4	43.9	-3.3	37.8	-17	1.16
Propane	62.4	60.4	-3.2	52.4	-16	1.15
Benzene	80.3	81.3	1.2	70.4	-12	1.15
urea	54.6	52.1	-4.6	43.3	-21	1.20
proionamide	76.7	74.2	-3.3	62.7	-18	1.18
α-Aminocaproic acid	126.0	134.7	6.9	113.7	-10	1.19
Tetramethyl ammonium	95.95	99.70	3.9	80.06	-17	1.25
Tetraethylammonium	163.2	163.7	0.3	139.1	-15	1.18

*Data from reference [8]

The literature molecular volumes were calculated manually using Van der Waals atomic increments. Some of the atomic increments are shown in Table 2.1. From Table 2.2, it can be seen that the molecular volumes calculated using Molecular Modeling Pro™ (Version 1.44) agree very well with the literature volumes. The average error is only -0.6%, the variation is about ±4%, while Insight II gives much bigger average relative error (about 16%) between the calculated and literature molecular volumes. However, the difference between molecular volumes calculated using different molecular modeling is systematic. The ratio of molecular volumes obtained from MMP™ to those from Insight II is about 1.2, which mean the molecular Van der Waals volume calculated using Insight II is about 20% lower than those using Molecular Modeling Pro™. The large molecular volume difference may be due to the degree of minimization or the methodology employed to create molecular volume. So, we can not justify which software gives the molecular volume close to the "true" value. However, it was found that the higher the degree of minimization, the smaller the volume were obtained.

In general, three methods are presently used to estimate molecular volume. The first method to obtain molecular volume is by dividing the molar volume of a solid or liquid by Avogadro's number. Molecular volume determined in this way is not appropriate for our study because this volume includes the "free volume" or "empty volume" between the molecules. Such a calculated molecular volume would be larger than the "true" value. The second way to obtain the molecular volume is to divide the partial molal volume by Avogadro's number. However, it was found that "*the empty volume associated with the solute molecule in aqueous solution is roughly the same as the empty volume associated with this molecule in the solid or liquid state at ordinary temperatures*" [8]. Thus this procedure would also overestimate the molecular volume. The most popular method to calculate molecular volume is the Van der Waals volume obtained from atomic increments. The Van der Waals atomic increments proposed by Bondi [6] are considered most appropriate because the environment (atoms or functional groups to which an atom is attached) of an atom was also considered. Molecular Modeling Pro™ employs the incremental method of Bondi to determine the molecular volume. Therefore, molecular volumes were calculated using the method described in Section 2.4.1.1.

2.4.2 AXIAL RATIO OF MOLECULE

2.4.2.1 DETERMINATION OF MOLECULAR LENGTH, WIDTH AND DEPTH

The axial ratio of a molecule was determined using Molecular Modeling Pro™. No other modeling program investigated allowed determination of this parameter. In the

ellipsoidal model (Perrin's model, Section 1.3.1.2), molecules were treated as ellipsoids. An ellipsoid is defined by three semi-axes: a; b; and c. The semi-axes are the axes of rotation, at a 90° angle to one another. In order to determine the extent of the influence of molecular shape on the absolute mobility, the axial ratio (b/a) of molecules had to be determined. The semi-axes (a, b, c) of the molecules were not automatically provided by the Molecular Modeling Pro™ Program. The program does provide the molecular length (X), width (Y) and depth (Z) with respect to the molecule's orientation on the screen. Molecular length is defined as the distance (in angstroms) from one end of the molecule along the screen X axis (right to left); molecular width is the width of the molecule along the y-axis (top to bottom); molecular depth is the width in and out of the screen (along the Z axis). To calculate the accurate axial ratio, it was necessary to manually rotate the molecule to ensure its position on the screen matched the predefined X, Y and Z direction. After the minimization, the molecule was rotated as follows:

1. Rotate the molecule along the Z axis to maximize its length. Since the direction of the molecular length and the X-axis may not be parallel at this moment, the molecular length obtained at this moment is the false maximum molecular length, as shown in Figure 2.3:

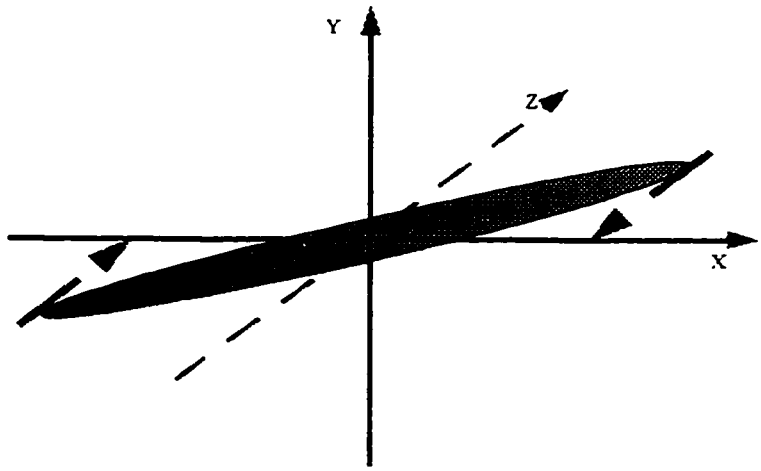

Figure 2.3 Rotate the molecule along Z axis to maximize its length.

2. Rotate the molecule along Y direction to maximum the molecular length once again. The direction of molecular length and the X axis should be parallel. This is the true maximum molecular length, which is indicated in the following diagram:

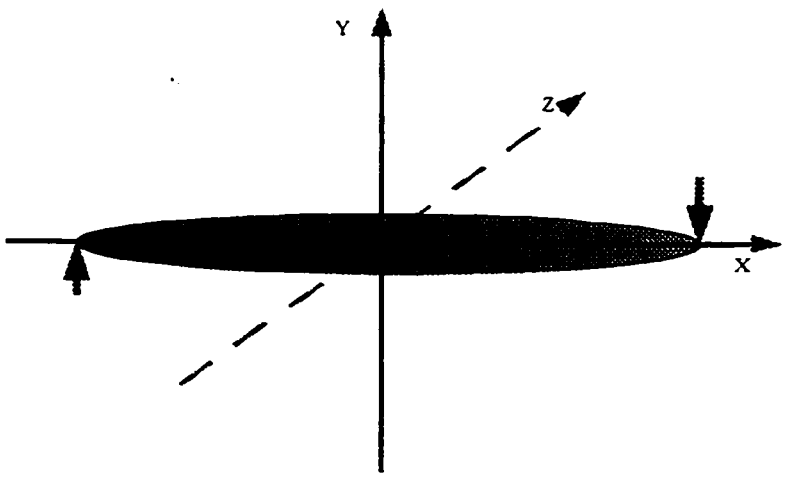

Figure 2.4 Rotate the molecule along Y direction to maximize its length

3. Rotate molecule along the X-axis to maximize its width or depth.

2.4.2.2 PROLATE AND OBLATE APPROXIMATIONS

Prolate or oblate approximations were used in the ellipsoidal model [5]. Prolate refers to a cigar-shaped ellipsoid, $a > b = c$, where the axial ratio $b/a < 1$ (Figure 2.5). An oblate is disk-shaped, $b = c > a$, $b/a > 1$ (Figure 2.5).

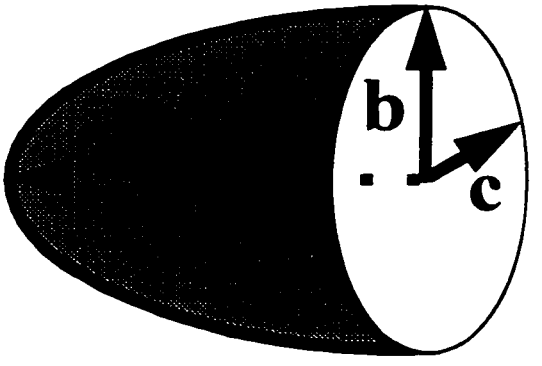

Figure 2.5 Schematic diagram of a prolate.

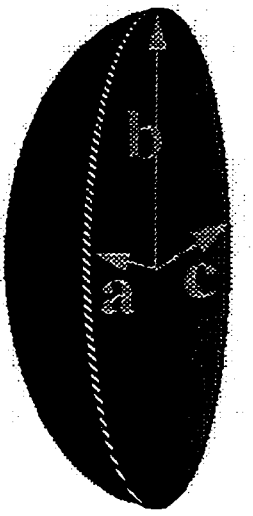

Figure 2.6 Schematic diagram of an oblate.

If any one (2a) of the three dimensions (molecular length, width or depth) was significantly larger than the other two (2b, 2c), then the molecule was treated as prolate (Figure 2.5). The longest dimension is defined as the molecular length, while the other two dimensions are molecular width and depth. For axes of similar length (*i.e.*, molecular width and depth), the geometric mean (equatorial semi-axis) was used for the b-length [5]:

$$b = \frac{1}{2}\sqrt{Width \times Depth} \qquad 2\text{-}1$$

In the same manner, if any two (2b, 2c) of the three dimensions (molecular length, width or depth) was significantly larger than the third one (2a), then the molecule was treated as oblate (Figure 2.6). In this case, the shortest dimension is defined as 2a, while

the other two dimensions are 2b and 2c. The two longest axes (2b and 2c) were used to calculate the geometric mean using Equation 2-1.

2.4.3 KIER'S KAPPA 2 SHAPE INDEX

Molecular Modeling Pro™ provides Kier's Kappa 2 shape index under the **Calculate/Connectivity index menu**. Kappa 2 shape index is an index relating to a topological property and degree of branching of a molecule [9]. For example, the shape indexes for five isomers of heptylamine are indicated in Table 2.3.

Table 2.3 Kappa shape indexes for 5 isomers of heptylamine

	Kappa Shape Index
$CH_3CH_2CH_2CH_2CH_2CH_2CH_2NH_3^+$	7.00
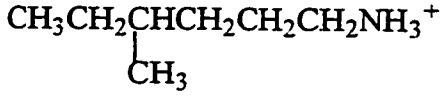	5.14
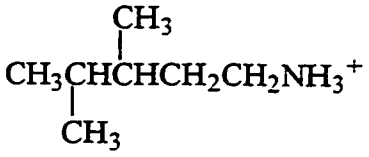	3.94
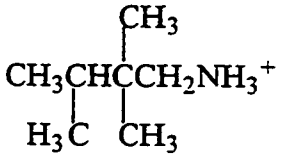	2.52
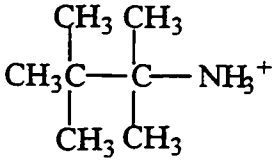	1.75

From Table 2.3, it can be seen that shape index can reflect the branching of a molecule. For isomers, the smaller the shape index, the higher the branching.

2.4.4 HYDRATION NUMBER

Intuitively, hydration of ions influences the effective molecular size [10]. The hydration number of a molecule was estimated using Molecular Modeling Pro™. In this program, McGowan's additive method [4] was employed to calculate the mean waters of

hydration. In this method, the waters of hydration associated with various functional groups have been estimated based on surfactant properties. Table 2.4 lists the mean waters of hydration for a number of functional groups and fragments:

Table 2.4 Mean waters of hydration of different functional groups.

Functional groups	mean water of hydration
Alkyl, Alkenyl, Alkynyl, Aryl	0
X-R (X = F^-, Cl^-, Br^-, I^-)	0
NH_4^+	12
R-N^+H_3	9
$R_1R_2N^+H_2$ (include ring system)	6
$R_1R_2R_3N^+H$	3
$R_1R_2R_3R_4N^+$	3
NH_3	9
R-NH_2	6
R_1R_2NH	3
$R_1R_2R_3N$	3
$RCOO^-$	5
RCOOH	2
R-O^-	4.5
ROH	1
R_1-O-R_2	1
RCN	3
R-NO_2	5
R_1-CONHR_2	4
R_1-CO-R_2	1.5
R-CHO	1.5
R-SO_3^-	10
R-SO_3H	7
R-SH	0
R_1-S-R_2	0

These waters of hydration are summed to estimate the hydration of the overall molecule. For example, the hydration number of each functional group of a Tris cation is indicated

in Figure 2.7.

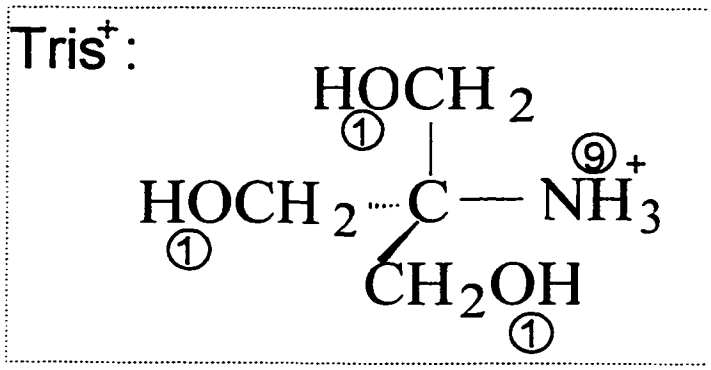

Figure 2.7 Hydration number of each functional group on $Tris^-$

Therefore, the total hydration number of $Tris^-$ is 12.

2.5 SUMMARY

Most of the physicochemical properties employed to predict the absolute mobilities were determined using Molecular Modeling Pro™ (Version 1.44, WindowChem Software™ Inc., Fairfield, CA). A higher level molecular modeling software, Insight II, was also employed to calculate the molecular volume.

2.6 REFERENCES

1. Azzaoui, K.; Lafosse, M.; Morin-Allory, L. *J. Liq. Chromatogr.* **1995**, *18*, 3021.

2. Lamare, V.; Bressot, C.; Casnati, A. *Separation Sci. Tech.* **1997**, *32*, 175.

3. Cardinael, P.; Ndzie, E.; Combret, J. C. *J. High. Resol. Chromatogr.* **1997**, *20*, 560.

4. WindowChem Software™ Inc.; *Molecular Modeling Pro™*, Revision 1.2; Fairfield, CA, 1994.

5. Edward, J. T.; Waldron-Edward, D. *J. Chromatog.* **1965**, 20, 563-571.

6. Bondi, A. *J. Phys. Chem.* **1964**, 68, 441.

7. Biosym Technologies; *Search-Compare user guide*, version 2.3; San Diego, CA, 1993.

8. Edward, J. T. *J. Chem. Education* **1970**, *47*, 261.

9. Kier, L. B., Hall, L. H.; Murray, W. J.; Randic, M. *J. Pharmaceutical Sci.* **1975**, 64, 1971.

10. Grossman, P. D.; Colburn, J. C.; Lauer, H. H. *Anal. Biochem.* **1989**, 179, 28-33.

CHAPTER 3 ABSOLUTE MOBILITY PREDICTION OF MONOAMINES

3.1 INTRODUCTION

Amines have been widely used as surfactants to form cationic micelles in Micellar Electrokinetic Chromatography (MEKC) [1][2] and to adjust electroosmotic flow (EOF) in CZE [3][4][5][6]. At a given pH, amines are fully or partially protonated. Therefore, they are one of the major classes of compounds that can be separated using capillary zone electrophoresis. In this chapter, many physicochemical parameters have been investigated to predict their absolute mobilities. It was found that absolute mobilities of monoamines can be predicted very well using two parameters (molecular weight and pK_b).

3.2 EXPERIMENTAL

3.2.1 CALCULATION OF MOLECULAR VOLUME AND HYDRATION NUMBER

Molecular volume and hydration number were calculated using the method described in Section 2.4.

3.2.2 CHEMICALS

All reagents and chemicals were from Aldrich (Milwaukee, WI), BDH Inc. (Toronto, Ontario) or CHEM SERVICE Inc. (West Chester, PA). These were of analytical grade or higher, and were used without any further purification. All solutions were prepared with distilled deionized water (18 MΩ) (NANOpure, Barnstead, NY) and

filtered (0.45 μm, MilliCup™, Millipore Corp., Bedford, MA) before use. Ultrasonic degassing was performed on buffer and sample solutions before separation.

3.2.3 ABSOLUTE MOBILITY DETERMINATION

3.2.3.1 BUFFER SELECTION AND PREPARATION

The running buffer selection is extremely important to the success of any capillary zone electrophoresis separation. In order to measure absolute mobilities accurately, the first key factor that needs to be considered is that all solutes in the buffer solution are fully ionized. Otherwise, the measured absolute mobilities are lower than the true values. For weak monoprotic acids (HA), there exists the following equilibrium in aqueous solution:

$$HA \rightleftharpoons H^- + A^- \qquad 3\text{-}1$$

$$K_a = [H^-][A^-]/[HA] \qquad 3\text{-}2$$

For a given pH, the fraction of the ionized form (A^-) can be calculated using Equation 3-3:

$$\alpha_{A^-} = \frac{[A^-]}{[A^-]+[HA]} = \frac{K_a}{[H^+]+K_a} \qquad 3\text{-}3$$

From Equation 3-3, it can be seen that in order to ensure more than 99.9% ionization of the acid, the K_a should be at least a thousand times greater than $[H^-]$. This means the pH of the buffer solution should be at least three or more pH units higher than the pK_a. For the same reason, in order to ensure more than 99.9% protonation of weak bases (amines), the pH of the running buffer solution must be at least three or more pH units lower than the pK_a of the analyte.

The measurements of absolute mobilities were performed in seven different ionic strength buffer solutions and the lowest ionic strength was about 10^{-3} M. Therefore, we should choose buffer solutions which have maximum buffer capacity at the pH of interest to keep the pH and electroosmotic flow constant. For a weak acid or base and its conjugate buffer system, the pH of a buffer depends on the ratio of the concentrations of the acid-base conjugate pair:

$$pH = pK_a + \log [A^-]/[HA] \qquad 3\text{-}4$$

At a given ionic strength ($[HA] + [A^-]$ = constant), the buffer capacity increases as the concentration ratio of the acid-base pair approaches unity.

So the ideal buffer should have the following properties: (1) High buffer capacity; (2) $pK_{a(buffer)}$ is at least three or more pH units higher than the $pK_{a(solute)}$ for weak acids and three or more pH units lower than the $pK_{a(solute)}$ for weak bases. The pK_a values for our 13 experimentally investigated aliphatic monoamines are given in Table 3.1.

Table 3.1 pK_a values of experimentally investigated monoamines.

Molecule	pK_a (25 °C)	Ionic Strength (M)
Ethylammonium	10.636[a]	0
t-Butylammonium	10.685[a]	0
Diallylammonium	9.29[a]	0
Cyclohexylammonium	10.64[a]	0
Cyclohexylmethylammonium	10.85[b,c]	0
2, 6-Dimethylpiperidinium	11.10[a,c]	0
Dibutylammonium	11.25[a]	0
2-Ethylhexylammonium	10.55[b,c]	0
Triallylammonium	8.31[a]	0
Dicyclohexylammonium	11.25[a]	0
Dodecyldimethylammonium	10.05[b,c]	0
Tetra-n-butylammonium	Permanently Charged	
Octadecyltrimethylammonium	Permanently Charged	

[a] Data from reference [7].

[b] Data were estimated using the method described in reference [8].

[c] Data were extrapolated to zero ionic strength using Equation 1.17 in reference [8].

It can be seen that the pK_a values for aliphatic amines are around 10.0. Any buffer system with $pK_{a(buffer)}$ less than 5.0 will ensure full protonation of all molecules listed in Table 3.1. The second criteria to choose an appropriate buffer system is to avoid electrodispersion which can cause skewed peaks (Section 3.2.3.2). In this aspect, the smaller the mobility difference between the analyte and the co-ions of the background buffer solution, the more symmetrical is the peak obtained. In consideration of all of these requirements, an acetic acid (HAc)-Lithium acetate (LiAc) buffer system (pH = 4.75) was selected, and it gives satisfactory peak shapes.

The HAc-LiAc buffer system was prepared by dissolving lithium hydroxide (LiOH) in distilled deionized water ($C_{LiOH} = C$). 1M HAc solution was added to adjust the pH to 4.75:

$$HAc + LiOH \rightleftharpoons H_2O + LiAc \qquad 3\text{-}5$$

At pH = pKa = 4.75, $[HAc] = [Ac^-] = C$, $[H^+] = 1.78 \times 10^{-5}$ M, $[OH^-] = 5.62 \times 10^{-10}$ M. The ionic strength of this buffer system can be calculated as follows:

$$I = 1/2\ \Sigma C_i Z_i^2$$

$$= 1/2\ \{[Li^+]\times 1^2 + [Ac^-]\times 1^2 + [OH^-]\times 1^2 + [H^+]\times 1^2\}$$

$$= 1/2\ (C + C + 5.62\times 10^{-10}\ M + 1.78\times 10^{-5}\ M) \approx C \qquad 3\text{-}6$$

The ionic strength of the stock acetate buffer was controlled to 0.1M. Serial dilution was performed to prepare I = 0.075 M, 0.05 M, 0.025 M, 0.01 M, 0.005 M and 0.001 M buffer solutions. After dilution, the pH of these buffers changed slightly, so pH adjustment was performed to keep the pH constant (4.75).

3.2.3.2 SAMPLE SOLUTION PREPARATION

In this study, we need to obtain accurate migration times of analytes to calculate the electrophoretic mobility. The concentration of the analyte can influence the width and shape of peaks [9]. Sharp and symmetrical peaks give most accurate migration times. Lower concentrations usually give narrower peaks.

In capillary electrophoresis, the perfect peak shape occurs when the conductivity of the sample matches that of the running buffer. When the solute zone has a different conductivity than that of the buffer solution, skewed peaks are observed. If the sample

zone conductivity is lower, we usually get peak tailing (Fig. 3.1A). If the sample zone conductivity is higher than that of the buffer, we observe peak fronting (Fig. 3.1B).

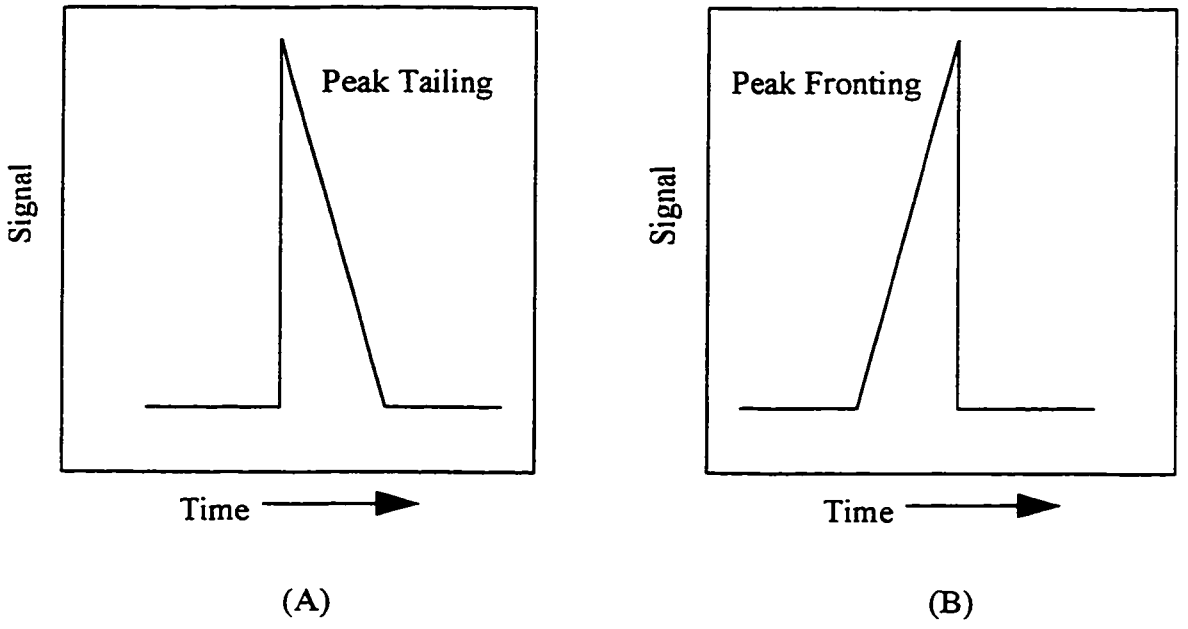

Figure 3.1 Skewed peaks due to mismatched sample and buffer conductivities.

Furthermore, some of the monoamines are surfactants. In order to obtain accurate absolute mobilities, micelle formation must not occur. The critical micelle concentrations (CMC) of two monoamines are listed in Table 3.2.

Table 3.2 CMC values of experimentally investigated monoamines*.

Molecule	CMC (M), 25 °C
Dodecyldimethylammonium	2.03×10^{-2}
Octadecyltrimethylammonium	4.00×10^{-4}

* Data from reference [10]

In order to avoid the formation of micelles, the sample concentration of all aliphatic monoamines was limited to 1.0×10^{-4} M. All the monoamines were dissolved in distilled deionized water. The pH of all the sample solutions was also adjusted to 4.75 with 0.1M HAc or 0.1M LiOH.

3.2.3.3 EXPERIMENTAL APPARATUS-CRYSTAL 300 CE SYSTEM

Commercial CE instruments have been available in recent years [11]. The instrument used to measure the absolute mobilities of monoamines was a Crystal 300 capillary electrophoresis system with a Crystal 1000 CE conductivity detector (Thermo CE, Boston, MA). The Crystal 1000 is the first commercially available conductivity detector developed specially for electrophoresis [11]. The efficient end-capillary detector has a detection volume of less than 2.5 nanoliters and permits more sensitive detection of small molecular weight ions over indirect conductivity detection methodologies [11]. A ConCap™ fused silica capillary (50 μm I.D.×52 cm) and an interchangeable finger tight ConTip™ (Thermo) conductivity sensor were used. The finger tight ConCap connector is placed on only one end of the fused capillary and connected to the conductivity detector. The tip of the ConCap and ConTip connectors needs to be cleaned in an ultrasonic bath of distilled deionized water for about 30 seconds before installation. During the experiment, the connectors need to be handled very carefully. First, never touch the O-ring on the connector with your bare hands because oils on the O-ring can extract slowly into the conductivity detection cell and cause drifting baselines. Second, do not clean or dry the

O-ring mechanically with a paper towel such as KimWipe®. The abrasive fiber will damage the O-ring surface and make the cell difficult to seal completely. The connector tip can be dried using clean pressurized air before assembling into the conductivity cell block. The users manual gives more detailed discussion of the detector configuration and handling [12].

3.2.3.3.1 CONDUCTIVITY DETECTOR

The conductance of a liquid is a measure of the electric current carried by positive and negative ions in solution when an electric field is applied. A standard measure of conductivity is the specific conductivity. The specific conductivity is obtained by measuring the reciprocal resistance in ohms of a 1 cm^3 volume cell composed of two opposing 1 cm^2 surfaces spaced 1 cm apart at a specific temperature. In this instrument, the specific conductance (C) is obtained when the conductivity value (c) is multiplied by a cell constant (K). In this study, only accurate migration times were needed for the calculations. Therefore the detector cell was not calibrated. The configuration of the Crystal 300 CE system is showing schematically in Figure 3.2.

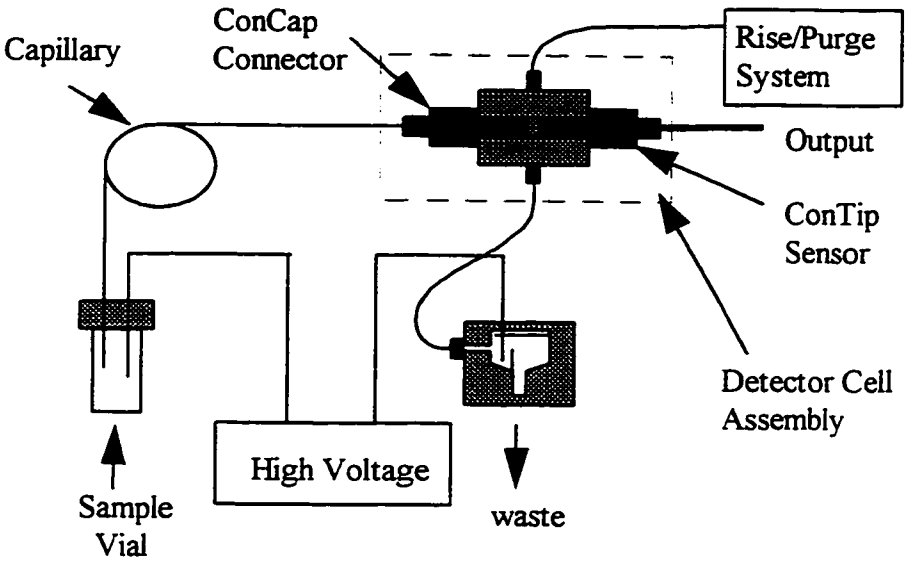

Figure 3.2 Schematic diagram of Crystal 300 CE system with conductivity detector (Adapted from reference [11])

The conductivity cell is constructed when the ConCap and the ConTip sensor are connected together. The anode and cathode of the cell are incorporated on the surface of the ConTip sensor to determine the conductivity.

3.2.3.3.2 INSTRUMENT SETTING

Applied Voltage In capillary electrophoresis, high voltages are used to provide fast analyses and efficient (sharp peaks) separations. However too high of a voltage will cause Joule heating within the capillary. Such heating would change the viscosity of the buffer, thus altering our measured mobility. The maximum applied voltage across the capillary was determined experimentally by plotting the current against the applied voltage. The highest voltage in the linear region of this plot was chosen as the applied

voltage. For HAc-LiAc buffer system (Ionic strength = 0.1 M), it was found that the applied voltage should be 6 kV. The Ohm's plot is shown in Figure 3.3.

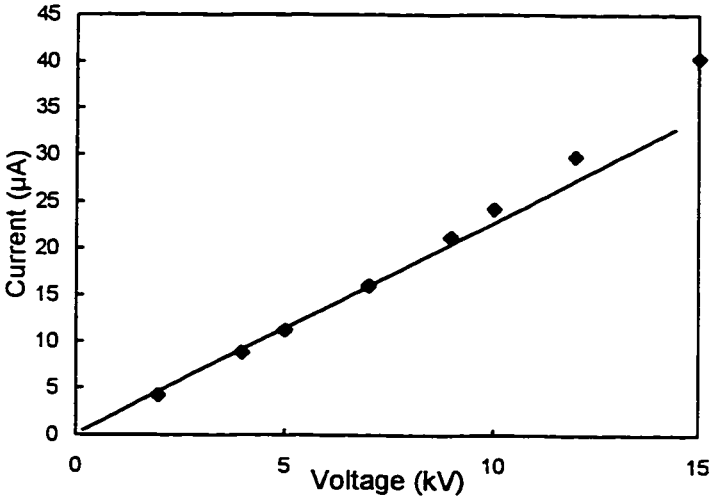

Figure 3.3 Ohm's plot of acetate buffer (HAc-LiAc, pH 4.75) at 0.1 M ionic strength.

Capillary Conditioning The capillary was rinsed before each run to ensure reproducible electroosmotic flow. The rinses were: 2 min high pressure rinsing (29 psi) with 0.1 M LiOH; then 1 min with distilled deionized water; and finally 2 min with running buffer solution.

Injection All sample injections were hydrodynamic (0.29 psi) for 0.2 min.

Detection Parameters The sensitivity range determines the output scale for the analog background conductivity signal. The available sensitivity ranges were 50, 100, 200, 500, 1000, and 2000 nS. Lower sensitivity values are more sensitive. For the phosphate buffer used, the sensitivity range was set at 500 nanosiemens (nS).

Cell Voltage Cell voltage is the voltage applied to the detector cell. Appropriate cell voltage is one of the key parameters determining the signal to noise ratio and signal linearity. The optimum cell voltage is inversely related to the background conductivity of the running buffer. High background buffers require low cell voltages. In this study, the auto cell voltage key, which determines the best applied cell voltage, was used for all the measurements.

Temperature The Crystal 300 CE system has no thermostatting devices. Thus all the experiments were performed at room temperature, which was about 25.4 °C.

Data Acquisition and Software A CHROM-1AT data acquisition board (Keithley MetraByte, Taunton, MA) was used for data acquisition. This board uses a voltage to frequency (V/F) converter and a complex counter device (five 16 bit counters) to obtain very high resolution and integration accuracy. The voltage to frequency converter has a scaling of approximately 100,000 counts/sec. The input ranges of +10V, +5V, +2V and +1V are software selectable. LabCalc™ software (Galactic, Salem, NH) was used for data analysis. The data acquisition rate (sampling rate) for all samples was set at 5 Hz.

3.2.3.4 PROCEDURE FOR ABSOLUTE MOBILITY DETERMINATION

Determination of Migration Times The migration times of the analyte (t_m) and electroosmotic flow (t_{eof}) are obtained directly from an electropherogram as shown in Figure 3.4.

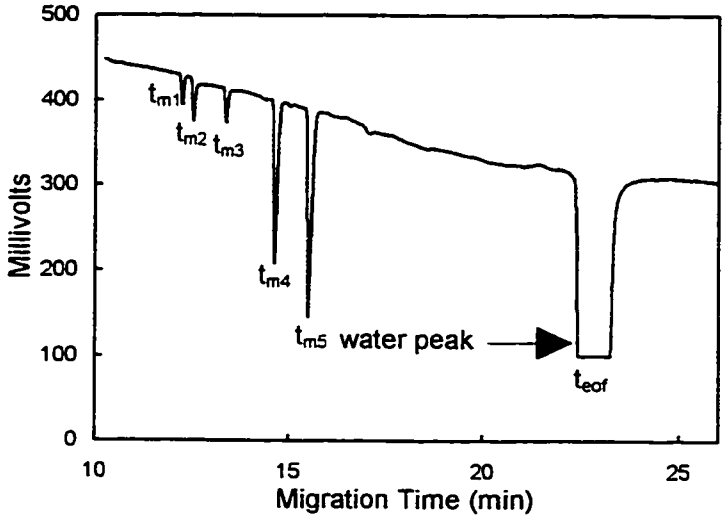

Figure 3.4 Electropherogram of five aliphatic monoamines

For conductivity detection, the water peak from the injected sample can be used as the electroosmotic flow marker, and no other EOF marker is needed. However, the water peak usually gives a truncated broad peak, as indicated in Figure 3.4. The water peak is about 0.84 min wide for this particular electropherogram. How can we determine the accurate migration time of the electroosmotic flow (t_{eof}) using the broad water peak? Which time is more accurate, the time corresponding to the front edge, the center or the rear edge of the water peak? In order to answer this question, we need to consider the **stacking** effect in capillary electrophoresis [13]. Since the solutes were dissolved in distilled deionized water and their concentrations were significantly lower than the concentration of the buffer solution, the conductivity in the sample zone was lower than that of the running buffer. Upon the application of the voltage, a much greater electric field strength develops across the sample zone, causing the ions to migrate faster. Once

the analyte cations reach the running buffer boundary, the electric field strength decreases and they move slower. This process continues until all of the analyte cations reach the boundary between the running buffer and the sample zone. This stacking causes the analytes to become concentrated into a smaller zone, as illustrated in Figure 3.5.

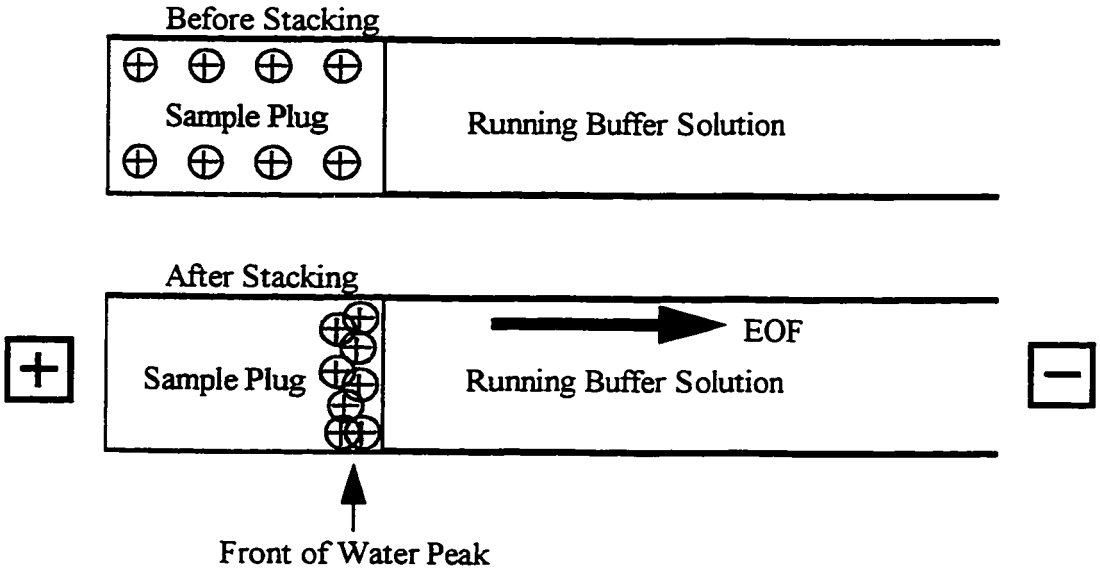

Figure 3.5 Schematic diagram of stacking effect.

It can be seen from Figure 3.5 that the best migration time to reflect the electroosmotic flow is the migration time of the front of the water peak.

For a capillary electrophoresis system, the time that the voltage is actually on (t_m) is the time under the constant applied (programmed) voltage (t_c) plus the ramp time (t_{ramp}). The ramp time is the time needed for the instrument to reach the programmed voltage. This is illustrated in Figure 3.6.

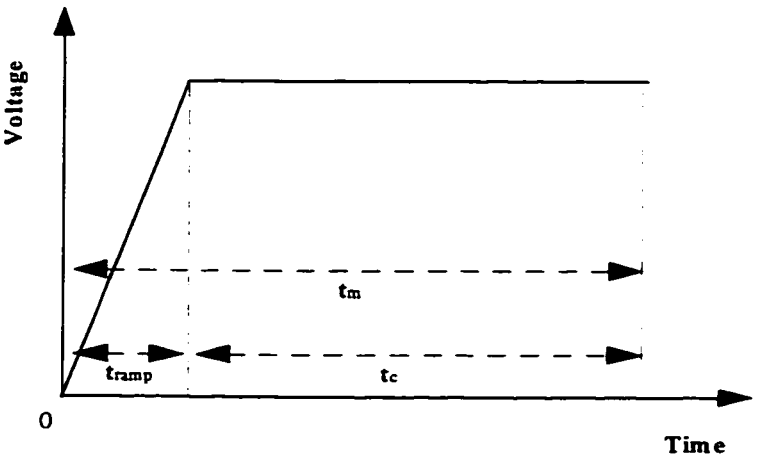

Figure 3.6 Ramp time of applied voltage.

Calculation of Electrophoretic Mobilities Williams and Vigh [14] have extensively discussed the influence of the voltage ramp time (t_{ramp}) on the calculated apparent electrophoretic mobility (electrophoretic mobility + electroosmotic mobility) of an analyte. Since the analytes migrate in a lower electric field strength during the ramp time, Williams and Vigh proposed that in the case of a linear voltage ramp, the correct apparent mobility can be calculated using Equation 3-7.

$$\mu_{app} = \frac{L_t L_d}{V(t_m - \frac{1}{2} t_{ramp})} \qquad 3\text{-}7$$

where μ_{app} is the apparent electrophoretic mobility, L_t is the total capillary length, L_d is the capillary length to the detector, V is the programmed (applied) voltage, and t_m is the apparent migration time of the analyte. For the Crystal 300 CE system, the default voltage ramp (6 kV/s) was used for all the experiments. Since the programmed voltage was 6 kV, the ramp time is 1 second.

Cations migrate in the same direction as the electroosmotic flow. For end-capillary conductivity ($L_t = L_d = L$) and cationic analytes, based on the migration times and the potential ramp time, the electrophoretic mobility of an analyte can be calculated using Equation 3-8.

$$\mu = \mu_{app} - \mu_{eof} = \frac{L}{V}\left(\frac{1}{t_m - \frac{1}{2}t_{ramp}} - \frac{1}{t_{eof} - \frac{1}{2}t_{ramp}}\right) \qquad 3\text{-}8$$

The default voltage ramp (6 k*V*/s) was used for all the experiments. Since the programmed voltage was 6 k*V*, the ramp time is 1 second.

Determination of Absolute Mobilities by Means of Extrapolation Although absolute mobilities of analytes are very important in capillary electrophoresis, they can not be determined directly in experiments. The only way to determine absolute mobilities is by extrapolating the electrophoretic mobilities of the analytes at finite buffer concentrations to infinite dilution (zero ionic strength). For reliable extrapolation, the relationship between electrophoretic mobilities and corresponding ionic strengths should be known.

Two effects, electrophoretic and relaxation effects, must be considered to derive the relationship between electrophoretic mobility and ionic strength [15]. In electrolyte solutions, every ion is surrounded by an ionic atmosphere of oppositely charged ions due to coulombic interaction. Upon the application of an external electric field, cations and anions will migrate in opposite directions, *i.e.*, each ion migrates in a medium which moves in the opposite direction. This **electrophoretic effect** caused by the counter-ion migration makes the observed mobilities lower than the absolute mobilities.

The second effect is the **relaxation effect**, which considers the influence of the deformation of the ionic atmosphere on the mobilities of ions. Upon application of an external electric field, the spherically symmetric ionic atmosphere deforms into an egg-shaped ionic cloud [16], as illustrated in Figure 3.7.

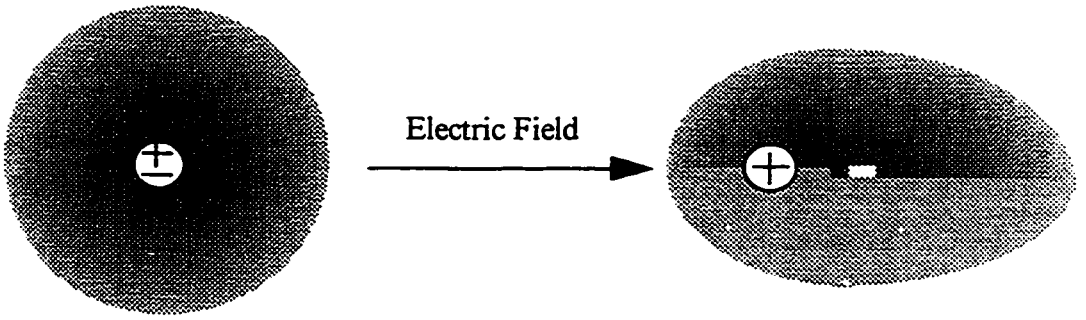

Figure 3.7 Deformation of ionic atmosphere around a moving central cation upon the application of an electric field.

The deformation of the ionic atmosphere (cloud) results in the shift of the charge center of the central ion from the center of charge of its cloud. Therefore, an electric force will develop between the moving ion and its lagging atmosphere which retards the migration of the central ion (relaxation effect). According to the suggestion of Debye and Hückel, Onsager incorporated electrophoretic and relaxation effects into the calculation of conductivity of an electrolyte. The resulting famous Debye-Hückel-Onsager limiting law of conductivity is given by [15]:

$$\Lambda = \Lambda^\circ - (A + B\Lambda^\circ)\sqrt{I} \qquad 3\text{-}9$$

where Λ is the molar conductivity, Λ° is the molar conductivity at infinite dilution, A and B are constants, and I is the ionic strength of the electrolyte solution.

Conductivity and mobility have the relationships:

$$\mu = \Lambda/F \qquad 3\text{-}10$$

$$\mu_0 = \Lambda_0/F \qquad 3\text{-}11$$

where μ is the mobility of an analyte, μ_0 is the absolute mobility, and F is the Faraday constant. Thus Equation 3-9 can be expressed as:

$$\mu = \mu_0 - (A/F + B\mu_0)\sqrt{I} \qquad 3\text{-}12$$

From Equation 3-12, it can be seen that the electrophoretic mobility of an analyte is proportional to the square root of the ionic strength ($\sqrt{I}$). This equation has been widely used in analytical chemistry [17][18] to represent the relationship between electrophoretic mobilities and ionic strengths. However, the Debye-Hückel-Onsager equation is valid for univalent strong electrolyte only up to 0.01 M ionic strength [15][17][18].

Since the ionic strength of many buffer systems used to determine the absolute mobilities in capillary electrophoresis is between 0.001 M and 0.1 M, the Debye-Hückel-Onsager limiting law is not valid. Indeed, significant curvature appeared in the electrophoretic mobility versus square root of ionic strength plots for the more than 20 analytes investigated experimentally in this study. For higher ionic strength buffer solutions, the ionic diameter (a), which is neglected in the Debye-Hückel-Onsager limiting law, must be considered. By considering the ionic diameter in the relaxation effect, the extended form of the Debye-Hückel-Onsager equation (Equation 3-13) was developed by Falkenhagen [19] and Pitts [20][21][15].

$$\Lambda = \Lambda^\circ - (A_1 + A_2\Lambda^\circ)\frac{\sqrt{I}}{1 + Ba\sqrt{I}} \qquad 3\text{-}13$$

where A_1, A_2 and B are constants, and a is the ionic diameter. For aqueous electrolyte solutions at 25 °C, B is equal to 0.33. As suggested by Güntelberg [22], if the ionic diameter is taken as 3.04 Å, Equation 5-9 can be simplified as:

$$\Lambda = \Lambda^\circ - (A_1 + A_2\Lambda^\circ)\frac{\sqrt{I}}{1+\sqrt{I}} \qquad 3\text{-}14$$

In terms of electrophoretic mobility, Equation 3-14 can be transformed to:

$$\mu = \mu_0 - (A_1/F + A_2\mu_0)\frac{\sqrt{I}}{1+\sqrt{I}} \qquad 3\text{-}15$$

Equation 3-15 is valid up to an ionic strength of about 0.1 M for univalent strong electrolytes [15].

Since the ionic strengths used in this study were from 0.001 to 0.1 M, Equation 3-15 was used to represent the relationship between electrophoretic mobilities and ionic strength. Therefore, the calculated electrophoretic mobilities were plotted against the corresponding $\frac{\sqrt{I}}{1+\sqrt{I}}$ for all the analytes investigated experimentally. Then linear regression was performed to extrapolate the electrophoretic mobilities to ionic strength equal to zero. In comparison with Equation 3-12, Equation 3-15 gives much better linear correlations under our experimental conditions (I = 0.001-0.1 M). Therefore, once the electrophoretic mobilities at different ionic strengths were calculated, they were plotted against the corresponding $\frac{\sqrt{I}}{1+\sqrt{I}}$. The electrophoretic mobility at zero ionic strength is the absolute mobility. This process can be illustrated in Figure 3.8.

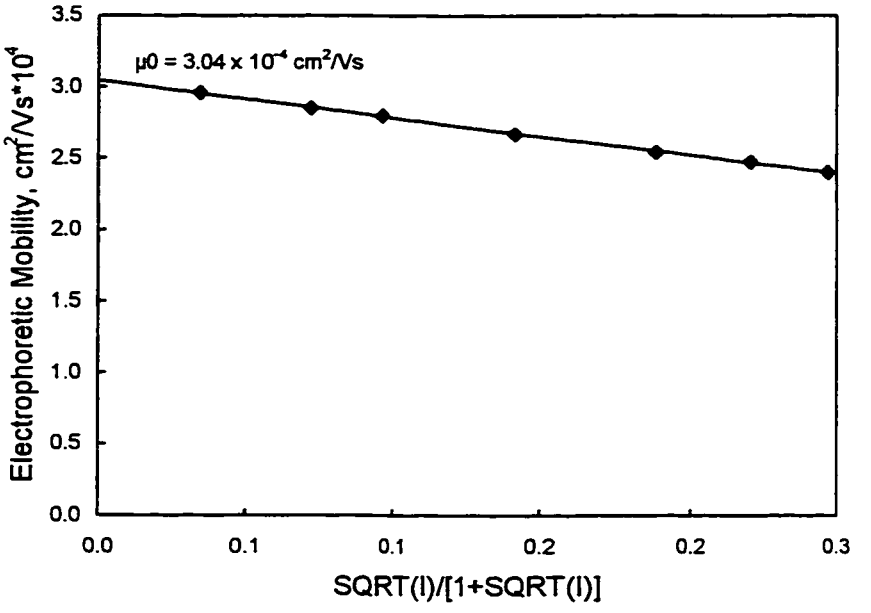

Figure 3.8 Absolute mobility determination using linear regression.

For multicharged ions, an empirical exponential relationship between electrophoretic mobilities and square root of ionic strength has been proposed by Friedl and coworkers [23], in which the absolute mobilities were determined by extrapolating a second-order polynomial fit of electrophoretic mobilities to zero ionic strength. This method is illustrated in Figure 3.9.

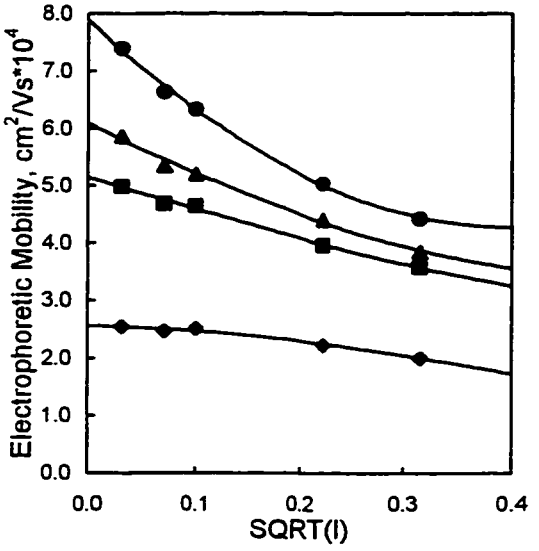

Figure 3.9 Dependence of electrophoretic mobility on the square root of the ionic strength. A second-order polynomial fit was performed to obtain the absolute mobility (Figure adapted from reference [23]). The charge number for each component is: ◆ = 1, ■ = 2, ▲ =3, ● =5.

Although Equation 3-15 was originally derived for 1-1 univalent strong electrolytes, it was found that this equation also gives a good linear relationship between electrophoretic mobility and $\frac{\sqrt{I}}{1+\sqrt{I}}$ for multicharged ions. This was demonstrated by applying Equation 3-15 to the data for multiply sulfonated dyes from reference [23]. The results are shown in Figure 3.10.

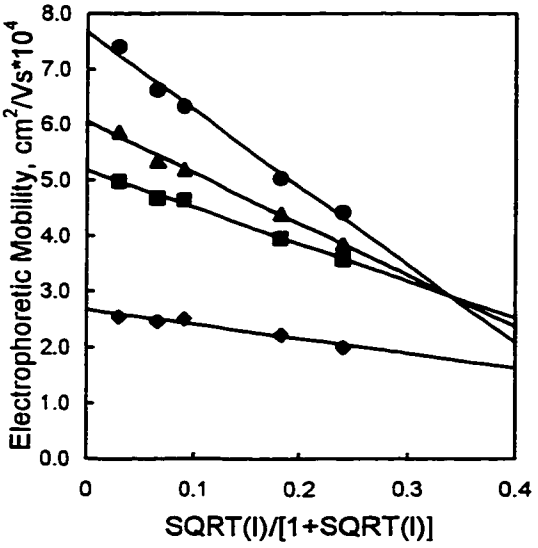

Figure 3.10 Dependence of electrophoretic mobility on $\frac{\sqrt{I}}{1+\sqrt{I}}$. Linear regression was performed to obtain the absolute mobility (Data from reference [23]). The charge number for each component is: ◆ = 1, ■ = 2, ▲ =3, ● =5.

It can be seen from Figure 3.10 that, even for highly charged ions, Equation 3-15 gives very high linear correlation coefficients (R = 0.9947 for charge number equal to 5, and 0.9961 for 3). Therefore, Equation 3-15 was used as the basis for all extrapolations to obtain absolute mobilities. For some analytes, we did observe a slight curvature in the mobility versus $\frac{\sqrt{I}}{1+\sqrt{I}}$ plots. This may be due to the simplification of ionic diameter (a) in Equation 3-13.

3.3 BEST FIT EQUATION GENERATION (EXCEL)

The best fit equation generation involves two steps. First, an absolute mobility

prediction model was constructed based on the knowledge of the physicochemical parameters that correlate to the friction coefficient of the analytes. For example, molecular volume can be used to represent the molecular size, suggested by the modified Stokes' Law [24][25]

$$\mu = \frac{Ze}{6\pi\eta r_s} \qquad 3\text{-}16$$

Equation 3-16 is also called the Hückel equation, where Z is the charge on the molecule, e is the charge on an electron, η is the viscosity of the solvent, and r_s is the Stokes' radius. The Stokes' radius, r_s, and molecular volume are correlated:

$$r_s \propto V^{1/3} \qquad 3\text{-}17$$

Thus, a model based on the molecular volume was constructed as:

$$\mu_0 = \frac{a}{V^b} \qquad 3\text{-}18$$

where μ_0 is the absolute mobility, V is the molecular volume, and a and b are constants. The second step is to determine the optimum constants in the constructed model. The optimum constants used in all of the models investigated were obtained using successive trials, or iterations. During each iteration, a new set of constants was used to calculate the *residual sum of squares* (the sum of the squared residuals, residual = measured value - predicted value) [26] between the literature values and the predicted values. Microsoft Excel (version 5.0) has a powerful optimization tool named **Solver** under the **Tool** menu, making the optimization process much easier to perform. The cell containing the *residual sum of squares* was set as the target cell and all cells containing the constants were set as changing cells. Then the optimization process was began until the minimum *residual sum*

of squares was found. The optimum constants used in the expressions can also be obtained using the **Curve Fitter** function of SlideWrite *Plus* (Version 2.0 for Windows, Advanced Graphics Software, Inc., Carlsbad, CA). Curve Fitter uses the iterative Levenberg-Marquardt algorithm which yields parameters based on the minimization of the sum of the squared deviation. Both **Solver** and **Curve Fitter** yielded the same constants. The uncertainties quoted in this study are the standard deviations of the fit constants determined using **Curve Fitter**. Such uncertainties could not be determined for equations that have more than two variables.

3.4 RESULTS

3.4.1 SPHERICAL MODEL

Using the Hückel equation (Equation 3-16), the predicted absolute mobilities were calculated for 34 monoamines. These are listed in Table 3.3.

Table 3.3 Physicochemical parameters and absolute mobilities of monoamines possessing no other functional groups.

Molecule	μ_0 (literature) $cm^2/Vs \times 10^4$	Molecular Volume ($Å^3$)	Molecular Radius r (Å)	u_0 (Hückel) $cm^2/Vs \times 10^4$
Octadecyltripropylammonium	1.78[a]	479.6	4.856	1.96
Octyltrimethylammonium	2.75[a]	215.3	3.718	2.56
Pentylammonium	3.83[a]	107.6	2.950	3.22
Piperidinum	3.86[a]	99.27	2.872	3.31
Tetra-n-butylammonium	2.02[a]	297.9	4.143	2.29
Tetradecyltrimethylammonium	2.23[a]	314.5	4.219	2.25
Dipropylammonium	3.31[b], 3.12[a]	126.9	3.117	3.05
Tetra-i-pentylammonium	1.86[a]	362.2	4.422	2.15
Tetra-n-pentylammonium	1.81[a]	363.5	4.427	2.15
Tetra-n-propylammonium	2.43[a]	232.4	3.814	2.49
Ammonium	7.62[c]	23.28	1.771	5.54
Tripropylammonium	2.79[b], 2.71[a]	177.3	3.485	2.72
Propyltrimethylammonium	3.80[c]	132.4	3.162	3.01
Octadecyltrimethylammonium	2.08[c], 2.06[a]	378.2	4.486	2.11
Methylammonium	6.20[b], 6.08[a]	42.02	2.157	4.41
Dimethylammonium	5.46[b], 5.37[a]	61.25	2.445	3.89
Trimethylammonium	5.03[b], 4.89[a]	80.44	2.678	3.54
Tetramethylammonium	4.43[f], 4.65[a]	99.70	2.877	3.3
Benzyltrimethylammonium	3.59[a]	171.9	3.449	2.76
i-Butylammonium	3.94[a]	91.59	2.796	3.4
Butyltrimethylammonium	3.48[a], 3.44[c]	149.33	3.291	2.89
Decyltrimethylammonium	2.53[a]	247.6	3.895	2.44
Dodecyltrimethylammonium	2.34[a]	281.0	4.063	2.33
Ethyltrimethylammonium	4.20[a], 4.27[c]	116.1	3.026	3.13
Hexadecyltrimethylammonium	2.17[a]	347.8	4.363	2.18
Hexyltrimethylammonium	3.07[a]	182.2	3.517	2.7
Octadecyltributylammonium	1.72[a]	528.0	5.014	1.89
Octadecyltriethylammonium	1.86[a]	428.7	4.678	2.03
Ethylammonium	4.85[c]	58.43	2.407	3.94
Propylammonium	4.30[c], 4.23[a]	91.34	2.794	3.4
n-Dodecylammonium	2.47[c]	222.5	3.759	2.53
Diethylammonium	3.89[c]	94.12	2.822	3.37
Triethyl ammonium	3.52[c]	129.6	3.140	3.03
Tetraethylammonium	3.39[c], 3.38[a]	163.7	3.394	2.8

[a] Data from reference [27]; [b] Data from reference [28]; [c] Data from reference [29]; [d] Data from reference [30]; [e] Data from reference [31]; [f] Data from reference [32].

The radius used in Equation 3-16 was obtained by treating the molecules as a sphere ($r = [V/(^4/_3\pi)]^{1/3}$, where V is the Van der Waals volume of a molecule). The correlation between the predicted absolute mobilities of monoamines and the literature absolute mobilities is shown below.

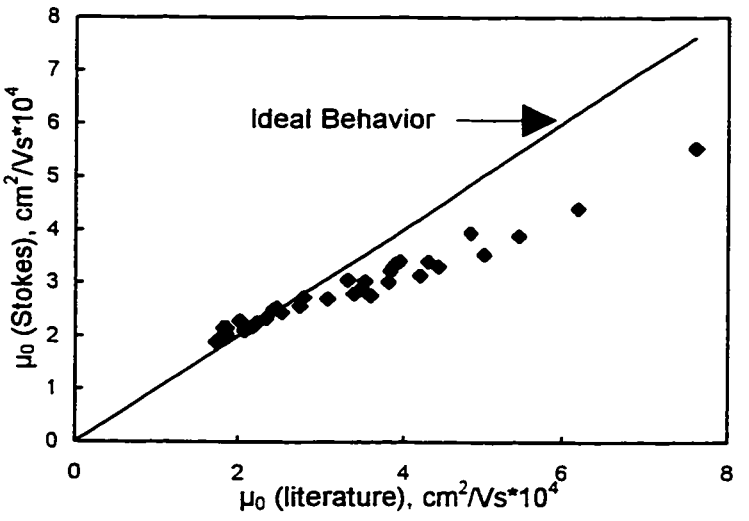

Figure 3.11 Plot of predicted absolute mobilities, μ_0, (Equation 3-16) vs. literature absolute mobilities for the monoamines in Table 3.3. The line is the expected behavior for perfect correlation between the literature and predicted values.

The line in Figure 3.11 indicates the ideal correlation (*i.e.*, if the calculated mobilities precisely matched the literature mobilities, slope = 1.00, intercept = 0.00). It can be seen that the mobilities determined using the Hückel equation deviate significantly from the literature values. The average relative error between the predicted absolute mobilities and the literature values is 13.9%. Edward [29][33] has suggested that the

numerical constant in the denominator of Equation 3-16 should be other than 6 for small ions. Indeed, the "6" in the denominator arises solely from the assumption of "stick" between the moving sphere and the surrounding continuum solvent. It has alternatively been proposed that it would be more appropriate to assume that the solvent "slips" past the surface of the solute sphere, in which case the constant should be "4" [34]. Allowing this constant to be an adjustable parameter (*i.e.*, equation of the form $\mu_0 = Ze/(n\pi\eta r_s)$ yields a numerical constant of 5.00, in agreement with Edward [29], but did not significantly alter the correlation. In this case, the average relative error between the predicted absolute mobilities and the literature mobilities is 15.2%.

3.4.2 PERRIN'S ELLIPSOIDAL MODEL

The use of an ellipsoidal rather than spherical approximation for the molecular shape would provide more flexibility in modeling the molecule, and thus presumably greater accuracy. In the 1930's, Perrin derived expressions for calculating the frictional resistance to moving an ellipsoid through continuum media [35][36]. Generally the frictional resistance of the ellipsoid is expressed as a ratio to that of a sphere of the same volume (*i.e.*, f/f_0 where f is the frictional coefficient of the ellipsoid and f_0 is the frictional coefficient for a sphere of the same volume). Thus Perrin's equation has the form:

$$\mu = \frac{Ze}{6\pi\eta r_s (f / f_0)} \qquad 3\text{-}19$$

An ellipsoid is defined by three semi-axes, a, b and c. The semi-axes are axes of rotation, at 90^0 angles to one another, going through the center of mass of a molecule. Once the

axial ratio of a molecule was determined as described in Chapter 2. The frictional correction term was calculated as follows.

For a prolate molecule (a > b = c, b/a < 1), the frictional correction is given by [37]:

$$\frac{f}{f_0} = \frac{[1-(b/a)^2]^{1/2}}{(b/a)^{2/3} Ln\{\frac{1+[1-(b/a)^2]^{1/2}}{(b/a)}\}} \qquad 3\text{-}20$$

while for a discus-shaped oblate molecule (b = c > a; b/a >1), the frictional ratio is given by [37]:

$$\frac{f}{f_0} = \frac{[(b/a)^2-1]^{1/2}}{(b/a)^{2/3} \tan^{-1}[(b/a)^2-1]^{1/2}} \qquad 3\text{-}21$$

Graphical representations [29] and tabulations [37] of the relationship between the axial ratio, b/a, and the frictional correction term have been given in the literature. Including Perrin's ellipsoidal shape correction into the Stokes' model, the predicted absolute mobilities and other parameters are listed in Table 3-4.

Table 3.4 Absolute mobilities, axial ratio and friction ratio of 34 monoamines.

Molecule	μ_0 (literature) $cm^2/Vs \times 10^4$	u_0 (ellip.) $cm^2/Vs \times 10^4$	Axial Ratio (b/a)	f/f_0
Octadecyltripropylammonium	1.78	2.06	0.293	1.142
Octyltrimethylammonium	2.75	2.83	0.385	1.084
Pentylammonium	3.83	3.65	0.452	1.058
Piperidinum	3.86	3.95	1.263	1.005
Tetra-n-butylammonium	2.02	2.71	0.658	1.016
Tetradecyltrimethylammonium	2.23	2.3	0.256	1.176
Dipropylammonium	3.31	3.39	0.389	1.078
Tetra-i-pentylammonium	1.86	2.54	0.672	1.014
Tetra-n-pentylammonium	1.81	2.52	0.608	1.022
Tetra-n-propylammonium	2.43	2.95	0.684	1.013
Ammonium	7.62	6.43	1.138	1.001
Tripropylammonium	2.79	3.15	1.935	1.038
Propyltrimethylammonium	3.80	3.55	0.658	1.016
Octadecyltrimethylammonium	2.08	2.1	0.229	1.208
Methylammonium	6.20	5.27	0.824	1.003
Dimethylammonium	5.46	4.59	0.655	1.016
Trimethylammonium	5.03	4.23	1.284	1.006
Tetramethylammonium	4.43	3.95	1.230	1.004
Benzyltrimethylammonium	3.59	3.24	0.617	1.021
i-Butylammonium	3.94	4.03	0.700	1.011
Butyltrimethylammonium	3.48	3.37	0.578	1.027
Decyltrimethylammonium	2.53	2.63	0.331	1.114
Dodecyltrimethylammonium	2.34	2.45	0.291	1.143
Ethyltrimethylammonium	4.20	3.73	0.766	1.006
Hexadecyltrimethylammonium	2.17	2.17	0.233	1.203
Hexyltrimethylammonium	3.07	3.08	0.466	1.053
Octadecyltributylammonium	1.72	2.05	0.342	1.107
Octadecyltriethylammonium	1.86	2.04	0.239	1.195
Ethylammonium	4.85	4.66	0.661	1.016
Propylammonium	4.30	3.93	0.518	1.039
n-Dodecylammonium	2.47	2.58	0.255	1.177
Diethylammonium	3.89	3.86	0.487	1.047
Triethyl ammonium	3.52	3.57	1.580	1.018
Tetraethylammonium	3.39	3.34	0.762	1.007

The correlation between the absolute mobilities predicted using Perrin's model and the literature values is shown in Figure 3.12.

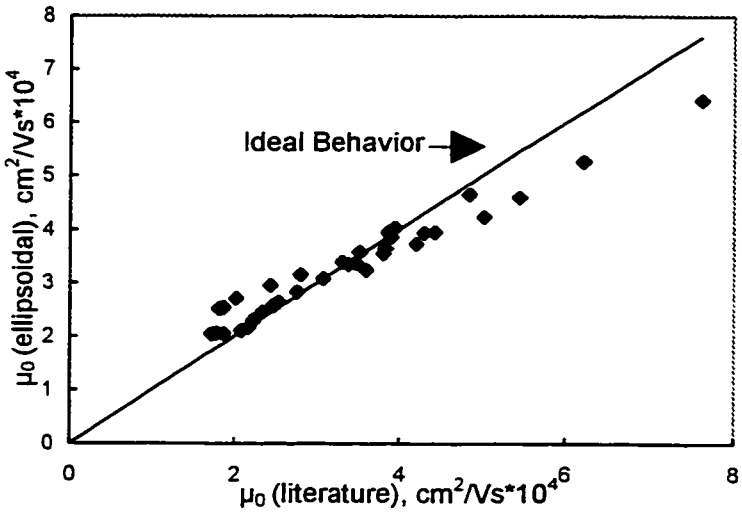

Figure 3.12 Plot of predicted absolute mobilities μ_0 (Equation 3-19) vs. literature absolute mobilities for the monoamines in Table 3.4. The line is the expected behavior for perfect correlation between the literature and predicted values.

It can be seen that Perrin's ellipsoidal model (Equation 3-19) provides a better approximation of the mobilities than the spherical model. The average relative error between the predicted absolute mobilities and the literature values is 10.0%. Interestingly, in the low mobility region (~ 2×10^{-4} cm^2/Vs), the mobilities predicted by Perrin's model are more scattered than observed using Stokes' model. Inspection of these points indicates that the deviations are related to the shape of the molecules. The upper points are amines with side chains longer than ethyl and the main chain has about the same length as the side chains, such as tetra-n-propylammonium, tetra-n-butylammonium, tetra-n-pentylammoniun, and tripropylammonium. The lower points are amines with long main chains and relatively short side chains, such as octadecyltrimethylammonium and

Tetradecyltrimethylammonium. This indicates that Perrin's model fails to adequately account for the effect of molecular shape for the aliphatic amines studied. Thus, not only does Perrin's model not provide precise approximation of the mobility, but it also induces a shape dependent deviation not previously noted with the Hückel equation.

3.4.3 MOLECULAR VOLUME MODEL

The Stokes' equation relates the diffusion coefficient to $(\text{radius})^{-1}$. Given this model's explicit assumption of a spherical model, it would be expected that the diffusion coefficient would be related to $(\text{volume})^{-0.33}$. Nevertheless, Wilke-Chang [38] and Hayduk [39] have found that optimum prediction of diffusion coefficients is achieved using molecular volume to the -0.6 and -0.589 power. Given that the frictional factors (f) are similar in both diffusion and electrophoretic mobility, it would not be surprising if the volume followed a similar power dependence.

Nonlinear curve fitting of the literature mobilities and volume using an equation of the form $\mu_0 = A/V^B$ yielded the following best fit equation, which gives the minimum *residual sum of squares*.

$$\mu_0 = \frac{(3.66 \pm 0.27) \times 10^{-3}}{V^{(0.481 \pm 0.016)}} \quad \text{cm}^2/\text{Vs} \qquad 3\text{-}22$$

where V is molecular volume (Å^3). The uncertainties in Equation 3-33 are 1 times the standard deviations. The correlation between the predicted absolute mobilities using Equation 3-22 and the literature values of amines listed in Table 3.4 is shown in Figure 3.13.

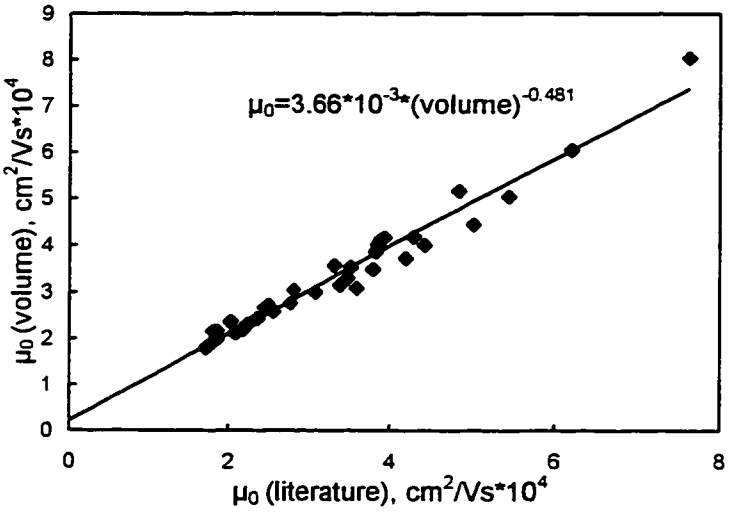

Figure 3.13 Correlation of absolute mobilities estimated using Equation 3-22 μ_0 (volume) with literature mobilities μ_0 (literature) for 34 amines in Table 3.4.

From Figure 3.13, it can be seen that Equation 3-22 yielded much better predictions of the absolute mobilities than those of spherical and ellipsoidal models. The average relative error between the predicted and literature absolute mobilities decreases significantly, to 6.6%. The correlation coefficient, slope and intercept of the linear regression line in Figure 3.13 are 0.9832, 0.9416 and 0.2061 respectively. This suggests that molecular size (volume) is the most important parameter governing electrophoretic mobility.

As discussed in Chapter 2, the volume obtained using Molecular Modeling Pro™ was not reproducible. However, the variation in the calculated molecular volume was generally very small, ranging from 0.04% RSD for ethylamine to 0.3% for octadecyltributylamine. An alternative more complicated molecular modeling software, Insight II, also gave comparable fluctuation in the calculated volumes. Fortunately, from

the discussion in Section 2.4, it can be seen that the calculated Van der Waals volumes using Molecular Modeling Pro™ agree very well with the corresponding literature values (calculated manually from Van der Waals atomic increments).

It was also observed that systematic errors do exist between the molecular volumes estimated using different molecular modeling softwares and even different versions of the same program (Sections 2.4.1.1 and 2.4.1.2). However, systematic molecular volume changes will not influence the power dependence of the molecular volume. This can be demonstrated as follows:

$$\mu_0 = \frac{A}{V^B} \tag{3-23}$$

$$\mu_0 = \frac{A}{(\beta V)^B} = \frac{A}{\beta^B \times V^B} = \frac{(A/\beta^B)}{V^B} = \frac{C}{V^B} \tag{3-24}$$

where A, B, and C are constants. From Equations 3-23 and 3-24, it can be seen that a systematic change in the molecular volume from V to βV does not alter the power dependence of the molecular volume. However, the constants in the numerator do vary with the systematic change in the molecular volume. This indicates that the predicted separation order will not be altered by a systematic error in the molecular volume.

3.4.4 MOLECULAR WEIGHT MODEL

As discussed in Chapter 1, molecular weight has been used to represent molecular size. Offord [40] suggested that the absolute mobilities of peptides can be predicted using molecular weight alone. Thus, molecular weight was investigated as a substitute for

molecular volume. If molecular weight is used instead of molecular volume in Equation 3-22, the best fit equation to predict the absolute mobilities of monoamines listed in Table 3.4 is:

$$\mu_0 = \frac{(3.12 \pm 0.20) \times 10^{-3}}{W^{(0.470 \pm 0.015)}} \quad \text{cm}^2/\text{Vs} \qquad 3\text{-}25$$

where W is the molecular weight of the monoamines. The correlation between the absolute mobilities predicted using Equation 3-25 and the literature mobilities is shown in Figure 3.14.

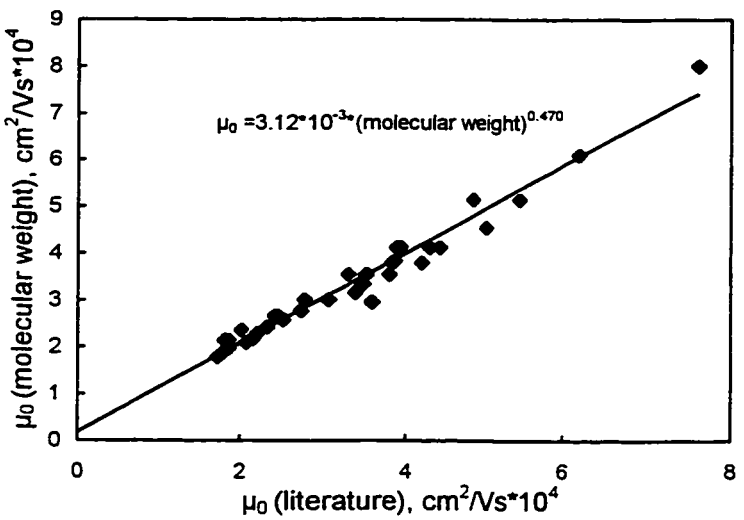

Figure 3.14 Correlation of the mobilities estimated using Equation 3-25 with the literature absolute mobilities for the 34 amines in Table 3.4.

The average relative error is 6.1%, which is slightly better than that achieved using molecular volume (Equation 3-22). The correlation coefficient, slope and intercept of the linear regression line in Figure 3.14 are 0.9836, 0.95 and 0.1793 respectively.

3.4.5 MOLECULAR VOLUME AND HYDRATION MODEL

Hydration obviously alters the size and shape of an ion, particularly small ions. Typically this effect is imbedded within the experimentally determined Stokes' radius that is used in the Hückel spherical model and Perrin ellipsoidal model. The Van der Waals volumes used in this work do not incorporate hydration. To rectify this, the mean waters of hydration are explicitly estimated using McGowan's additive method. These can be calculated using Molecular Modeling Pro™ or manually using the increments listed in Table 2.1. The mean waters of hydration for 34 monoamines are listed in Table 3-5.

Table 3.5 Mean waters of hydration for 34 monoamines

Molecule	Hydration Number (H)
Octadecyltripropylammonium	3
Octyltrimethylammonium	3
Pentylammonium	9
Piperidinum	6
Tetra-n-butylammonium	3
Tetradecyltrimethylammonium	3
Dipropylammonium	6
Tetra-i-pentylammonium	3
Tetra-n-pentylammonium	3
Tetra-n-propylammonium	3
Ammonium	12
Tripropylammonium	3
Propyltrimethylammonium	3
Octadecyltrimethylammonium	3
Methylammonium	9
Dimethylammonium	6
Trimethylammonium	3
Tetramethylammonium	3
Benzyltrimethylammonium	3
i-Butylammonium	9
Butyltrimethylammonium	3
Decyltrimethylammonium	3
Dodecyltrimethylammonium	3
Ethyltrimethylammonium	3
Hexadecyltrimethylammonium	3
Hexyltrimethylammonium	3
Octadecyltributylammonium	3
Octadecyltriethylammonium	3
Ethylammonium	9
Propylammonium	9
n-Dodecylammonium	9
Diethylammonium	6
Triethyl ammonium	3
Tetraethylammonium	3

Incorporating hydration number into the molecular volume model (Equation 3-22) reduces the average relative error from 6.6% to 5.0%. The best fit equation is:

$$\mu_0 = \frac{(7.8 \pm 1.2) \times 10^{-3}}{V^{(0.619 \pm 0.028)} + (0.287 \pm 0.087) \times H} \quad \text{cm}^2/\text{Vs} \qquad 3\text{-}26$$

where H is the hydration number of a molecule. The correlation between the predicted and the literature values is shown in Figure 3.15.

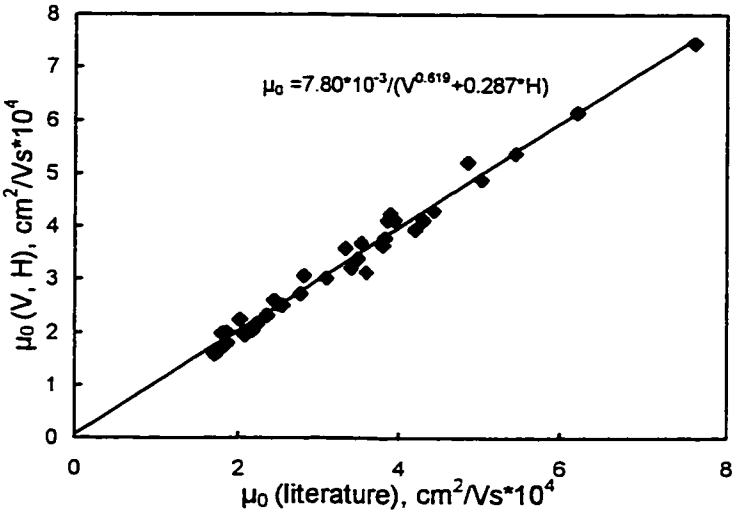

Figure 3.15 Correlation of the mobilities estimated using Equation 3-26 with the literature absolute mobilities for the 34 amines in Table 3.4.

The correlation coefficient, slope and intercept in Figure 3.15 are 0.9903, 0.982 and 0.0595 respectively. As can be seen in Figure 3.15, the absolute mobilities predicted using Equation 3-26 closely match the literature mobilities. Furthermore, the slope and intercept of the linear regression line in Figure 3.15 are very close to the ideal behavior (slope = 1.00, intercept = 0.00).

3.4.6 MOLECULAR WEIGHT AND HYDRATION MODEL

If molecular weight (W) is used instead of molecular volume (V) in Equation 3-26,

the best fit equation is:

$$\mu_0 = \frac{(5.55 \pm 0.72) \times 10^{-3}}{W^{(0.579 \pm 0.026)} + (0.171 \pm 0.054) \times H} \quad \text{cm}^2/\text{Vs} \qquad 3\text{-}27$$

where W is the molecular weight and H is the hydration number. The average relative error between the predicted absolute mobilities using molecular weight and hydration model (Equation 3-27) and literature mobilities is only 4.5%, which is significantly less than that of the molecular weight model (Equation 3-25, 6.1%) and slightly better than that of using the molecular volume and hydration model (Equation 3-26). The correlation between predicted absolute mobilities using Equation 3-27 and literature mobilities is shown in Figure 3.16.

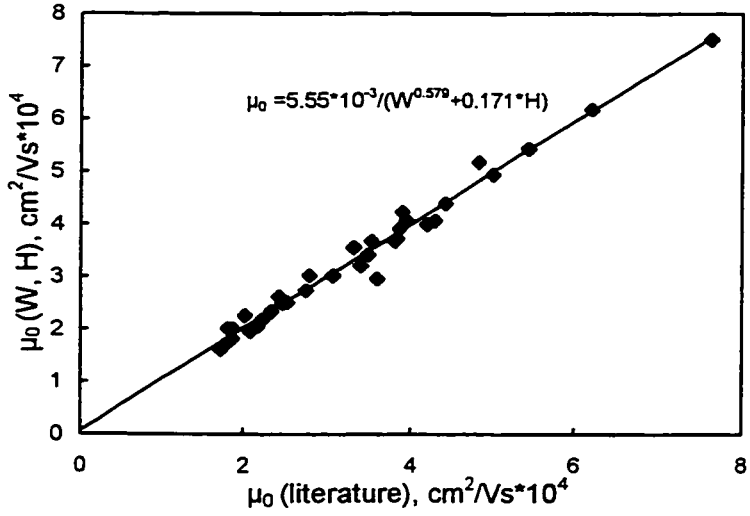

Figure 3.16 Correlation of the mobilities estimated using Equation 3-27 with the literature absolute mobilities for the 34 amines in Table 3.4.

The correlation coefficient, slope and intercept of the linear regression line in Figure 3.16 are 0.9906, 0.9818 and 0.0613 respectively.

3.4.7 MOLECULAR VOLUME AND pK_b MODEL

3.4.7.1 CONCEPT OF DIELECTRIC FRICTION

It has previously been noted that the agreement between the Hückel equation and the behavior of small (< 5 Å) ions is poor [33]. Further, for very small ions (< 1.5 Å, *e.g.*, K^-, Na^-, Li^-), the mobility is actually inversely related to the crystallographic radii [41]. This paradoxical behavior is believed to result from mobility depending upon a friction in addition to the hydrodynamic friction (f_H) incorporated in the Hückel equation [41]:

$$\mu = \frac{Ze}{f_H + f_D} \qquad 3\text{-}28$$

As discussed in Chapter 1, this additional or "dielectric" friction (f_D) is due to the interaction between the moving ion and the adjacent solvent dipoles. This interaction imposes a retarding force on the migrating ion. Although Hubbard and Onsager have provided the most thorough treatment of this effect [42][43][44], their proposed models have not been highly successful at *a priori* prediction of mobilities in aqueous solution, especially for alkali metal and halide ions [44][41]. However, from Equation 1-24, it can be seen that for infinitely dilute aqueous solutions at a constant temperature and pressure, the Debye dielectric relaxation time, τ_D, and the low and high frequency dielectric constants of water are constants. Therefore, the dielectric term in Equation 1-24 can be simplified as ke^2/r_i^3, where k is a constant. In other words, the dielectric friction is only

related to the

charge density of the ion under certain conditions. The dielectric friction concept led us to investigate the physicochemical parameters which can be used to reflect the charge distribution or dielectric friction of ions.

3.4.7.2 MOLECULAR VOLUME AND pK_b MODEL

As will be described in Chapter 4 (Section 4.3), the pK_a value of a molecule can reflect the charge distribution of carboxylates. For amines, pK_b is the preferred descriptor of charge distribution. pK_b values of 34 monoamines are listed in Table 3.6.

Table 3.6 pK_b of 34 amines at zero ionic strength.

Molecule	pK_b (25 °C)
Octadecyltripropylammonium	0
Octyltrimethylammonium	0
Pentylammonium	3.403[a]
Piperidinum	2.877[a]
Tetra-n-butylammonium	0
Tetradecyltrimethylammonium	0
Dipropylammonium	3.00[a]
Tetra-i-pentylammonium	0
Tetra-n-pentylammonium	0
Tetra-n-propylammonium	0
Ammonium	4.75[c]
Tripropylammonium	3.34[a]
Propyltrimethylammonium	0
Octadecyltrimethylammonium	0
Methylammonium	3.36[a]
Dimethylammonium	3.226[a]
Trimethylammonium	4.200[a]
Tetramethylammonium	0
Benzyltrimethylammonium	0
i-Butylammonium	3.52[a]
Butyltrimethylammonium	0
Decyltrimethylammonium	0
Dodecyltrimethylammonium	0
Ethyltrimethylammonium	0
Hexadecyltrimethylammonium	0
Hexyltrimethylammonium	0
Octadecyltributylammonium	0
Octadecyltriethylammonium	0
Ethylammonium	3.364[a]
Propylammonium	3.434[a]
n-Dodecylammonium	3.37[b]
Diethylammonium	3.067[a]
Triethyl ammonium	3.285[a]
Tetraethylammonium	0

[a] Data from reference [7]

[b] Data from reference [45]

[c] Data from reference [27]

Note that the pK_b values for quaternary amines (permanently charged) were arbitrarily defined as zero. For any permanently charged species, its pK_b value has no physical meaning. However, the stronger the protonation ability of a monoamine, the smaller its pK_b. Since quaternary amines are permanently charged, in analogy to permanently protonated, we assume its pK_b to be zero.

This assumption is also supported by the results of carboxylates and sulfonates (Chapter 4 and Chapter 5). For weak acids (*e.g.*, carboxylic acids), the stronger the electron withdrawing substituent on the molecule, the stronger the acid and the smaller the pK_a. The result is lower charge density and dielectric friction. For example, the pK_a of trichloroacetic acid is only 0.90, which is much less than that of acetic acid ($pK_a = 4.76$). This should result in its higher charge distribution or lower dielectric friction, and in turn higher absolute mobility than those of other ions with the same size and with lower charge distribution. Indeed, CCl_3COO^- ($pK_a = 0.90$) and $n\text{-}C_4H_9COO^-$ ($pK_a = 4.84$) have about the same size (their molecular volume are 104.3 and 105.3 respectively), but CCl_3COO^- has a much higher absolute mobility (3.62×10^{-4} cm^2/Vs) than that of $n\text{-}C_4H_9COO^-$ (2.98×10^{-4} cm^2/Vs). It was also observed that the dielectric friction term can be neglected for very strong organic acids (sulfonic acids in Chapter 5). Therefore, we can assume the pK_a values of permanently charged organic acids to be zero. By the same analogy, we define the pK_b of permanently charged quaternary amines to be zero.

Including pK_b of monoamines into the molecular volume model, the equation that gives the minimum *residual sum of squares* is:

$$\mu_0 = \frac{(7.8 \pm 1.3) \times 10^{-3}}{V^{(0.620 \pm 0.032)} + (0.66 \pm 0.23) \times pK_b} \quad \text{cm}^2/\text{Vs} \qquad 3\text{-}29$$

Using Equation 3-29, the average relative error between the predicted absolute mobilities and the literature values for amines listed in Table 3.4 is 4.5%. The correlation between the predicted and literature absolute mobilities is shown in Figure 3.17.

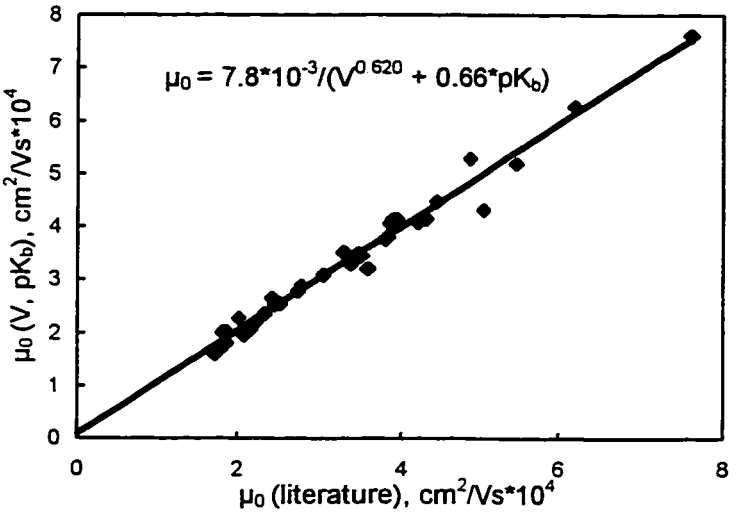

Figure 3.17 Correlation of the mobilities estimated using Equation 3-29 with the literature absolute mobilities for the 34 amines in Table 3.4.

The correlation coefficient, slope and intercept of the linear regression line in Figure 3.17 are 0.9887, 0.9766 and 0.079 respectively.

3.4.8 MOLECULAR WEIGHT AND pK_b MODEL

Using molecular weight and pK_b as the parameters to predict the absolute

mobilities of monoamines, nonlinear regression gave the best fit equation:

$$\mu_0 = \frac{(5.48 \pm 0.79) \times 10^{-3}}{W^{(0.578 \pm 0.029)} + (0.39 \pm 0.14) \times pK_b} \quad \text{cm}^2/\text{Vs} \qquad 3\text{-}30$$

The correlation between the predicted absolute mobilities and the literature values is shown in Figure 3.18.

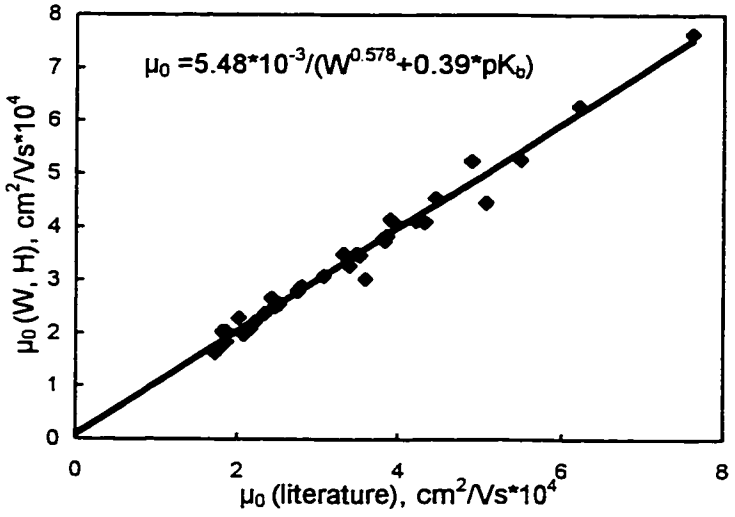

Figure 3.18 Correlation of the mobilities estimated using Equation 3-30 with the literature absolute mobilities for the 34 amines in Table 3.4.

The average error between the predicted absolute mobilities and the literature values is 4.3%. In comparison with other single or two parameter models, the molecular weight and pK_b model gives us the best prediction of the absolute mobilities of monoamines investigated. The correlation coefficient, slope and intercept of the linear regression line in Figure 3.18 are 0.9894, 0.9767 and 0.080 respectively.

3.4.9 MODELS INCLUDING SHAPE CORRECTION

Molecular shape is another important factor we need to consider in estimating the absolute mobilities of small organic ions in aqueous solution. The molecular shape correction parameters, including the frictional ratio (f/f_0), Kappa shape index (K) and an empirical shape factor (S), are listed in Table 3.7.

Table 3.7 Molecular shape correction parameters for monoamines.

Molecules	f/f_0	Kappa 2 (K)	Shape Factor(S)
Octadecyltripropylammonium	1.142	21.70	19.0
Octyltrimethylammonium	1.084	6.51	18.0
Pentylammonium	1.058	5.00	6.0
Piperidinum	1.005	2.22	3.0
Tetra-n-butylammonium	1.016	11.11	4.0
Tetradecyltrimethylammonium	1.176	12.06	30.0
Dipropylammonium	1.078	6.00	2.0
Tetra-i-pentylammonium	1.014	10.68	3.3
Tetra-n-pentylammonium	1.022	14.92	4.0
Tetra-n-propylammonium	1.013	7.41	4.0
Ammonium	1.001	0.00	1.0
Tripropylammonium	1.038	7.11	3.0
Propyltrimethylammonium	1.016	2.34	8.0
Octadecyltrimethylammonium	1.208	15.88	38.0
Methylammonium	1.003	0.00	2.0
Dimethylammonium	1.016	2.00	2.0
Trimethylammonium	1.006	1.33	3.0
Tetramethylammonium	1.004	1.00	4.0
Benzyltrimethylammonium	1.021	3.60	16.0
i-Butylammonium	1.011	2.25	5.0
Butyltrimethylammonium	1.027	3.11	10.0
Decyltrimethylammonium	1.114	8.32	11.0
Dodecyltrimethylammonium	1.143	10.17	26.0
Ethyltrimethylammonium	1.006	1.63	6.0
Hexadecyltrimethylammonium	1.203	13.96	34.0
Hexyltrimethylammonium	1.053	4.76	14.0
Octadecyltributylammonium	1.107	24.64	15.2
Octadecyltriethylammonium	1.195	18.78	25.3
Ethylammonium	1.016	2.00	3.0
Propylammonium	1.039	4.00	4.0
n-Dodecylammonium	1.177	12.00	13.0
Diethylammonium	1.047	4.00	2.0
Triethyl ammonium	1.018	4.17	3.0
Tetraethylammonium	1.007	3.92	4.0

Among the shape corrections we have studied (including prolate and oblate approximations, Kappa shape index and empirical shape factor), neither ellipsoidal approximations nor Kier's Kappa shape index gave the results we expected. In comparison with Equation 3-30, multiplying the molecular weight term by either the

Perrin frictional correction factors (f/f_0) or Kier's shape index (K) actually increased the prediction errors. The results are shown in Table 3.8.

Table 3.8 Models incorporating ellipsoidal approximation (f/f_0) or Kier's Kappa shape index (K) for amines listed in Table 3.7.

Best Fit Equation		Average Relative Error (%)
1. $\mu_0 = \frac{A}{(f/f_0)\times W^B}$,	$A = 2.80\times10^{-3}$, $B = 0.437$	6.6 (34 amines)
2. $\mu_0 = \frac{A}{K\times W^B}$,	$A = 1.95\times10^{-5}$, $B = -0.859$	23.2 (34 amines)
3. $\mu_0 = \frac{A}{(f/f_0)\times W^B + C\times pK_b}$,	$A = 3.99\times10^{-3}$, $B = 0.505$, $C = 0.185$	6.2 (34 amines)
4. $\mu_0 = \frac{A}{K\times W^B + C\times pK_b}$,	$A = 1.79\times10^{-5}$, $B = -0.877$, $C = 0.0062$	28.6 (34 amines)
5. $\mu_0 = \frac{A}{(f/f_0\times W)^B + C\times pK_b}$,	$A = 4.50\times10^{-3}$, $B = 0.534$, $C = 0.250$	5.1 (34 amines)
6. $\mu_0 = \frac{A}{(K\times W)^B + C\times pK_b}$,	$A = 1.15\times10^{-3}$, $B = 0.205$, $C = -0.0636$	4.9 (34 amines)

From Equations 2 and 4 listed in Table 3.8, it can be seen that incorporating Kier's Kappa 2 shape index into the molecular weight term gives unrealistic results. That is, the molecular weight is raised to a negative power. This suggests that increased molecular weight results in higher absolute mobility of an analyte. This is physically unrealistic.

However, inspection of the deviations between the literature mobilities and those predicted using the molecular weight and pK_b model (Equation 3-30) reveled some general shape dependence. The mobilities of large symmetric quaternary amines such as tetra-n-butylammonium were overestimated. Meanwhile, the mobilities of large

asymmetric quaternary amines were generally underestimated. Errors for smaller solutes were not systematic. From Figure 3-18, it was noted that benzyltrimethylammonium is an outliner because, being aromatic, its shape is distinctively different from the rest of the monoamines which were aliphatic. It was noted that the length of the main chain, number of side chains on the nitrogen atom and the average carbon atoms in the side chains all seemed to correlate with the prediction deviations. Based on these observations, an empirical shape index (S) was developed, and is defined as:

$$S = \frac{(N_L + 1) \times (B + 1)}{(N_S + 1)} \qquad 3\text{-}31$$

where N_L is the number of carbon atoms in the longest chain, B is the number of side chains on the amine (primary amines, B=0; secondary amines, B=1; tertiary amines, B=2 and for quaternary amines, B=3), and N_S is the average number of carbon atoms in the side chains. Incorporation of this shape factor yielded the best fit regressions:

$$\mu_0 = \frac{8.11 \times 10^{-3}}{\left(V^{0.636} + 0.698 pK_b - 0.116S\right)} \quad \text{cm}^2/\text{Vs} \qquad 3\text{-}32$$

$$\mu_0 = \frac{5.70 \times 10^{-3}}{\left(W^{0.595} + 0.404 pK_b - 0.085S\right)} \quad \text{cm}^2/\text{Vs} \qquad 3\text{-}33$$

Equation 3-32 and 3-33 reduce the average relative error down to 4.0% and 4.1%, respectively. In comparison with Equation 3-29 and 3-30, it can be seen that incorporation of shape correction did improve the prediction slightly, but it is just a very minor factor. In consideration of simplicity and predictability, the molecular weight and pK_b model (Equation 3-30) is the recommended equation for the prediction of absolute mobilities.

3.4.10 TEST OF EXPRESSIONS

In order to confirm the effectiveness of the equations developed to predict the absolute mobilities of monovalent amines, the following two tests were performed.

3.4.10.1 AMINES WITH OTHER FUNCTIONAL GROUPS

The best fit equations developed above were used to predict the absolute mobilities of seven monovalent amines possessing additional functional groups. This mobility data was obtained from the literature, and is listed in Table 3.9.

Table 3.9 Physicochemical parameters and absolute mobilities of amines with other functional groups

Molecules	Mole. Weight (g/mol)	Mole. Volume ($Å^3$)	Hydration Number (H)	Shape Factor (S)	pK_b (25 °C, I=0)	μ_0 (lit.) $cm^2/Vs \times 10^4$
$^+NH_3CH_2CH_2OH$	62.09	67.33	10	4.0	4.502*	4.37[a]
$(HOCH_2)_3CNH_3^+$	122.14	118.00	12	3.0	5.925*	2.95[c]
$HOCH_2CH_2N^+(CH_3)_3$	104.17	125.03	4	8.0	0	3.96[b]
$^+NH_3(CH_2)_5COOH$	132.18	136.17	11	8.0	3.196*	2.88[c]
$C_3H_3N_2$-$CH_2CH(COOH)NH_3^+$	156.16	139.20	17	8.0	4.92*	2.96[c]
$CH_3NHCOCH_2N^+(CH_3)_3$	131.20	148.50	7	10.0	0	3.46[b]
$(HOCH_2CH_2)_2(CH_3)_2N^+$	134.20	149.69	5	6.0	0	3.48[b]

[a] Data from reference [27]
[b] Data from reference [29]
[c] Data from reference [30]
* Data from reference [7]

The predictive accuracy of different models for the amines listed in Table 3.9 is given in Table 3.10.

Table 3.10 Summary of the accuracy of absolute mobilities predicted using the expressions developed herein for amines listed in Table 3.9.

Equation	Average Relative Error
Volume-based	
Equation 3-22 (volume model)	12.9%
Equation 3-26 (volume and hydration model)	8.2%
Equation 3-29 (volume and pK_b model)	6.7%
Equation 3-32 (volume, pK_b and shape correction model)	3.6%
Weight-based	
Equation 3-25 (weight model)	7.8%
Equation 3-27 (weight and hydration model)	7.2%
Equation 3-30 (weight and pK_b model)	**5.0%**
Equation 3-33 (weight, pK_b and shape correction model)	5.0%

3.4.10.2 EXPERIMENTALLY MEASURED ABSOLUTE MOBILITIES

Further evaluation of the absolute mobility prediction models was performed by comparing the experimentally measured absolute mobilities of 13 monoamines with the predicted mobilities. These monoamines were chosen to give a range in size and shape, and are listed in Table 3.11.

Table 3.11 Physicochemical parameters and absolute mobilities of experimentally investigated molecules.

Molecule	mole. weight (g/mol)	Mole. Volume ($Å^3$)	Hydr. Number (H)	Shape Factor (S)	pK_b (25° C, I=0)	μ_0 (meas.) $cm^2/Vs \times 10^4$
Ethylammonium	46.09	58.4	9	3	3.364[a]	5.32
t-Butylammonium	74.15	91.5	9	5	3.315[a]	3.73
Diallylammonium	98.17	116.8	6	2	4.71[a]	3.55
Cyclohexylammonium	100.18	114.5	9	7	3.36[a]	3.58
Cyclohexylmethylammonium	114.21	132.6	6	7	3.15[b]	3.41
2, 6-Dimethylpiperidinium	114.21	133.2	6	8	2.90[a]	3.28
Dibutylammonium	130.25	159.7	6	2	2.75[a]	2.92
2-Ethylhexylammonium	130.25	158.3	9	9	3.45[b]	3.04
Triallylammonium	138.23	166.4	3	3	5.69[a]	3.09
Dicyclohexylammonium	182.33	205.4	6	2	2.75[a]	2.64
Dodecyldimethylammonium	214.41	260.8	3	19.5	3.95[b]	2.47
Tetra-n-butylammonium	242.47	279.9	3	4	0	2.24
Octadecyltrimethylammonium	312.60	378.2	3	38	0	1.89

[a] Data from reference [7].

[b] Data were estimated using Equation 3.2, 3.3 and 3.4 in page 23 of reference [8], and then extrapolated to zero ionic strength using Equation 1.17 of the same reference.

The average relative errors between the predicted absolute mobilities using some of the best fit equations and the measured mobilities are given in Table 3.12.

Table 3.12 Summary of the accuracy of absolute mobilities predicted using the expressions developed herein for amines listed in Table 3.11.

Equation	Average Relative Error
Volume-based	
Equation 3-22 (volume model)	5.5%
Equation 3-26 (volume and hydration model)	4.0%
Equation 3-29 (volume and pK_b model)	4.4%
Equation 3-32 (volume, pK_b and shape correction model)	4.5%
Weight-based	
Equation 3-25 (weight model)	4.0%
Equation 3-27 (weight and hydration model)	2.8%
Equation 3-30 (weight and pK_b model)	4.1%
Equation 3-33 (weight, pK_b and shape correction model)	4.9%

From Table 3.12, it can be seen that all models gave pretty good prediction of the absolute mobilities of experimentally investigated monoamines. This may be due to the large experimental error associated with the absolute mobility determination of monoamines using Crystal 300 CE system. The average error between the experimentally measured absolute mobilities and the literature values for ethylammonium, tetra-n-butylammonium and octadecyltrimethylammmoniumInspection is 9.9%. Therefore, this data set can be treated only as a rough test. However, inspection of the results listed in Table 3.10 and 3.12 suggests that molecular shape correction is not important for the monoamines investigated. Actually, the only case that the prediction of absolute mobilities improved is the incorporation of shape correction into the molecular volume and pK_b model for amines with other functional groups. For all other cases, incorporation of the molecular shape

correction did not improve the prediction of the absolute mobilities or slightly worsened the predictions. Furthermore, it can be seen that the molecular weight and pK_b model (Equation 3-30) gives excellent prediction of absolute mobilities for all test amines. In general, models including hydration of analytes also give very good prediction of the behavior of monoamines.

3.5 SUMMARY OF OBSERVATIONS

Both hydrodynamic friction and dielectric friction need to be considered for the prediction of the behavior of monoamines. The molecular weight and pK_b model (Equation 3-30) gives the lowest prediction error (4.3%) for the 34 monoamines listed in Table 3.4. Two independent tests confirmed the effectiveness of this model. Using the molecular weight and pK_b model, very good agreement was achieved between the predicted absolute mobilities and the literature mobilities of 7 amines possessing other functional groups (5.0% error), as well as for 13 experimentally investigated monoamines (4.1% error). In general, molecular weight-based models give slightly better predictions of the absolute mobilities. The physical significance of parameters used and the constants in the best fit regression equations is discussed in detail in Chapter 6.

3.6 REFERENCES

1. Burton, D.; Sepaniak, M.; Maskarinec, M. *J. Chromatogr. Sci.* **1987**, *25*, 514.

2. Tsuda, T. *J. High Resolut. Chromatogr. Chromatogr. Commun.* **1987**, *10*, 622.

3. Lucy, C. A.; Underhill, R. A. *Anal. Chem.* **1996**, *68*, 300-305.

4. Yeung, K. K.-C.; Lucy, C. A. *Anal. Chem.* **1997**, *69*, 3435.

5. Yeung, K. K.-C.; Lucy, C. A. *J. Chromatogr. A* In Press.

6. Tavares, M. F. M.; Colombara, R.; Massaro, S. *J. Chromatogr. A* **1997**, 772, 171-178.

7. Martell, A. E.; Smith, R. M. *Critical Stability Constants*, Volume 2; Plenum Press: New York, 1975.

8. Perrin, D. D.; Dempsey, B.; Serjeant, E. P. *pK_a Prediction for Organic Acids and Bases*; Chapman and Hall: New York, 1981; p. 23.

9. Mikkers, F. E. P.; Everaerts, F. M.; Verheggen, Th. P. E. M. *J. Chromatogr.* **1979**, 169, 1-10.

10. Mukerjee, P.; Mysels, K. J. *Critical Micelle Concentration of Aqueous Surfactant Systems*, NSRDS-NBS 36; US Government Printing Office: Washington, D.C., 1970; pp 41-60.

11. Haber, C.; Jones, W. R.; Soglia, J.; Surve, M. A.; McGlynn, M.; Caplan, A.; Reineck, J. R.; Krstanovic, C. *J. Cap. Elec.* **1996**, 3, 1-11.

12. Thermo; *Crystal 1000 CE Conductivity Detector Users Manual*, Version 1.1; Boston, MA, 1994.

14. Williams, B. A.; Vigh, Gy. *Anal. Chem.* **1996**, 68, 1174-1180.

15. Erdey-Grúz, T. *Transport Phenomena in Aqueous Solutions*; Halsted Press: New York, 1974; 294-326.

16. Bockris, J. O'M.; Reddy, A. K. N.; *Modern Electrochemistry*, Vol. 1; Plenum Press: New York, 1970. pp 420-440.

17. Edward, J. T.; Crawford, R. *J. Chromatogr.* **1958**, 1, 449-456.

18. Tiselius, A.; Svensson, H. *Trans. Faraday Soc.* **1940**, 36, 16-22.

19. Falkenhagen, H.; Kelbg, G. *Z. Elektrochemie* **1954**, 58, 653.

20. Pitts, E. *Proc. Roy. Soc.* **1953**, A.217, 43.

21. Pitts, E.; Tabor, B. E.; Daly, J. *Trans. Faraday Soc.* **1970**, 66, 693.

22. Güntelberg, E. *Z. Phys. Chem.* **1926**, 123, 199.

23. Friedl, W.; Reijenga, J. C.; Kenndler, E. *J. Chromatogr. A* **1995**, 709, 163-170.

24. Abramson, H. A., Moyer, L. S.; Gorin, M. H. *Electrophoresis of Protein*; Hafner Publishing Co. Inc.: New York, 1964; pp 105-172.

25. Grossman, P. D.; Colburn, J. C.; Lauer, H. H. *Anal. Biochem.* **1989**, *179*, 28-33.

26. Caulcutt, R.; Boddy, R. *Statistics for Analytical Chemists;* Chapman and Hall: New York, 1983. p 52.

27. *Handbook of Chemistry and Physics*, 1st Student Edition; Weast, R. C., Ed.; CRC Press: Boca Raton, FL, 1991; pp D-106.

28. Moor, T. S.; Winmill, T. F. *J. Chem. Soc.* **1912,** *101*, 1635.

29. Edward, J. T. In *Advances in Chromatography*; Giddings, J. C., Keller, R. A., Eds.; Marcel Dekker: New York, 1966; Vol. 2, pp 63-98.

30. Hirokawa, T.; Kiso, Y. *J. Chromatogr.* **1982,** *252*, 33.

31. Kuhn, D. W.; Kraus, C. A. *J. Am. Chem. Soc.* **1950**, *72*, 3676.

32. Beckers, J. L.; Everaerts, F. M. *J. Chromatogr.* **1989**, *470*, 277.

33. Edward, J. T. *J. Chem. Education* **1970**, *47*, 261.

34. Cussler, E. L. *Diffusion: mass transfer in fluid systems*; Cambridge University Press: New York, 1984, Sec. 5.2.

35. Perrin, F. *J. Phys. Radium* **1934**, *5*, 497.

36. Perrin, F. *J. Phys. Radium* **1936**, *7*, 1.

37. Eisenberg, D.; Crothers, D. *Physical Chemistry with Applications to the Life Sciences*; Benjamin/Cummings: Menlo Park, CA, 1979; pp 718-724.

38. Wilke, C. R.; Chang, P. *AIChE J.* **1955**, *1*, 264-270.

39. Hayduk, W.; Laudie, H. *AIChE J.* **1974**, *20*, 611-615.

40. Offord, R. E. *Nature* **1966**, *211*, 591.

41. Evans, D. F.; Tominaga, T.; Hubbard, J. B.; Wolynes, P. G. *J. Phys. Chem.* **1979**, *83*, 2669.

42. Hubbard, J.; Onsager, L. *J. Chem. Phys.* **1977**, *67*, 4850.

43. Hubbard, J. B. *J. Chem. Phys.* **1978**, *68*, 1649.

44. Kay, R. L. *Pure Appl. Chem.* **1991**, *63*, 1393.

45. Perrin, D. D. *Dissociation Constants of Organic Bases In Aqueous Solution*; Butterworths: London, 1965; p 51.

CHAPTER 4 PREDICTION OF ABSOLUTE MOBILITIES FOR ALIPHATIC CARBOXYLATES

4.1 INTRODUCTION

Capillary electrophoresis has been widely used to separate organic acids. For aliphatic carboxylates, indirect UV detection [1][2] is the most popular detection method due to its versatility and simplicity, and also because most commercial CE instruments are equipped with UV absorbance detectors. Low molecular weight carboxylates can also be detected by conductivity detection [3]. No matter which detection method is used, separations of aliphatic carboxylates are based on the mobility differences of the carboxylates. Many efforts have been made to measure the absolute mobilities of carboxylates [4][5][6]. However, measurements of absolute mobilities using experimental methods are very time-consuming.

In this chapter, we investigate the physicochemical parameters determining the absolute mobilities of aliphatic carboxylates and then use these parameters to predict the absolute mobilities of carboxylates. As described in Chapter 3 (amines), dielectric friction is one of the major factors which influences the absolute mobility of an analyte. In this chapter, both hydrodynamic friction and dielectric friction are considered in order to predict the absolute mobilities of carboxylates. It was found that the absolute mobilities of aliphatic carboxylates can be predicted very well using molecular volume and pK_a.

4.2 DETERMINATION OF PHYSICOCHEMICAL PARAMETERS

4.2.1 MOLECULAR VOLUME

The molecular volumes of 15 aliphatic or substituted carboxylates were calculated using Molecular Modeling Pro™ (version 1.44) and Insight II (version 95.0.2). The procedures for drawing each molecule, minimizing its strain energy and calculating its molecular volume are as described in Chapter 2 (molecular modeling).

4.2.2 HYDRATION NUMBER

The mean waters of hydration for each molecule were calculated using Molecular Modeling Pro™. McGowan's Additive method was employed in the calculation of hydration number, as described in Section 2.4.

4.3 pK_a VALUES

As discussed in Chapter 3, hydrodynamic and dielectric frictions are the two main resistive forces which influence the absolute mobilities. For practical application in analytical chemistry, we are more interested in easily obtainable physicochemical parameters which can represent or reflect the extent of these effects. As demonstrated in Chapter 3, molecular volume or molecular weight can reflect the molecular size of the analyte, which is one of the major factors determining the hydrodynamic friction. However, many factors such as the ion charge, solvent viscosity, dielectric constant of the solvent, the dielectric relaxation time of the pure solvent, etc., have a significant effect on

the dielectric friction of a moving ion. The dielectric friction coefficient (f_D) of a moving ion can be calculated using equation 4-1 [7]:

$$f_D = (\frac{17}{280})\frac{\tau_D e^2}{r^3}(\frac{\varepsilon_0 - \varepsilon_\infty}{\varepsilon_0^2}) \qquad 4\text{-}1$$

where e is the ion charge, ε_0 and ε_∞ are the low (zero) and high (infinite) frequency dielectric constants of the pure solvent, τ_D is the Debye dielectric relaxation time of the pure solvent, and r is the ionic radius. This equation was derived assuming that the ion is moving in a continuum viscous fluid. From equation 4-1, it can be seen that not only the ion charge (e), but also the distribution of the charge (*i.e.*, radius of charge) has significant influence on the dielectric friction. For a monocharged ion, a larger ion (larger r) results in a smaller charge density and from Equation 4-1 a much smaller dielectric coefficient ($f_D \propto 1/r^3$). For monocharged aliphatic carboxylates at infinite dilution in aqueous solution (25 °C), the low and high frequency dielectric constants (ε_0 = 78.6 and ε_∞ = 5.5) [7], viscosity (η = 0.8904 cP) and dielectric relaxation of the water ($\tau_D = 8.2\times10^{-12}$ s) can be considered as constants. We can imagine that if a spherical molecule with a uniform charge distribution on the surface is moving in a continuum medium, the drag force produced from the dielectric interaction between the moving ion and the solvent will be much smaller than that if the charge is localized in a particular functional group. Now the distribution of the charge becomes the predominant factor determining the dielectric friction of a particular molecular ion.

For aliphatic or substituted aliphatic acids, the charge distribution of carboxylate anions has significant influence on the pK_a values [8]. For a weak acid, the acid dissociation equilibrium is:

$$HA + H_2O \rightleftharpoons H_3O^+ + A^- \qquad 4\text{-}2$$

The thermodynamic ionization constant or acid dissociation constant of the acid (HA) is:

$$K_a = \frac{a_{H_3O^+} \times a_{A^-}}{a_{HA} \times a_{H_2O}} \qquad 4\text{-}3$$

where $a_{H_3O^+}$, a_{A^-}, a_{HA}, and a_{H_2O} are the activity of the hydrogen ion, the acid anion, undissociated acid and water respectively. Almost all K_a measurements are made in dilute aqueous solution where the concentration of water is effectively a constant. Therefore the activity of water can be taken as unity. Equation 4-3 can be simplified as:

$$K_a = \frac{a_{H_3O^+} \times a_{A^-}}{a_{HA}} \qquad 4\text{-}4$$

pK_a is the negative logarithm of the acid dissociation (ionization) constant. Many factors can influence the magnitude of the acid dissociation constant. The major factor which modifies the dissociation constants of aliphatic carboxylates is electron-delocalization. Other factors such as conformational differences and steric factors [8] also modify pK_a's. All of these factors are discussed in more detail below.

4.3.1 ELECTRON-DELOCALIZATION EFFECTS [8]

Electrical work must be done to remove a proton from the neutral acid (HA in

Equation 4-2) to the solvent molecules (H_2O in equation 4-2). The amount of work needed depends on the location and distribution of the dipoles and electrical charges of the acid. For aliphatic carboxylates, charge distribution is produced mainly by inductive and (or) electrostatic effects. The inductive effects change the distribution of the charge directly through the bonds in the acid molecules, while the electrostatic effects modify the charge distribution indirectly, e.g., through the solvent molecules. Because these two effects usually occur at the same time and operate in about the same direction, it is very difficult to separate them. In the following discussion, only the term inductive effect will be used, but it refers to both the inductive and electrostatic effects.

A substituent has acid-strengthening effects (increase K_a, decrease pK_a) if its addition decreases the electron density on the carboxyl group [8]. For example, in monochloroacetic acid, the electronegative substituent (-Cl) withdraws charge from the $-COO^-$ group, which decreases the electron density on the $-COO^-$ group. Therefore, the pK_a of monochloroacetic acid is lower than that of acetic acid. The magnitude of the inductive effect decreases quickly as the distance separating the substituent from the charge center increases. Thus the pK_a of the following substituted acids are:

$$ClCH_2COOH < ClCH_2CH_2COOH < ClCH_2CH_2CH_2COOH$$

Since inductive effects are approximately additive, the pK_a of mono-, di- and tri-chloroacetic acids are:

$$Cl_3CCOOH < Cl_2CHCOOH < ClCH_2COOH$$

From the above discussion, it can be seen that the charge density of the carboxylic acid anions is reflected by their corresponding pK_a values. In general, a lower pK_a means a

lower charge density, and thus a lower dielectric friction.

For an acid, its thermodynamic pK_a is a constant for a given solvent and temperature. It is obtained by extrapolating pK_a values measured at a series of ionic strengths to zero ionic strength. For acids which dissociate according to equation 4-2, the relationship between the mixed acid dissociation constant (here concentrations of acid and base species instead of activities are used in equation 4-4) and ionic strength is given by Equation 4-5 (based on the Debye-Hückel extended equation) [8]:

$$pK_a' = pK_a - A\frac{\sqrt{I}}{1+\sqrt{I}} + 0.1\,I \qquad 4\text{-}5$$

where pK_a' is the negative logarithm of mixed acid dissociation constant, pK_a is the zero ionic strength (thermodynamic) pK_a, A is a constant equal to 0.5115 for aqueous solution at 25 °C, and I is the ionic strength of the solution. The 0.1 in the rightmost term is an empirical parameter valid for 1:1 electrolytes. Equation 4-5 is valid up to an ionic strength of 0.1 M. Since all pK_a values listed in reference [9] are concentration constants (concentrations instead of activity of hydrogen ion, acid and base species are used in Equation 4-4), they must be converted to mixed constants before the application of Equation 4-5. For monoprotic acids, pK_a increments listed in Table 4.1 need to be added to obtain the corresponding mixed acid dissociation constants [9]:

Table 4.1 pK_a increment used to convert concentration constant to mixed constant.

Ionic Strength	Increase in pK_a
0.05	0.09
0.10	0.11
0.15	0.12
0.20	0.13
0.50	0.15
1.0	0.14
2.0	0.11
3.0	0.07

In this study, absolute (infinite dilution) mobilities are predicted for aliphatic acids. Therefore the corresponding pK_a's at infinite dilution are used. The thermodynamic pK_a's of the 15 aliphatic or substituted aliphatic acids investigated are given in Table 4.2.

Table 4.2 pK_a values and the corresponding ionic strength of carboxylates[‡].

Molecules	pK_a (25 °C)	Ionic Strength (M)
$HCOO^-$	3.75	0
CH_3COO^-	4.76	0
CH_2ClCOO^-	2.87	0
$CH_3CH_2COO^-$	4.87	0
$CH_2ClCH_2COO^-$	4.11	0
$CHCl_2COO^-$	1.30	0
$CH_3CH_2CH_2COO^-$	4.82	0
CCl_3COO^-	0.90[†]	0[†]
$n\text{-}C_4H_9COO^-$	4.84	0
$(CH_3)_3CCOO^-$	5.03	0
$n\text{-}C_5H_{11}COO^-$	4.86	0
$n\text{-}C_6H_{13}COO^-$	4.86	0
$n\text{-}C_7H_{15}COO^-$	4.89	0
$n\text{-}C_8H_{17}COO^-$	4.96[†]	0[†]
$n\text{-}C_9H_{19}COO^-$	4.96*	0*

‡ Data from reference [9].

* pK_a value is estimated from the pK_a values of $n\text{-}C_5$ to $n\text{-}C_{10}$ carboxylates.

† pK_a values were calculated using Equation 4-5. For CCl_3COOH, its pK_a' is 0.77 at ionic strength 0.1 M; the pK_a' of $n\text{-}C_8H_{17}COOH$ is equal to 4.95 at ionic strength 0.0004 M.

4.3.2 STERIC EFFECTS [8]

Obviously, not only the inductive effect but also steric effects can influence the acid dissociation constant. Bulky aliphatic chains around the carboxyl group will make the solvation of the carboxylate ion more difficult. An increase in the pK_a value is the result. The influence of steric hindrance on pK_a values of carboxylates can be illustrated using the following isomer pair (Figure 4.1 and 4.2), which represent the extreme situation among

the aliphatic carboxylates investigated.

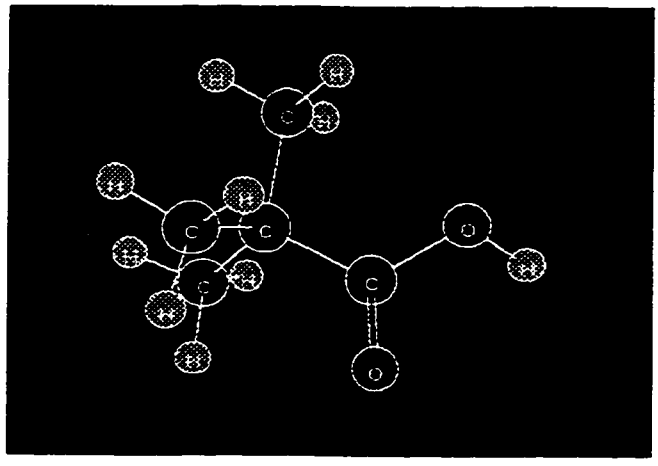

Figure 4.1 Pivalic acid ($(CH_3)_3CCOOH$): $pK_a = 5.03$.

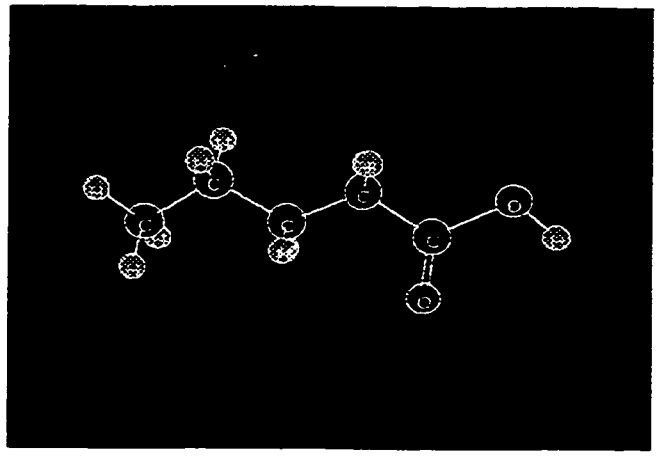

Figure 4.2 Pentanoic acid (C_4H_9COOH): $pK_a = 4.84$.

Pivalic acid ($pK_a = 5.03$) is a weaker acid than pentanoic acid ($pK_a = 4.84$). The pK_a difference results from steric hindrance to the solvation the carboxyl anion formation in

pivalic acid [8]. Crowding by the three methyl groups around the carboxyl group of pivalic acid increases the difficulty of deprotonating the carboxyl group. This steric hindrance makes pivalic acid a weaker acid than pentanoic acid, and also weaker than hexanoic, heptanoic, octanoic and decanoic acids. In comparison with pentanoic acid, the pK_a of pivalic acid is increased by 3.9%. This is the largest steric effect among the molecules investigated.

In contrast, the pK_a of monochloroacetic acid and dichloroacetic acid are decreased by about 40% and 73%, respectively, due to inductive effects. Thus, in general, the influence of steric effects on the acid dissociation constants in Table 4.2 is much smaller than that due to inductive effects. Since the influence of dielectric friction is much smaller than that of hydrodynamic friction, it can be expected that the $\leq$3.9% pK_a differences resulting from steric hindrance will have only a negligible contribution on the predicted absolute mobilities.

4.4 ABSOLUTE MOBILITIES

The absolute mobilities of all carboxylates investigated were compiled from numerous literature sources and are listed in Table 4.3. These absolute mobilities were determined by isotachophoresis [4][5] or calculated from the limiting equivalent conductivity [11][12]. The relationship between absolute mobility and limiting equivalent conductivity is given by:

$$\mu_0 = \frac{\Lambda^0}{F} \qquad 4\text{-}6$$

where μ_0 is the absolute mobility, Λ^0 is the limiting equivalent conductivity and F is the Faraday constant.

Table 4.3 Literature absolute mobilities of carboxylates.

Molecule	Absolute Mobility ($cm^2/Vs \times 10^4$)
$HCOO^-$	5.71[a]
CH_3COO^-	4.24[b]
~~ICH_2COO^-~~	~~4.21[e]~~
CH_2ClCOO^-	4.19[a], ~~4.37[b]~~
$CH_3CH_2COO^-$	3.69[a] ,3.71[d]
$CH_2ClCH_2COO^-$	3.68[a]
$CHCl_2COO^-$	3.94[a]
$CH_3CH_2CH_2COO^-$	3.37[a]
CCl_3COO^-	3.62[a]
n-$C_4H_9COO^-$	2.98[c]
$(CH_3)_3CCOO^-$	3.16[a]
n-$C_5H_{11}COO^-$	3.05[a]
n-$C_6H_{13}COO^-$	2.87[a]
n-$C_7H_{15}COO^-$	2.74[a]
n-$C_8H_{17}COO^-$	2.67[a]
n-$C_9H_{19}COO^-$	2.21[a]

[a] Data from reference [4], [b] Data from reference [5], [c] Data from reference [10], [d] Data from reference [11], [e] Data from reference [12].

Note, the absolute mobility of monoiodoacetate is not included in our studies because the molecular modeling softwares used did not contain parameters for iodine. Also, the absolute mobilities of monochloroacetate obtained from different sources were significantly different (4.19×10^{-4} cm^2/Vs and 4.37×10^{-4} cm^2/Vs). For consistancy with the absolute mobilities of other molecules, we use the absolute mobilities from the same

source if possible. Therefore, 4.19×10^{-4} cm^2/Vs was used to investigate the correlation between absolute mobilities and physicochemical parameters of analytes.

4.5 RESULTS

Different physicochemical parameters were investigated for the prediction of the absolute mobilities of aliphatic carboxylates. These included molecular volume, molecular weight, acid dissociation constant (pK_a), and hydration number. These parameters are listed in Table 4.4 and Table 4.2.

Table 4.4 Physicochemical parameters of aliphatic carboxylates

Molecules	Weight (g/mol)	Molecular Modeling Pro™		Insight II
		Molecular Volume ($Å^3$)	hydration Number	Molecular Volume ($Å^3$)
$HCOO^-$	45.02	39.75	5	28.51
CH_3COO^-	59.04	55.95	5	42.88
CH_2ClCOO^-	93.49	70.12	5	57.86
$CH_3CH_2COO^-$	73.07	72.73	5	57.21
$CH_2ClCH_2COO^-$	107.5	86.75	5	77.25
$CHCl_2COO^-$	127.9	88.27	5	73.22
$CH_3CH_2CH_2COO^-$	87.10	89.07	5	71.71
CCl_3COO^-	162.4	104.3	5	88.40
$n\text{-}C_4H_9COO^-$	101.1	105.3	5	86.37
$(CH_3)_3CCOO^-$	101.1	110.1	5	86.10
$n\text{-}C_5H_{11}COO^-$	115.2	122.0	5	101.0
$n\text{-}C_6H_{13}COO^-$	129.2	138.4	5	115.4
$n\text{-}C_7H_{15}COO^-$	143.2	154.6	5	129.8
$n\text{-}C_8H_{17}COO^-$	157.2	171.1	5	145.0
$n\text{-}C_9H_{19}COO^-$	171.3	187.6	5	158.8

4.5.1 MOLECULAR VOLUME MODEL

4.5.1.1 VOLUMES OBTAINED FROM MOLECULAR MODELING PRO™.

As discussed in Chapter 3, molecular weight or volume is the predominant factor determining the hydrodynamic friction of monoamines. Is the same true for aliphatic carboxylates? By using nonlinear best fit regression, it was found that the following equation gave the minimum *residual sum of squares*:

$$\mu_0 = \frac{(3.94 \pm 0.67) \times 10^{-3}}{V^{(0.535 \pm 0.038)}} \qquad \text{cm}^2/\text{Vs} \qquad 4\text{-}7$$

where V is the molecular volume (Å^3) determined using Molecular Modeling Pro™. The uncertainties in Equation 4-7 are the standard deviations of the parameters determined by nonlinear regression using SlideWrite's cuve fitter function. The correlation between the predicted absolute mobilities using Equation 4-7 and the literature mobilities is shown in Figure 4.3.

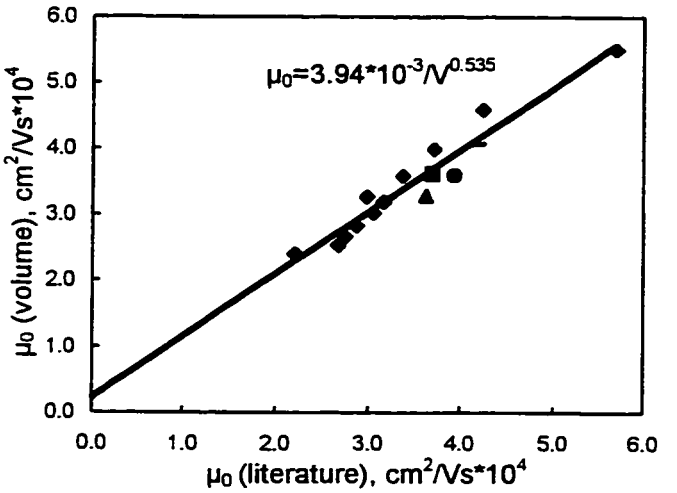

Figure 4.3 Plot of predicted absolute mobilities μ_0 (molecular volume, MMP™) vs. literature absolute mobilities for aliphatic carboxylates listed in Table 4.4, where ▲ = CCl_3COO^-, ■ = $CH_2ClCH_2COO^-$, ● = $CHCl_2COO^-$, - = CH_2ClCOO^-.

It can be seen from Figure 4.3 that the correlation between the predicted and literature absolute mobilities is fair (correlation coefficient r = 0.9657). The slope and intercept of Figure 4.3 are 0.9366 and 0.2197 respectively. Using only one physicochemical parameter (molecular volume), the average relative error between the predicted absolute mobilities and the literature mobilities is 5.2%. In Figure 4.3, all of the chlorinated solutes are given a different symbol for reasons which will be discussed in Section 4.5.2.

4.5.1.2 VOLUMES OBTAINED FROM INSIGHT II

If the molecular volume from Molecular Modeling Pro™ in Equation 4-7 is replaced by the molecular volume calculated from the more advanced molecular modeling

software Insight II, the nonlinear regression gives the following best fit equation:

$$\mu_0 = \frac{(2.75 \pm 0.43) \times 10^{-3}}{V^{(0.477 \pm 0.038)}} \qquad \text{cm}^2/\text{Vs} \qquad 4\text{-}8$$

Figure 4.4 shows the correlation between the predicted absolute mobilities using Equation 4-8 and the literature absolute mobilities. The correlation coefficient (r), slope and intercept of Figure 4.4 are 0.9580, 0.9175 and 0.2866 respectively. All of these parameters are slightly worse than those of Figure 4.3. The average relative error between the absolute mobilities predicted using Equation 4-8 and the literature absolute mobilities is 5.8%. However, the power dependence of volume in Equations 4-7 and 4-8 is statistically equivalent as predicted in Sections 3.4.3 and 2.4.

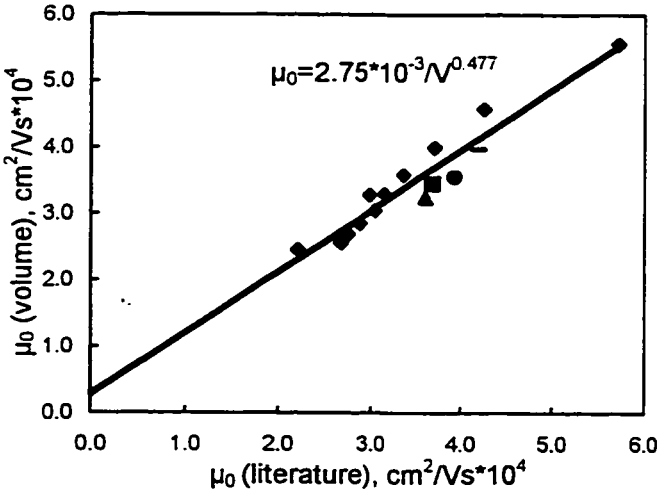

Figure 4.4 Plot of predicted absolute mobilities μ_0 (molecular volume, Insight II) vs. literature absolute mobilities for aliphatic carboxylates listed in Table 4.4, where ▲ = CCl_3COO^-, ■ = $CH_2ClCH_2COO^-$, ● = $CHCl_2COO^-$, - = CH_2ClCOO^-.

4.5.2 MOLECULAR WEIGHT MODEL

Using molecular weight as a single physicochemical parameter, the best fit equation for predicting the absolute mobilities of aliphatic carboxylates is:

$$\mu_0 = \frac{(3.6 \pm 1.5) \times 10^{-3}}{W^{(0.506 \pm 0.090)}} \qquad \text{cm}^2/\text{Vs} \qquad 4\text{-}9$$

where W is the molecular weight. The correlation between predicted and literature absolute mobilities is shown in Figure 4.5:

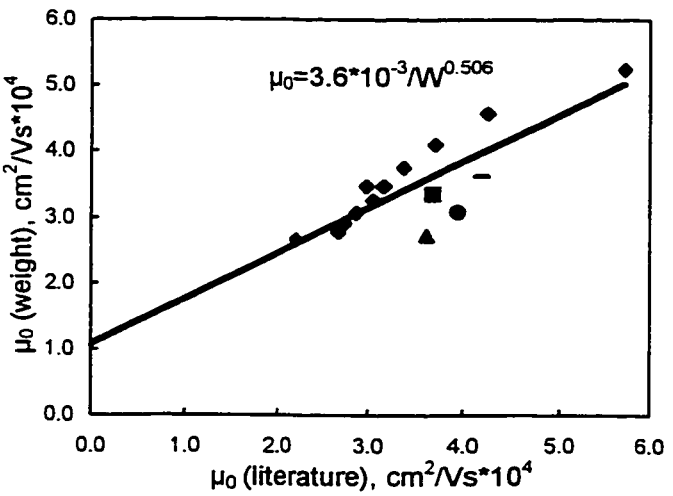

Figure 4.5 Plot of predicted absolute mobilities μ_0 (molecular weight) vs. literature absolute mobilities for the aliphatic carboxylates listed in Table 4.4, where ▲ = CCl_3COO^-, ■ = $CH_2ClCH_2COO^-$, ● = $CHCl_2COO^-$, - = CH_2ClCOO^-.

It can be seen that the predicted absolute mobilities using the molecular weight model did not agree well with literature absolute mobilities. The average relative error is 11.8%, which is much worse than that of the molecular volume models. The correlation

coefficient, slope and intercept of Figure 4.5 are 0.8249, 0.6933 and 1.063 respectively. In comparison with Figure 4.4, it was found that molecular weights can not represent the molecular sizes of chlorinated aliphatic carboxylates. For the chlorinated aliphatic carboxylates in Table 4.3, the average relative error between the predicted absolute mobilities using Equation 4-9 and the literature mobilities is about 17%.

However, if the four halogenated aliphatic carboxylates are not included, molecular weight works as good as molecular volume. The results are shown in the following plot:

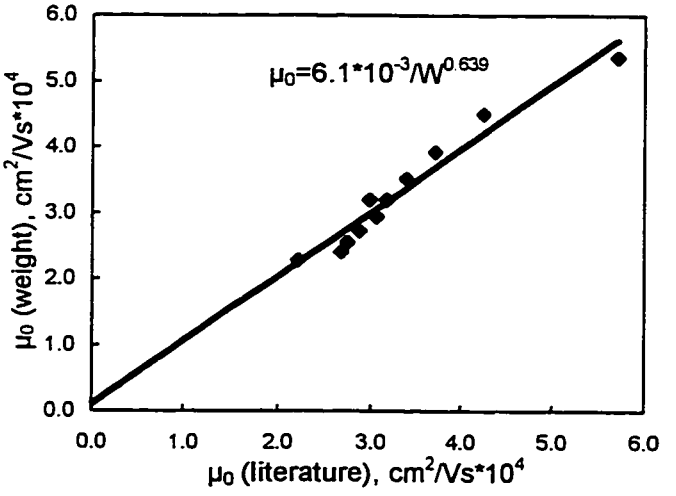

Figure 4.6 Plot of predicted absolute mobilities μ_0 (molecular weight) vs. literature absolute mobilities for the nonchlorinated aliphatic carboxylates listed in Table 4.4.

Nonlinear regression produced the following best fit equation for predicting the absolute mobilities of nonchlorinated aliphatic carboxylates:

$$\mu_0 = \frac{(6.1 \pm 1.2) \times 10^{-3}}{W^{(0.639 \pm 0.046)}} \qquad \text{cm}^2/\text{Vs} \qquad 4\text{-}10$$

Excluding all the chlorinated carboxylates, the average relative error between the predicted absolute mobilities using Equation 4-10 and the literature mobilities decreases significantly to 5.4%. The deviations may result from the different molecular volume to molecular weight ratio for different atomic groups. The correlation coefficient (r), slope and intercept of the linear regression line in Figure 4.6 are 0.9752, 0.9691, and 0.0986 respectively.

4.5.3 VOLUME AND pK_a MODEL

4.5.3.1 VOLUMES OBTAINED FROM MOLECULAR MODELING PRO™.

Both hydrodynamic and dielectric frictions need to be considered in predicting the absolute mobilities of carboxylates. As discussed in Section 4.3, pK_a can be used as a measure of the charge density on the carboxylate. Thus it should be related to the dielectric friction. Incorporation of the pK_a of the aliphatic carboxylates into the molecular volume model yielded the expression:

$$\mu_0 = \frac{(6.5 \pm 1.2) \times 10^{-3}}{V^{(0.613 \pm 0.038)} + (0.62 \pm 0.24) pK_a} \qquad \text{cm}^2/\text{Vs} \qquad 4\text{-}11$$

Using Equation 4-11, the predicted absolute mobilities of aliphatic carboxylates agree very well with the literature absolute mobilities (Figure 4.7). The average relative error between the predicted and literature absolute mobilities drops to only 3.7%. This relative error is very close to that of literature absolute mobilities obtained from different sources.

The uncertainties of available literature absolute mobilities (data not shown) is 3.8% for all classes (aromatic, aliphatic, monocharged, and multicharged) of amines, carboxylates, and sulfonates. Theoretically, it is not necessary to add any more physicochemical parameters in to Equation 4-11 to further reduce the uncertainty of prediction.

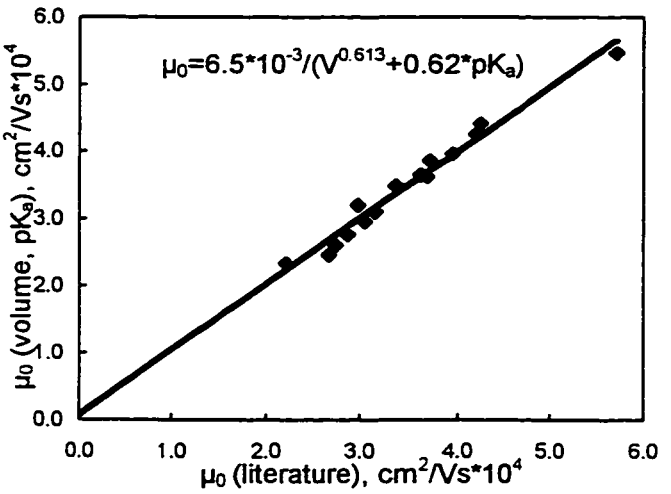

Figure 4.7 Plot of predicted absolute mobilities μ_0 (molecular volume, MMP™, pK_a) vs. literature absolute mobilities for the aliphatic carboxylates in Table 4.4.

The correlation coefficient (r) of the linear regression line of Figure 4.7 is 0.9861, which is much better than molecular volume alone (Section 4.5.1) or molecular weight alone (Section 4.5.2) models. Furthermore, the slope (0.9816) and intercept (0.062) of the linear regression line in Figure 4.7 are very close to the ideal behavior (ideal slope 1.00, ideal intercept 0.00).

4.5.3.2 VOLUMES OBTAINED FROM INSIGHT II.

If molecular volumes calculated from Insight II were used instead of those from MMP™, the best fit expression is:

$$\mu_0 = \frac{(4.9 \pm 0.9) \times 10^{-3}}{V^{(0.568 \pm 0.036)} + (0.54 \pm 0.19) pK_a} \quad \text{cm}^2/\text{Vs} \qquad 4\text{-}12$$

Again, the power dependence of the volume is statistically equivalent between the two molecular modeling programs. Figure 4.8 illustrates the correlation between the absolute mobilities predicted using Equation 4-12 and the literature mobilities.

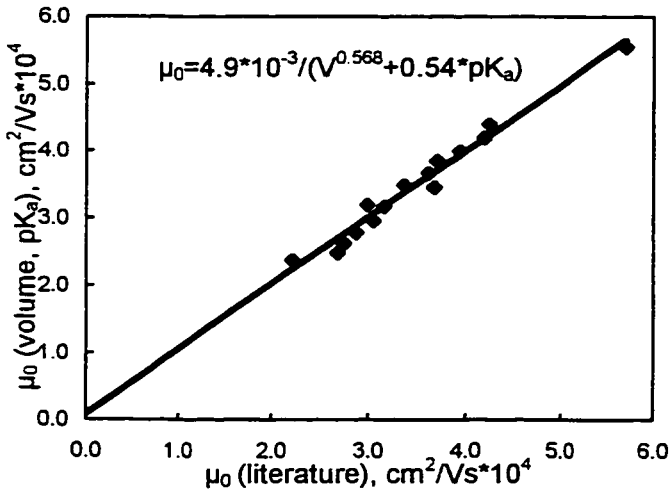

Figure 4.8 Plot of predicted absolute mobilities μ_0 (molecular volume, Insight II, pK_a) vs. literature absolute mobilities for the aliphatic carboxylates in Table 4.4.

The predicted absolute mobilities from Equation 4-12 also agree very well with the literature mobilities. The average relative error is only 3.6%, almost the same as that of the volume (MMP™) and pK_a model (Section 4.5.3.1). The volume (Insight II) and pK_a

model gives compatible correlation coefficient, slope and intercept (0.9864, 0.9790 and 0.072 respectively) to the volume (MMP™) and pK_a model.

4.5.4 VOLUME AND HYDRATION MODEL

Addition of mean waters of hydration into the molecular volume model (MMP™) (Section 4.5.1.1) yielded only slight improvements over the use of volume alone. The average relative error between the predicted absolute mobilities and literature mobilities drops slightly from 5.2% to 5.0%. The slope (0.9339), intercept (0.2298) and correlation coefficient (0.9670) of the volume (MMP™) and hydration model are compatible with those of volume (MMP™) model.

4.6 SUMMARY OF OBSERVATIONS

Both hydrodynamic and dielectric frictions must be considered to accurately predict the absolute mobilities of aliphatic carboxylates. Using molecular volume and pK_a as parameters, the predicted absolute mobilities agree very well with the literature absolute mobilities. The average relative error between the predicted and literature absolute mobilities was only about 3.7% using Equation 4-10 or 4-11. For halogenated aliphatic carboxylates, molecular volume better reflects the hydrodynammic friction than the molecular weight. Including hydration number into the volume model only improves the prediction slightly. However, including pK_a of the carboxylic acid into the molecular volume model significantly improves the prediction of absolute mobilities. This is consistent with the hypothesis that the magnitude of pK_a can be used to represent the

distribution of charge on the carboxylate anion. The significance of the constants and parameters used to predict the absolute mobilities in the best fit equations is discussed in detail in Chapter 6.

4.7 REFERENCES

1. Dabek-Zlotorzynska, E.; Dlouhy, J. F. *J. Chromatogr. A* **1994**, 685, 145-153.
2. Harrold, M. P.; Wojtusik, M. J.; Riviello, J.; Henson, P. *J. Chromatogr.* **1993**, 640, 463-471.
3. Huang, X.; Luckey, J. A.; Gordon, M. J.; Zare, R. N. *Anal. Chem.* **1989**, 61, 766-770.
4. Hirokawa, T.; Nishino, M.; Kiso, Y. *J. Chromatogr.* **1982**, 252, 49-65.
5. Beckers, J. L.; Everaerts, F. M. *J. Chromatogr.* **1989**, 470, 277-287.
6. Beckers, J. L. *J. Chromatogr.* **1985**, 320, 147-158.
7. Hubbard, J. B. *J. Chem. Phys.* **1978**, 68, 1649-1664.
8. Perrin, D. D.; Dempsey, B.; Serjeant, E. P. *pKa Prediction for Organic Acids and Bases*; Chapman and Hall: New York, 1981; p. 12.
9. Martell, A. E.; Smith, R. M. *Critical Stability Constants*, Volume 3; Plenum Press: New York, 1977.
10. Edward, J. T. In *Advances in Chromatography*; Giddings, J. C., Keller, R. A., Eds.; Marcel Dekker: New York, 1966; Vol. 2. p. 75.

11. Robinson, R. A.; Stokes, R. H. *Electrolyte Solutions*, Second Edition; Butterworths: London, 1959; p. 463.

12. Landolt-Börnstein *Zahlenwerte und Funktionen*, 6 Aufl. Bd. II, Teil 7; Springers: Berlin, 1960; pp 264.

CHAPTER 5 ABSOLUTE MOBILITY PREDICTION OF SULFONATES

5.1 INTRODUCTION

Sulfonic acids or their salts are widely used as surfactants in a wide range of applications as diverse as in the oil industry to enhance oil recovery [4] and as ion-pairing reagents in high performance liquid chromatography [3]. They can be determined using capillary electrophoresis with direct and indirect UV absorbance [1] or conductivity detection [2]. Capillary zone electrophoresis has been used to test the purity of sulfonic acids of varying chain lengths [3] and to separate various sulfonates, such as alkylaromatic sulfonates [4], alkanesulfonates [5] and azo dyes with 1 to 6 sulfonate groups [6]. In this chapter, we develop expressions to predict the absolute mobility of sulfonates before separation, which will help us to predict the separation order and identify unknown peaks. It was found that a much simpler model can be used to predict the absolute mobilities of sulfonates than was necessary for carboxylates and monoamines. Using just one parameter (molecular volume), the predicted absolute mobilities agree very well with the experimentally measured absolute mobility values.

5.2 EXPERIMENTAL

5.2.1 CALCULATION OF MOLECULAR VOLUME AND HYDRATION NUMBER

The molecular volumes and hydration number of 10 sulfonates were determined using Molecular Modeling Pro™ Program (Version 1.44, WindowChem Software,

Fairfield, CA) and Insight II (Version 95.0.2, Biosym Technologies, San Diego). The procedures of drawing molecules, minimization of strain energy and calculation of the molecular Van der Waals volume and mean waters of hydration were as described in Chapter 2. The calculated molecular volumes and hydration numbers are listed in Table 5.1:

Table 5.1 Molecular modeling of sulfonates.

Molecule	Weight (g/mol)	MMP™		Insight II
		Volume $(Å)^3$	Hydr. Number	Volume $(Å)^3$
1-Butanesulfonic Acid	137.2	118.8	10	101.2
1-Hexanesulfonic Acid	165.2	148.1	10	123.1
1-Octanesulfonic Acid	193.3	181.6	10	159.1
1-Tetradecanesulfonic Acid	277.4	279.5	10	246.0
Benzenesulfonic Acid	157.2	126.0	10	104.4
p-Chlorobenzenesulfonic Acid	191.6	140.2	10	119.6
p-Toluenesulfonic Acid	171.2	148.2	10	119.0
5-Amino-2-chlorobenzenesulfonic Acid	206.6	156.4	15	128.4
2-Naphthalenesulfonic Acid	207.2	166.6	10	141.6
2-Amino-5-chloro-4-methylbenzenesulfonic Acid	220.7	174.1	15	143.5

5.2.2 CHEMICALS

Reagents and chemicals were from Aldrich (Milwaukee, WI), BDH Inc. (Toronto, Ontario), CHEM SERVICE Inc. (West Chester, PA), Eastman Kodak Co. (Rochester, New York) and Fisher Scientific (Fair Lawn, New Jersey). These were of analytical grade or higher, and were used without further purification. All solutions were prepared with distilled deionized water (18 MΩ) (NANOpure, Barnstead, NY). Ultrasonic degassing

was performed on the buffer and sample solutions before separation.

5.2.3 ABSOLUTE MOBILITY DETERMINATION

The absolute mobilities of 6 aromatic and 4 aliphatic sulfonic anions were determined experimentally using either Beckman P/ACE 2100 (aromatic) or Thermo Crystal 300 (aliphatic) capillary electrophoresis system.

5.2.3.1 AROMATIC SULFONATES

5.2.3.1.1 BUFFER SELECTION AND PREPARATION

As discussed in detail in Section 3.2.3, the first criteria to select the proper buffer system is that all solutes in the buffer solution must be fully ionized. In addition, the buffer capacity should be as high as possible. To meet these requirements, the pK_a of the buffer ($pK_{a(buffer)}$) must be at least three or more pH units higher than the pK_a of the solute ($pK_{a(solute)}$). The aromatic sulfonates investigated and their corresponding pK_a's are listed in Table 5.2.

Table 5.2 Acid dissociation constants of aromatic sulfonates.

Molecule	pK_a (25°C)
2-Naphthalenesulfonic Acid	0.57[a]
5-Amino-2-chlorobenzenesulfonic Acid	Not available
2-Amino-5-chloro-4-methylbenzenesulfonic Acid	Not available
Benzenesulfonic Acid	0.70[b]
p-Chlorobenzenesulfonic Acid	Not available
p-Toluenesulfonic Acid	Not available

[a] Data from reference [7], [b] Data from reference [8].

From these data, it can be seen that the pK_a's of sulfonic groups are very low. Most of the buffer systems that are available will guarantee full ionization. However we also need to consider whether the pH of the buffer system will cause the amino groups such as on 5-amino-2-chlorobenzenesulfonic acid to protonate. Unfortunately, the pK_a's of 5-amino-2-chlorobenzenesulfonic acid and 2-amino-5-chloro-4-methylbenzenesulfonic acid are not available. However, p-chloroaniline, which has a similar structure to 5-amino-2-chlorobenzenesulfonic acid and 2-amino-5-chloro-4-methylbenzenesulfonic acid, has a pK_a of 3.46 at 25°C[7]. By considering all the above-mentioned factors, we chose sodium tetraborate ($Na_2B_4O_7$) to prepare all the buffer solutions. In aqueous solution, $Na_2B_4O_7$ will dissociate:

$$Na_2B_4O_7 + 5H_2O \rightarrow 2Na^+ + 2H_2BO_3^- + 2H_3BO_3 \qquad pK_{a1} = 9.24 \qquad 5\text{-}1$$

In the solution, $[H_2BO_3^-]$ is equal to $[H_3BO_3]$. Therefore, pH is equal to the pK_a. That is, $[H^+]$ is equal to $10^{-9.24}$ M (5.75×10^{-10} M), and $[OH^-]$ is equal to 1.74×10^{-5} M. The ionic strength of the buffer solutions can be calculated according to the following equation:

$$I = 1/2\ \Sigma C_i Z_i^2$$

$$= 1/2\ \{[Na^+]\times 1^2 + [H_2BO_3^-]\times 1^2 + [OH^-]\times 1^2 + [H^+]\times 1^2\}$$

If $[Na_2B_4O_7]=C$, then $[Na^+] = 2C$, $[H_2BO_3^-] = 2C$

$$I = 1/2\ (2C + 2C + 1.74\times 10^{-5}\ M + 5.75\times 10^{-10}\ M) \approx 2C + 8.69\times 10^{-6}\ M \qquad 5\text{-}2$$

The highest ionic strength of the buffer was 0.100 M. Dilutions were then performed to prepare lower ionic strength solutions (0.075 M, 0.05 M, 0.025 M, 0.01 M, 0.005 M and 0.001 M). After dilution, the pH of all buffer solutions was adjusted to 9.24.

5.2.3.1.2 SAMPLE SOLUTION PREPARATION

As described in Section 3.2.3.2, the influence of sample concentrations on the peak shape must also be considered. By considering this effect, we decided to make the sample concentration about 10^{-4} M and prepare the sample in buffer at about the same ionic strength as the running buffer. For all of the analytes, this gave satisfactory peak shapes. A typical electropherogram is given in Figure 5.2.

The procedures for making aromatic sample solutions were as follows:

1. Prepare 10^{-3} M stock solution of each analyte in distilled deionized water.
2. 10^{-4} M sample solutions were prepared by diluting the stock solutions in the corresponding running buffer. Mesityl Oxide ($(CH_3)_2C=CHCOCH_3$), UV detectable at 214 nm) was added to the sample solutions as a neutral electroosmotic flow marker. Its concentration was about 10^{-4} M.
3. To eliminate any factors which can influence the mobility of analyte or the electroosmotic flow, the pH of the sample solutions was also adjusted to 9.24. This is the same pH as the running buffer solutions.

5.2.3.1.3 EXPERIMENTAL APPARATUS - BECKMAN 2100 CE SYSTEM

The absolute mobility measurements of all aromatic sulfonates were performed using a Beckman P/ACE 2100 capillary electrophoresis system (Fullerton, CA) equipped with a UV absorbance detector. The ultraviolet detector in this instrument employs a deuterium lamp as a light source with a range of 190-380 nm and there are four selectable wavelength filters transmitting at 200, 214, 254 and 280 nm. The selected detector

wavelength was 214 nm. The separation capillary was made from fused silica, 50 μm I.D. and 365 μm O.D. (Polymicro Technologies Inc., Phoenix, AZ). The total length was 37.0 cm and the distance from the injector to the detector was 30.0 cm. This capillary was wound on a spiral mandrel and mounted in a sealed cartridge. This was then positioned in the instrument, which enables the circulation of liquid coolant around the capillary.

New capillaries were conditioned before use by pressure (20 psi) induced rinsing with 0.1 M sodium hydroxide for 20 min, followed by distilled deionized water for 10 min. The capillary was thermostated at 25.0 °C. Based on the plot of Ohm's law (current versus applied voltage, as shown in Figure 5.1), the applied voltage was chosen at 6000 V to ensure no Joule heating during the separation.

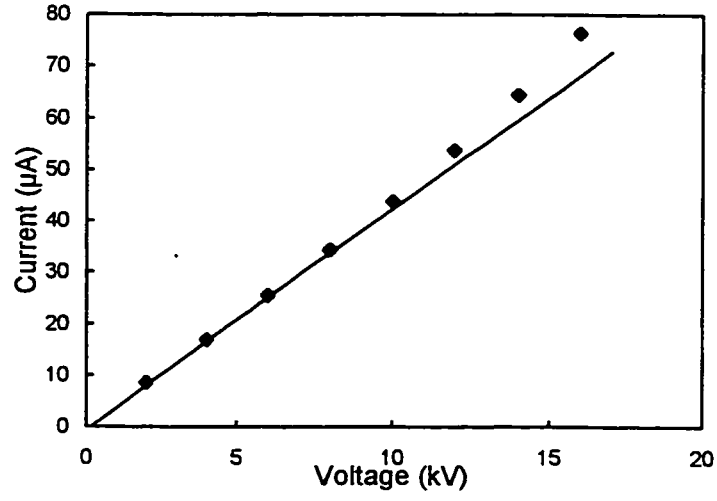

Figure 5.1 Ohm's plot of borate buffer (pH 9.24) at 0.1M ionic strength.

The capillary was rinsed as follows before each run so that it gives a reproducible

electroosmotic flow. The rinses were: 2 min high pressure rinsing (20 psi) with 0.1 M NaOH; then 1 min with distilled deionized water; and finally 6 min with running buffer solution. The long buffer solution rinse was carried out to ensure that the pH and ionic strength of the buffer solution in the capillary was constant. Otherwise, residual NaOH rinsing solution may influence the measured mobilities. The injections were hydrodynamic (0.5 psi) for 2 seconds. System Gold™ (Version 8.1) was used as the control software. This package provides automated instrument control and a sophisticated data analysis capability. The detector rise time was set at 1 second, and data acquisition rate at 5 Hz.

5.2.3.1.4 PROCEDURE FOR ABSOLUTE MOBILITY DETERMINATION

The procedures to determine the absolute mobilities of aromatic sulfonates are as follows:

1. Obtain electropherograms for each analyte at seven different ionic strength borate buffer solutions using a P/ACE 2100 CE system.

2. Determine accurate migration times (t_{eof}, t_m) from the electropherograms. The migration times of the analyte (t_m) and electroosmotic flow (t_{eof}) at seven different ionic strength buffers were obtained directly from the corresponding electropherograms as shown in Figure 5.2.

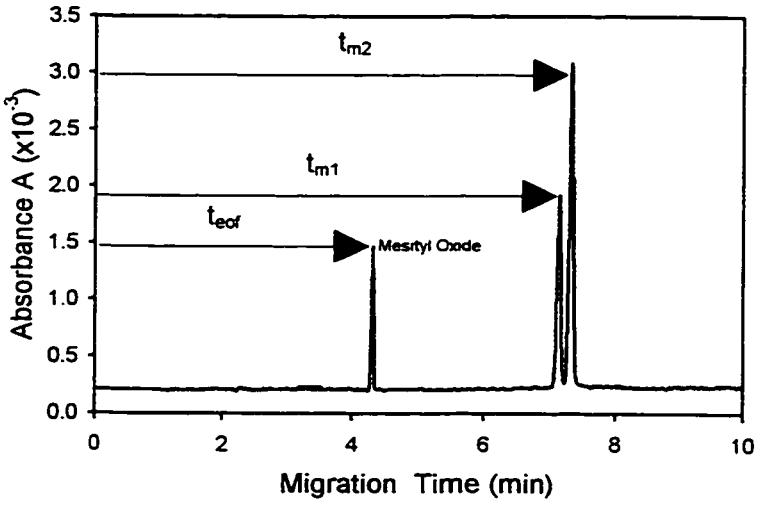

Figure 5.2 Electropherogram of two sulfonates with electroosmotic flow marker (Mesityl Oxide).

3. calculation of electrophoretic mobilities. Once we obtained the migration times of the electroosmotic flow and the analytes, similar calculations were performed as discussed in Section 3.2.3.4. Anions migrate against the electroosmotic flow. For all the aromatic sulfonates investigated, the electrophoretic mobilities were smaller than the electroosmotic mobilities. Based on the migration times and the potential ramp time, the electrophoretic mobility can be calculated using:

$$\mu = \mu_{eof} - \mu_{app} = \frac{L_t L_d}{V}\left(\frac{1}{t_{eof} - \frac{1}{2}t_{ramp}} - \frac{1}{t_m - \frac{1}{2}t_{ramp}}\right) \qquad 5\text{-}3$$

The P/ACE 2100 CE system takes at least 0.17 min for the voltage to reach the programmed value. Therefore 0.17 min was used as the default value for t_{ramp} in all calculations.

4. Determine absolute mobilities using linear regression method. The calculated electrophoretic mobilities were plotted against $\frac{\sqrt{I}}{1+\sqrt{I}}$. Then linear regression was performed to obtain the absolute mobility, as described in Section 3.2.3.4.

5.2.3.2 ALIPHATIC SULFONATES

5.2.3.2.1 BUFFER SELECTION AND PREPARATION

Since the dissociation constants of aliphatic sulfonates are very big ($pK_a << 1$), the sulfonates will be fully dissociated in most buffer systems used in capillary electrophoresis. The mobility of the selected buffer must also be considered. The Crystal CE 300 with a conductivity detector was used for measurements of the aliphatic sulfonates. Conductivity detection is a universal detection technique, which is based on the mobility difference between the analyte ion and the electrolyte co-ion in the running buffer. Therefore, the higher the mobility difference, the higher the detection sensitivity. However, high mobility differences usually cause skewed peaks (Section 3.2.3). In order to obtain sharp and symmetrical peaks, the mobility difference between the analyte and the background buffer should be small. Added to this is the complication that the aliphatic sulfonates range significantly in molecular size, and thus in electrophoretic mobility.

Phosphate buffer (KH_2PO_4-K_2HPO_4, pH=7.21) was chosen as the running buffer. This buffer gave satisfactory detection sensitivity and peak shape for all aliphatic sulfonates. The phosphate buffer system was prepared by dissolving KH_2PO_4 in distilled

deionized water ($C_{KH_2PO_4}$ = C). 1M KOH solution was then added to adjust the pH to 7.21:

$$H_2PO_4^- + OH^- \rightleftharpoons HPO_4^{2-} + H_2O \qquad 5\text{-}4$$

At pH = pKa_2 = 7.21, $[H_2PO_4^-] = [HPO_4^{2-}] = 1/2C$, $[H^-] = 6.16 \times 10^{-8}$ M, $[OH^-] = 1.62 \times 10^{-7}$ M. The ionic strength of this buffer system can be calculated as follows:

$$I = 1/2\ \Sigma C_i Z_i^2$$

$$= 1/2\ \{[K^+]\times 1^2 + [H_2PO_4^-]\times 1^2 + [HPO_4^{2-}]\times 2^2 + [OH^-]\times 1^2 + [H^-]\times 1^2\}$$

$$= 1/2\ (3/2C + 1/2C + 2C + 6.16\times 10^{-8}\ M + 1.62\times 10^{-7}\ M) \approx 2C + 3.08\times 10^{-8}\ M +$$

$$8.1\times 10^{-8}\ M \approx 2C \qquad 5\text{-}5$$

The ionic strength of the stock phosphate buffer was adjusted to 0.1M. Serial dilution was performed to prepare I = 0.075 M, 0.05 M, 0.025 M, 0.01 M, 0.005 M and 0.001 M buffer solutions. After dilution, the pH of these buffer changed slightly, so pH adjustment was performed to keep the pH constant (7.21).

5.2.3.2.2 SAMPLE SOLUTION PREPARATION

To prepare sample solutions of aliphatic sulfonates, the influence of sample concentration on the peak shape must also be considered, as was discussed in Section 3.2.3.2. As some of the aliphatic sulfonates were surfactants, one very important factor to be consider is their critical micelle concentration (CMC) [9]. The critical micelle concentration is the concentration at which the micelles make their first appearance.

Below this concentration, the surfactants exist in solution as monomers. For tetradecanesulfonic acid, its CMC is 2.7×10^{-3} M (39.5°C) [10]. Unfortunately, no CMC is available for tetradecanesulfonic acid at 25°C.

The formation of micelles in capillary zone electrophoresis is detrimental to the measurement of absolute mobilities because the hydrophobic and electrostatic interactions between the analytes and the formed micelles will change the electrophoretic mobilities of the analytes. Since the electroosmotic flow (EOF) is generally faster than the migration velocity of the micelles, the more the solute interacts with the micelle the shorter is the apparent migration time and the smaller is the calculated electrophoretic mobility. This is illustrated in Figure 5.3.

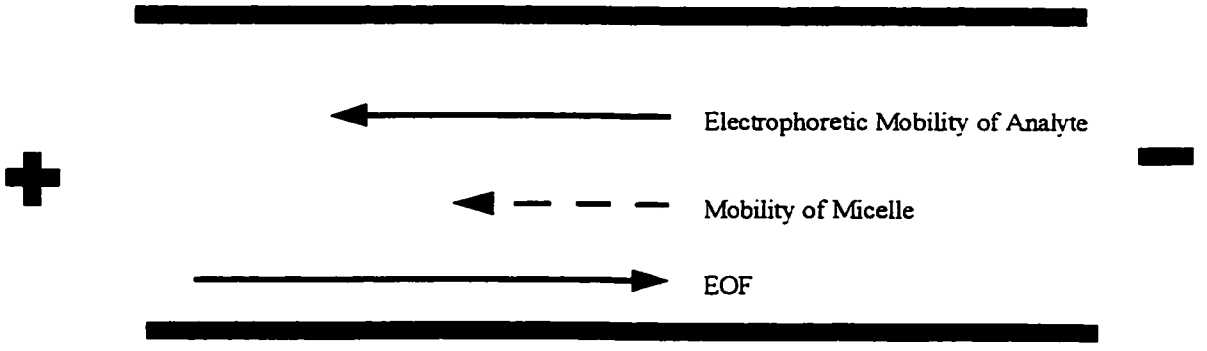

Figure 5.3 Schematic diagram of the magnitudes and direction of electroosmotic flow and mobilities of analytes and micelle.

In order to avoid the formation of micelles, the sample concentration of all aliphatic sulfonates was limited to 10^{-4} M. The pH of all the sample solutions was also

adjusted to 7.21.

5.2.3.2.3 EXPERIMENTAL APPARATUS

The instrument employed was a Crystal 300 capillary electrophoresis system with a Crystal 1000 CE conductivity detector (Thermo CE, Boston, MA), as described in more detail in Section 3.2.3.3. A ConCap™ fused silica capillary (50 μm I.D.×52 cm) and a interchangeable finger tight ConTip™ (Thermo) conductivity sensor were used. The users manual gives more detail discussion of the conductivity detector configuration and handling [11]. The instrument settings are:

Applied Voltage The maximum applied voltage across the capillary was determined experimentally by plotting the current against the applied voltage. The highest voltage in the linear region of this plot was chosen as the applied voltage. For potassium phosphate buffer (Ionic strength = 0.1 M), it was found that the applied voltage should be 6 kV. The Ohm's law plot is shown in Figure 5.4.

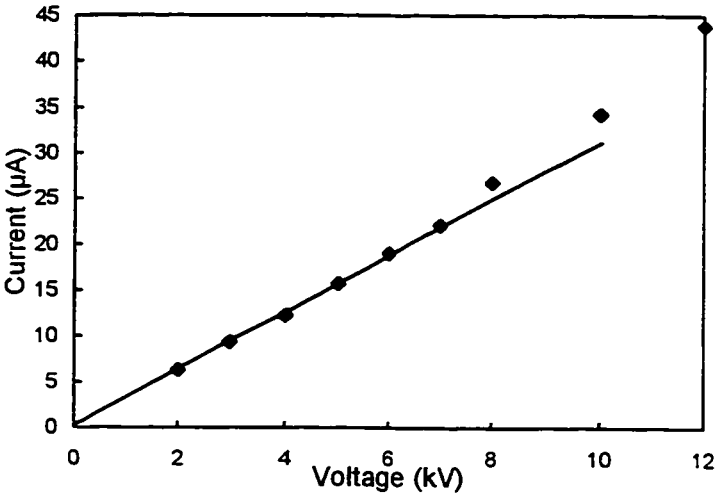

Figure 5.4 Ohm's plot of potassium phosphate buffer (pH 7.21) at 0.1M ionic strength.

Capillary Conditioning The procedures of capillary conditioning were as described in the aromatic sulfonic acid mobility determination (Section 5.2.3.1.3) to ensure steady electroosmotic flow.

Injection All sample injections were hydrodynamic (0.29 psi) for 0.2 min.

Detection Parameters The sensitivity range determines the output scale for the analog background conductivity signal. The available sensitivity ranges were 50, 100, 200, 500, 1000, and 2000 nS. Lower sensitivity values are more sensitive. For the phosphate buffer used, the sensitivity range was set at 500 nanosiemens (nS).

Cell Voltage Cell voltage is the voltage applied to the detector cell. Appropriate cell voltage is one of the key parameters determining the signal to noise ratio and signal

linearity. The optimum cell voltage is inversely related to the background conductivity of the running buffer. High background conductivities require low cell voltages. In this study, the auto cell voltage key, which determines the best applied cell voltage, was used for all the measurements.

Temperature The Crystal 300 CE system has no thermostatting devices. Thus all the experiment were performed at room temperature, which was about 25.4 °C.

Data Acquisition and Software

Data acquisition and software were exactly as described in Section 3.2.3.3.

5.2.3.2.4 PROCEDURES OF ABSOLUTE MOBILITY DETERMINATION

The basic procedures to determine the absolute mobilities of aliphatic sulfonates are as follows:

1. Obtain electropherograms for each analyte at seven different ionic strength potassium phosphate buffer solutions using the Crystal 300 CE system.

2. Determine accurate migration times (t_{eof}, t_m) from the electropherograms. For conductivity detection, the water peak from the injected sample can be used as the electroosmotic flow marker (Section 3.2.3.4). No other EOF marker is needed. However, the water peak usually gives a truncated broad peak, as indicated in Figure 5.5.

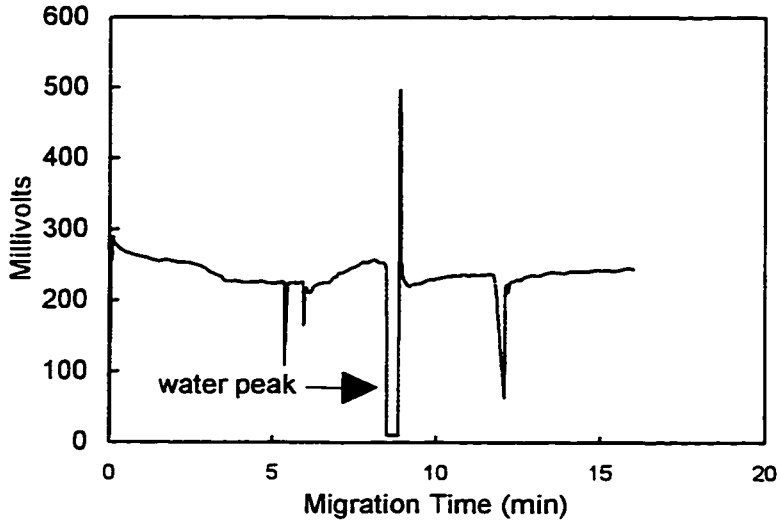

Figure 5.5 Electropherogram of aliphatic sulfonates.

The water peak is about 0.33 min wide for this particular electropherogram. As discussed in Section 3.2.3.4, **stacking** causes the analytes to become concentrated into a smaller zone, as illustrated in Figure 5.6.

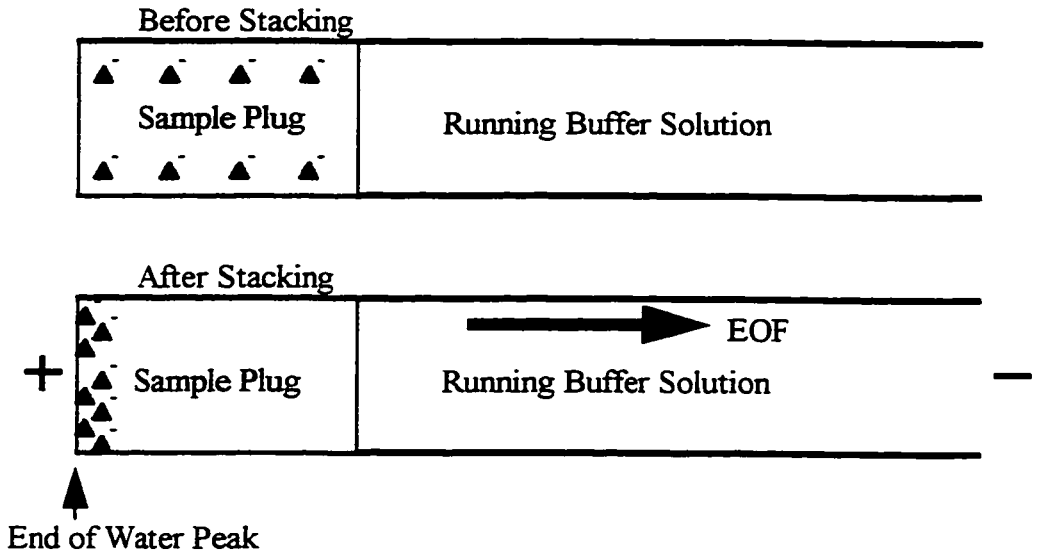

Figure 5.6 Schematic diagram of stacking effect.

It can be seen from Figure 5.6 that the best migration time to reflect the electroosmotic flow of sulfonates is the migration time of the end of the water peak.

3. Calculation of the electrophoretic mobilities.

Once we obtained the migration times of the electroosmotic flow and the analytes, similar calculations were performed as discussed in section 5.2.3.1.4. For end-capillary conductivity ($L_t = L_d = L$), Equation 5-3 is modified to:

$$\mu = \mu_{eof} - \mu_{app} = \frac{L^2}{V}\left(\frac{1}{t_{eof} - \frac{1}{2}t_{ramp}} - \frac{1}{t_m - \frac{1}{2}t_{ramp}}\right) \qquad 5\text{-}6$$

The default voltage ramp (6 kV/s) was used for all the experiments. Since the programmed voltage was 6 kV, the ramp time is 1 second.

4. Determine absolute mobilities using linear regression method.

The calculated electrophoretic mobilities were plotted against $\frac{\sqrt{I}}{1+\sqrt{I}}$. Then linear regression was performed to obtain the absolute mobility, as described in Section 3.2.3.4.

5.3 RESULTS

5.3.1 MOLECULAR VOLUME MODEL

The experimentally measured absolute mobilities of 10 sulfonates are listed in Table 5.3.

Table 5.3 Experimentally measured absolute mobilities of sulfonates.

Molecule	μ_0(meas.) $cm^2/Vs \times 10^4$	MMP™ μ_0(volume) $cm^2/Vs \times 10^4$	Insight II μ_0(volume) $cm^2/Vs \times 10^4$
1-Butanesulfonic Acid	3.64	3.63	3.57
1-Hexanesulfonic Acid	3.26	3.20	3.21
1-Octanesulfonic Acid	2.84	2.85	2.80
1-Tetradecanesulfonic Acid	2.21	2.23	2.22
Benzenesulfonic Acid	3.48	3.51	3.51
p-Chlorobenzenesulfonic Acid	3.26	3.30	3.26
p-Toluenesulfonic Acid	3.21	3.20	3.27
5-Amino-2-chlorobenzenesulfonic Acid	3.04	3.10	3.14
2-Naphthalenesulfonic Acid	3.03	2.99	2.98
2-Amino-5-chloro-4-methylbenzenesulfonic Acid	2.97	2.92	2.96

5.3.1.1 VOLUMES OBTAINED FROM MOLECULAR MODELING PRO™

By using the method described in Section 3.3, it was found that the following best fit equation gives the minimum *residual sum of squares* for sulfonates.

$$\mu_0 = \frac{(5.45 \pm 0.61) \times 10^{-3}}{V^{0.567 \pm 0.022}} \quad \text{cm}^2/\text{Vs} \qquad 5\text{-}7$$

where V is the molecular volume ($Å^3$) calculated using Molecular Modeling Pro™. The mobilities predicted for the sulfonates by Equation 5-7 are also shown in Table 5.3. The correlation between the predicted absolute mobilities using Equation 5-7 and the experimentally measured mobilities is shown in Figure 5.7. It can be seen that the predicted absolute mobilities agree extraordinarily well with those measured experimentally using only one molecular physical parameter (molecular volume). The average relative error between the predicted and measured absolute mobilities is only 1.09%. Furthermore, Equation 5-7 gives almost an ideal slope and intercept, which are 0.99 and 0.04, respectively.

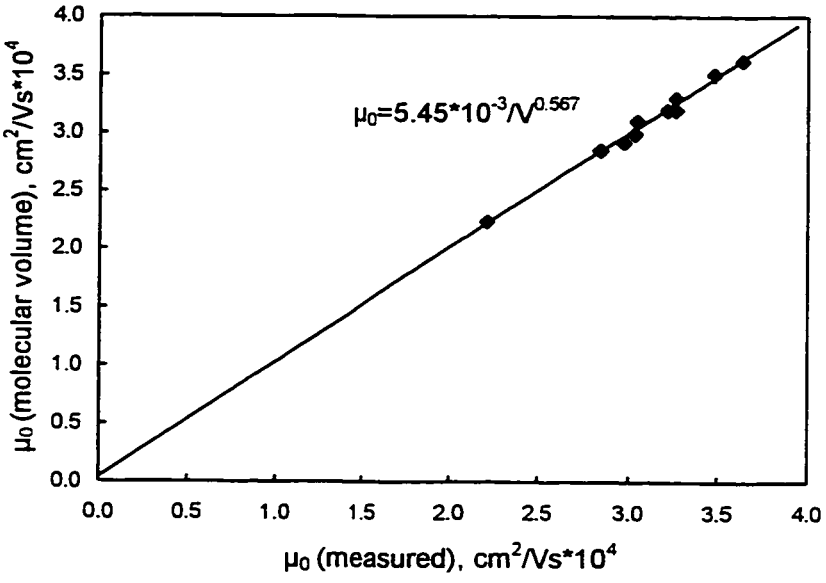

Figure 5.7 Plot of μ_0 (predicted, molecular volume model, Molecular Modeling Pro™) vs. experimentally measured absolute mobility μ_0 (measured) for sulfonates.

5.3.1.2 VOLUMES OBTAINED FROM INSIGHT II

Using molecular volumes calculated from Insight II yielded a similar best fit equation:

$$\mu_0 = \frac{(4.22 \pm 0.59) \times 10^{-3}}{V^{0.535 \pm 0.029}} \qquad \text{cm}^2/\text{Vs} \qquad 5\text{-}8$$

The absolute mobilities predicted for the sulfonates by Equation 5-8 are also listed in Table 5.3. Using Equation 5-8, the average relative error between the predicted absolute mobilities and the measured absolute mobilities is 1.33%, which is slightly higher than that using Equation 5-7. The correlation between the predicted absolute mobilities and the

measured mobilities is shown in Figure 5.8.

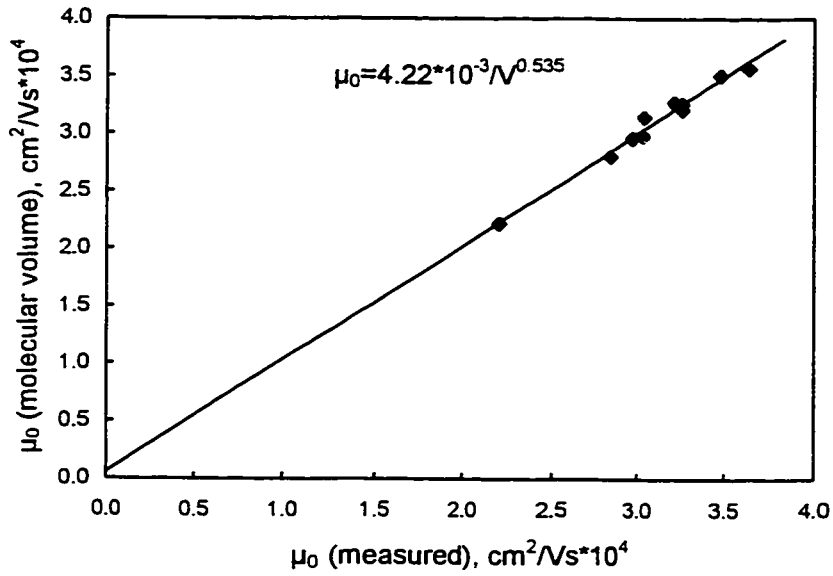

Figure 5.8 Plot of μ_0 (predicted, molecular volume model, Insight II) vs. experimentally measured absolute mobility μ_0 (measured) for sulfonates.

The slope and intercept of Figure 5.8 are 0.98 and 0.06 respectively, which are also slightly worse than those of Figure 5.7.

5.3.2 MOLECULAR VOLUME AND HYDRATION MODEL

In order to investigate the influence of hydration on the absolute mobility, the hydration number calculated using McGowan's additive method was incorporated into the molecular volume model. The best fit equation to predict the absolute mobility is given by:

$$\mu_0 = \frac{(5.61 \pm 0.79) \times 10^{-3}}{V^{(0.571 \pm 0.026)} + (0.018 \pm 0.047)H} \quad \text{cm}^2/\text{Vs} \qquad 5\text{-}9$$

where H is the mean waters of hydration calculated using Molecular Modeling Pro™ software. It was found that incorporating hydration number into the volume model did not improve the prediction. Also the constant associated with the waters of hydration was not statistically significant. Using Equation 5-9, the average error between the predicted and measured absolute mobilities is 1.10%, almost the same as that of molecular volume model. The slope and intercept obtained using the molecular volume and hydration model were compatible with those of molecular volume model.

5.3.3 MOLECULAR WEIGHT MODELS

In general, models including molecular weight instead of molecular volume for sulfonates gave much worse prediction of absolute mobilities. The average errors between the predicted and measured absolute mobilities for both the molecular weight model and the molecular weight and hydration model were above 3.5% (4.48% for molecular weight model, 3.52% for molecular weight and hydration model). Furthermore, the observed slopes and intercepts are far from the ideal behavior (intercepts above 0.41, slopes below 0.87). However, if all halogenated molecules were excluded, the relative error dropped to 3.0% for the molecular weight model, but the the slope and intercept were still far from the ideal behavior (0.93 and 0.22 respectively). Further investigation revealed that if only aliphatic sulfonates were used to generate the absolute mobility prediction model, we could significantly improve the prediction. In this case, the average relative error between

the predicted absolute mobilities and the experimentally measured mobilities is only 0.84%. The slope and intercept were very close to the ideal behavior (0.995 and 0.016 respectively). This confirms our assumption (discussed in aliphatic carboxylate chapter) that molecular volume represents molecular size better than does molecular weight for halogenated molecules. The results also indicate that molecular weight can represent mollecular size of aliphatic sulfonates better than that of aromatic sulfonates.

5.4 CONCLUSION

The absolute mobilities of sulfonates of different sizes and shapes can be predicted by using a very simple molecular volume model. Excellent agreement between the predicted absolute mobilities and the experimentally measured mobilities was achieved using equation 5-7. Including hydration number into the volume model did not give any better prediction. For sulfonates investigated, molecular volume models give much better prediction than molecular weight models.

5.5 REFERENCES

1. Nielen, M. W. F. *J. Chromatogr.* **1991**, 588, 321-326.

2. Haber, C.; Jones, W. R.; Soglia, J.; Surve, M. A.; McGlynn, M.; Caplan, A.; Reineck, J. R.; Krstanovic, C. *J. Cap. Elec.* **1996**, 3, 1-11.

3. Boden, J.; Feige, K.; Meyer, B. *Chromatographia* **1997**, 45, 116.

4. Desbene, P. L. *J. Chromatogr.* **1992**, 608, 375-383.

5. Chen, S.; Pietrzyk, D. J. *Anal. Chem.* **1993**, 65, 2770-2775.

6. Friedl, W.; Reijenga, J. C.; Kenndler, E. *J. Chromatogr. A* **1995**, 709, 163-170.

7. *Handbook of Chemistry and Physics*, 1st Student Edition; Weast, R. C., Ed.; CRC Press: Boca Raton, FL, 1991; pp D-102.

8. *The Merck Index*, Eleventh Edition; Budavari, S., Ed. MERCK & CO., Inc.: Rahway, NJ, 1989; pp-167.

9. Sepaniak, M. J.; Powell, A. C.; Swaile, D. F.; Cole, R. O. In *Capillary Electrophoresis*; Grossman, P. D., Colburn, J. C., Eds.; Academic Press, Inc.: San Diego, CA, 1992; pp136-189.

10. Mukerjee, P.; Mysels, K. J. *Critical Micelle Concentration of Aqueous Surfactant Systems*, NSRDS-NBS 36; US Government Printing Office: Washington, D.C., 1970; pp 123.

11. Thermo; *Crystal 1000 CE Conductivity Detector Users Manual*, Version 1.1; Boston, MA, 1994.

CHAPTER 6 DISCUSSION AND CONCLUSIONS

6.1 SUMMARY AND DISCUSSION OF BEST FIT EQUATIONS

In consideration of simplicity and accuracy, the best fit equations developed herein for the prediction of absolute mobilities of small molecules and some major electrophoretic mobility equations are summarized in Table 6.1. The area of application of each expression along with its underlying assumptions is also included in this table.

Table 6.1 Summary of electrophoretic mobility relationships

Equation	Application	Assumption	Average Error (%)
$\mu_0 = \frac{Ze}{6\pi\eta r_s}$	general expression for zero ionic strength	derived from Stokes' law using a spherical molecule [1][2]	13.9 (34 amines)
$\mu_0 = \frac{Ze}{6\pi\eta r_s (f / f_0)}$	small molecules	molecule approximated as ellipsoid [3][4]	10.0 (34 amines)
$\mu_0 = \frac{Ze}{6\pi\eta r_i + \frac{1}{16.5}\frac{(Ze)^2(\tau_D / \eta)[(\varepsilon_0 - \varepsilon_\infty)/\varepsilon_0^2]}{r_i^3}}$	ions with a symmetrical charge distribution moving in a continuum media	both hydrodynamic and dielectric frictions considered [5][6][7]	12.9 (34 amines)
$\mu = \frac{KZ}{W^{2/3}}$	peptides in paper electrophoresis and CZE [8]	empirically based [9]	15.7 (34 amines)
$\mu_0 = \frac{5.5 \times 10^{-3}}{W^{0.58} + 0.39 pK_b}$	monoamines at zero ionic strength	derived herein (Equation 3-30)	4.3 (34 amines)
$\mu_0 = \frac{6.5 \times 10^{-3}}{V^{0.61} + 0.62 pK_a}$	aliphatic carboxylates at zero ionic strength	derived herein (Equation 4-11)	3.7 (15 solutes)
$\mu_0 = \frac{5.5 \times 10^{-3}}{V^{0.57}}$	sulfonates at zero ionic strength	derived herein (Equation 5-7)	1.1 (10 solutes)

e = charge on an electron
ε_0 = low frequency dielectric constant
ε_∞ = high frequency dielectric constant
f / f_0 = frictional ratio
H = mean waters of hydration
I = ionic strength
r_i = crystallographic ionic radius
η = viscosity of the solvent
r_s = Stokes' radius
τ_D = Dielectric relaxation constant
W = molecular weight
Z = charge number on the molecule

6.1.1 POWER DEPENDENCE

Equations 3-30, 4-11, and 5-7 in Table 6.1 were developed herein for the absolute mobility prediction of monoamines, aliphatic carboxylates and sulfonates, respectively. The power dependences on volume in these equations are very similar, 0.58, 0.61, and 0.57 respectively. This power dependence is significantly different from that predicted from the traditional spherical (Hückel) model, which predicts a dependence of 0.33. However, the observed power dependence is very close to that of Wilke-Chang's empirical diffusion model, which is 0.6. Thus independent of whether a small ion is moving due to random motion or an electric field, the frictional drag is related to the molecular size to a power very close to 0.6. The physical meaning of this value is not known. It could be related to the radius of gyration of ions.

6.1.2 PARAMETERS REFLECTING MOLECULAR SIZE

As discussed in Chapter 2, the volume obtained using Molecular Modeling Pro™ was not reproducible. However, the variation in the calculated molecular volume was generally very small, ranging from 0.04% RSD for ethylamine to 0.3% for octadecyltributylamine. An alternative more complicated molecular modeling software, Insight II, also gave comparable fluctuation in the calculated volumes. Fortunately, from the discussion in Section 2.4.1.2, it can be seen that the calculated Van der Waals volumes using Molecular Modeling Pro™ agree very well with the corresponding literature values (calculated manually from Van der Waals atomic increments).

It was also observed that systematic errors do exist between the molecular volumes estimated using different molecular modeling softwares and even different versions of the same program (Section 2.4.1.1 and 2.4.1.2). However, systematic molecular volume changes will not influence the power dependence of the molecular volume (Section 3.4.3) and the predicted separation order. Therefore, although Molecular Modeling Pro™ is not perfect, we believe the calculated molecular volume is appropriate for our study.

It was found that, in general, molecular weight can also be used to represent the molecular size for nonhalogenated molecules. For monoamines, the use of molecular weight instead of molecular volume gave unambiguous and excellent prediction of the absolute mobilities. Since halogenated molecules were included in both aliphatic carboxylates and sulfonates, molecular volume is the preferred parameter to reflect the molecular size.

6.1.3 PARAMETERS REFLECTING CHARGE DISTRIBUTION

6.1.3.1 HYDRATION-(WHAT IS HYDRATION?)

As discussed in Chapter 4, incorporating hydration effects into the molecular size (molecular volume or molecular weight) models significantly improves the absolute mobility prediction. In order to understand how physicochemical parameters govern the solute behavior, we have to clarify what the hydration really means.

If hydration really meant hydration, we would expect that its major influence on the solute behavior would be on the molecular size and shape. However, it was found that

the second term in the denominator of Equation 3-26 and 3-27 can not be incorporated into the molecular size term. That is, the following transformation can not be used to reduce the absolute mobility prediction uncertainty:

$$\mu_0 = \frac{A}{V^B + C \times H} \not\longrightarrow \mu_0 = \frac{A}{(V + C \times H)^B} \qquad 6\text{-}1$$

Indeed, if the above transformation was performed on Equation 3-26, the prediction uncertainty increased by 0.5%. This suggests that the hydration number in Equation 6-1 may reflect something else. Further investigation revealed that hydration number and the charge density of the nitrogen atom on a monoamine molecule are highly correlated. The correlation coefficient is 0.978. This result further confirms that hydration really reflects something else, which we believe is the dielectric friction (or charge distribution), as discussed in Chapter 3.

6.1.3.2 pK

The recommended parameter to reflect the charge distribution for monoamines and aliphatic carboxylates is the pK value (pK_b for monoamines and pK_a for aliphatic carboxylates). When pK_b was used to reflect the charge distribution of monoamines, very interesting results were observed. Almost identical best fit equations for the prediction of absolute mobility of monoamines were obtained:

Table 6.2 Comparison of hydration and pK_b.

$\mu_0 = \frac{5.5 \times 10^{-3}}{W^{0.58} + 0.39 pK_b}$	3-30
$\mu_0 = \frac{5.6 \times 10^{-3}}{W^{0.58} + 0.17 H}$	3-27

In comparison with Equation 3-27 and 3-30, it can be seen that the molecular weight is raised to the same power, and the constants in the numerator are almost the same. The main difference is the variation of the constants in the second term in the denominator. However, the relative influence of the second term in the denominators are very similar. This result further confirms that both hydration and pK_b represent the same thing, which we believe is the dielectric friction.

6.1.4 SIGNIFICANCE OF DIELECTRIC FRICTION ON SULFONATES

From Table 6.1, it can be seen that the best fit equation for sulfonates (Equation 5-7) does not have second term in the denominator. This suggests that the dielectric friction is not significant for sulfonates. This abnormal behavior can be explained as follows. First, sulfonic acids are very strong organic acids ($pK_a < 1$) in comparison with carboxylic acids. Therefore, their anionic form has much higher charge distribution and in turn much lower dielectric friction than carboxylic acids. Second, the sulfonate functional group ($-SO_3^-$) has a larger radius (r = 2.28 Å) than that of carboxylic functional group ($-CO_2^-$) (r = 2.09 Å). From the Hubbard equation (Equation 4-1), it can be seen that a larger ionic species has a much smaller dielectric friction. That is, the dielectric friction is inversely

proportional to the ionic radius raised to the power of 3. Therefore, due to these effects, the dielectric friction of sulfonates would not be expected to be significant.

6.2 SHAPE CORRECTION

In general, molecular shape correction is only a minor factor influencing the absolute mobilities of analytes. For monoamines, independent tests (Sections 3.4.11.1 and 3.4.11.2) demonstrated that molecular shape correction had only a small influence on the predictability of the proposed models. Indeed, for experimentally measured absolute mobilities for 13 monoamines, including molecular shape correction resulted in slightly poorer predictions of the absolute mobilities.

6.3 CONCLUSIONS

Based on the results for small organic cations (monoamines) and anions (aliphatic carboxylates and sulfonates), it was found that:

1. Both hydrodynamic and dielectric frictions must be considered for the absolute mobility prediction.

2. Hydrodynamic friction can be reflected very well using molecular size (molecular weight or molecular volume).

3. The power dependence of the molecular size is close to 0.6, which is significantly different from that of classical spherical model.

4. pK value can be used to reflect dielectric friction.

5. Molecular shape correction is only a minor factor.

6.4 REFERENCES

1. Hiemenz, P. C. *Principles of Colloid and Surface Chemistry*, 2nd edition; Marcel Dekker: New York, 1986; p.747.
2. Grossman, P. D.; Colburn, J. C.; Lauer, H. H. *Anal. Biochem.* **1989**, *179*, 28.
3. Perrin, F. *J. Phys. Radium* **1934**, 1934, *5*, 497.
4. Perrin, F. *J. Phys. Radium* **1936**, 1934, *7*, 1.
5. Hubbard, J.; Onsager, L. *J. Chem. Phys.* **1977**, *67*, 4850.
6. Hubbard, J. B. *J. Chem. Phys.* **1978**, *68*, 1649.
7. Kay, R. L. *Pure Appl. Chem.* **1991**, *63*, 1393.
8. Adamson, N.; Riley, P. F.; Reynolds, E. C. *J. Chromatogr. A* **1993,** *646*, 391.
9. Offord, R. E. *Nature* **1966**, *211*, 591.

CHAPTER 7 FUTURE WORK

7.1 MOBILITY PREDICTION FOR ANY GIVEN STRENGTH

In this initial study, we only investigated the electrophoretic mobility prediction at zero ionic strength (absolute mobility). However, in real separation processes, the migrating analyte ions are moving in a buffer solution with a certain ionic strength. In order to understand the solute behavior under real separation conditions, it is essential for us to investigate the relationship between the electrophoretic mobility and the ionic strength of the running buffer solution. This issue is significant in capillary electrophoresis because, until now, no thorough investigation has been performed in this area. Our initial study demonstrated that the extended Debye-Hückel-Onsager equation (Section 5.2.3.1.4) works very well for monocharged small organic ions and multicharged species up to 0.1 M ionic strength. That is, the electrophoretic mobility varies linearly with $\sqrt{I} / (1+\sqrt{I})$. However, extensive investigation must be performed to confirm if this relationship holds for different ion species with different charges.

7.2 ABSOLUTE MOBILITY PREDICTION FOR MULTICHARGED SPECIES

All the ionic species investigated were monocharged. In order to predict their absolute mobilities, our focus is on the frictional force of a molecule. It will be very interesting to investigate how variation in the total charge on a molecule would influence the driving force and the drag force.

7.3 ABSOLUTE MOBILITY PREDICTION FOR COMPLEX MOLECULES

Capillary electrophoresis has been widely employed to investigate large molecules such as peptides and proteins. It is the natural trend for us to investigate the physicochemical parameters governing their behavior during separation. In comparison with small organic ions, peptides and proteins have not only multiple charges, but also charged functional groups are uniformly distributed over the entire molecule. It would be very interesting to see if our current hydrodynamic friction and dielectric friction concepts also hold for macromolecules.

BIBLIOGRAPHY

Abramson, H. A., Moyer, L. S.; Gorin, M. H. *Electrophoresis of Protein*; Hafner Publishing Co. Inc.: New York, 1964; pp 105-172.

Adamson, N.; Riley, P. F.; Reynolds, E. C. *J. Chromatogr. A* **1993**, *646*, 391-396.

Azzaoui, K.; Lafosse, M.; Morin-Allory, L. *J. Liq. Chromatogr.* **1995**, *18*, 3021.

Beckers, J. L. *J. Chromatogr.* **1985**, 320, 147-158.

Beckers, J. L.; Everaerts, F. M. *J. Chromatogr.* **1989**, 470, 277-287.

Biosym Technologies; *Search-Compare user guide*, version 2.3; San Diego, CA, 1993.

Bockris, J. O'M.; Reddy, A. K. N.; *Modern Electrochemistry*, Vol. 1; Plenum Press: New York, 1970. pp 420-440.

Boden, J.; Feige, K.; Meyer, B. *Chromatographia* **1997**, 45, 116.

Bondi, A. *J. Phys. Chem.* **1964**, 68, 441.

Bruin, G. J. M.; Chang, J. P.; Kuhlman, R. H.; Zegers, K.; Kraak, J. C.; Poppe, H. *J. Chromatogr.* **1989**, *471*, 429-436.

Burgreen, D.; Nakache, F. R. *J. Phys. Chem.* **1964**, *68*, 1084-1091.

Burton, D.; Sepaniak, M.; Maskarinec, M. *J. Chromatogr. Sci.* **1987**, *25*, 514.

Cao, C.-X. *J. Chromatogr.* **1997**, *771*, 374-378.

Cardinael, P.; Ndzie, E.; Combret, J. C. *J. High. Resol. Chromatogr.* **1997**, *20*, 560.

Caulcutt, R.; Boddy, R. *Statistics for Analytical Chemists;* Chapman and Hall: New York, 1983. p 52.

Chen, S.; Pietrzyk, D. J. *Anal. Chem.* **1993**, 65, 2770-2775.

Cheng, P. V.; Schachman, H. K. *J. Polymer Sci.* **1955**, *16*, 19.

Compton, B. J. *J. Chromatogr.* **1991**, *559*, 357-366.

Compton, B. J.; O'Grady, E. A. *Anal. Chem.* **1991**, *63*, 2597-2602.

Cussler, E. L. *Diffusion: mass transfer in fluid systems*; Cambridge University Press: New York, 1984, Sec. 5.2.

Dabek-Zlotorzynska, E.; Dlouhy, J. F. *J. Chromatogr. A* **1994**, 685, 145-153.

Desbene, P. L. *J. Chromatogr.* **1992**, 608, 375-383.

Edward, J. T. *J. Chem. Education* **1970**, *47*, 261-270.

Edward, J. T. In *Advances in Chromatography*; Giddings, J. C., Keller, R. A., Eds.; Marcel Dekker: New York, 1966; Vol. 2. Ch. 2.

Edward, J. T. *Scient. Proc., R. D. S.* **1957**, *27*, 273.

Edward, J. T. *Scient. Proc., R. D. S.* **1957**, *27*, 287.

Edward, J. T. Crawford, R. *J. Chromatogr.* **1958**, *1*, 449-456.

Edward, J. T.; Waldron-Edward, D. *J. Chromatog.* **1965**, 20, 563-571.

Eisenberg, D.; Crothers, D. *Physical Chemistry with Applications to the Life Sciences*; Benjamin/Cummings: Menlo Park, CA, 1979; pp 718-724.

Erdey-Grúz, T. *Transport Phenomena in Aqueous Solutions*; Halsted Press: New York, 1974; 294-326.

Evans, D. F.; Tominaga, T.; Hubbard, J. B.; Wolynes, P. G. *J. Phys. Chem.* **1979**, *83*, 2669-2677.

Falkenhagen, H.; Kelbg, G. *Z. Elektrochemie* **1954**, 58, 653.

Friedl, W.; Reijenga, J. C.; Kenndler, E. *J. Chromatogr. A* **1995**, 709, 163-170.

Gaus, H.-J.; Beck-Sickinger, A. G.; Bayer, E. *Anal. Chem.* **1993**, *65*, 1399.

Grossman, P. D. *Capillary Electrophoresis: Theory and Practice*, Grossman, P. D.; Colburn, J. C., Eds.; Academic Press: San Diego, 1992. Ch. 4.

Grossman, P. D.; Colburn, J. C.; Lauer, H. H. *Anal. Biochem.* **1989**, *179*, 28-33.

Güntelberg, E. *Z. Phys. Chem.* **1926**, 123, 199.

Haber, C.; Jones, W. R.; Soglia, J.; Surve, M. A.; McGlynn, M.; Caplan, A.; Reineck, J. R.; Krstanovic, C. *J. Cap. Elec.* **1996**, 3, 1-11.

Handbook of Chemistry and Physics, 1st Student Edition; Weast, R. C., Ed.; CRC Press: Boca Raton, FL, 1991; pp D-102-106.

Harrold, M. P.; Wojtusik, M. J.; Riviello, J.; Henson, P. *J. Chromatogr.* **1993**, 640, 463-471.

Hayduk, W.; Laudie, H. *AIChE J.* **1974**, *20*, 611-615.

Hayes, M. A.; Kheterpal, I.; Ewing, A. G. *Anal. Chem.* **1993**, *65*, 27.

Hiemenz, P. C. *Principles of Colloid and Surface Chemistry*, 2nd edition; Marcel Dekker: New York, 1986; p.747.

Hirokawa, T.; Kiso, Y. *J. Chromatogr.* **1982**, *252*, 33-36.

Hirokawa, T.; Nishino, M.; Kiso, Y. *J. Chromatogr.* **1982**, 252, 49-65.

Huang, X.; Luckey, J. A.; Gordon, M. J.; Zare, R. N. *Anal. Chem.* **1989**, 61, 766-770.

Hubbard, J. B. *J. Chem. Phys.* **1978**, *68*, 1649-1664.

Hubbard, J.; Onsager, L. *J. Chem. Phys.* **1977**, *67*, 4850-4857.

Jandik, P.; Bonn, G. *Capillary Electrophoresis of Small Molecules and Ions*; VCH: New York, 1993; p. 15.

Jones, J. H.; Spuhler, F. J.; Felsing, W. A. *J. Am. Chem. Soc.* **1942**, *64*, 965.

Jorgenson, J. W.; Lukacs, K. D. *Anal. Chem.* **1981**, *53*, 1298-1302.

Kašicka, V.; Prusík, Z.; Mudra, P.; Štepánek, J. *J. Chromarogr. A.* **1995**, *709*, 31.

Kay, R. *Pure & Appl. Chem.* **1991**, *63*, 1393-1399.

Kier, L. B., Hall, L. H.; Murray, W. J.; Randic, M. *J. Pharmaceutical Sci.* **1975**, 64, 1971.

Kuhn, D. W.; Kraus, C. A. *J. Am. Chem. Soc.* **1950**, *72*, 3676.

Lamare, V.; Bressot, C.; Casnati, A. *Separation Sci. Tech.* **1997**, *32*, 175.

Landolt-Börnstein *Zahlenwerte und Funktionen*, 6 Aufl. Bd. II, Teil 7; Springers: Berlin, 1960; pp 264.

Li, S. F. Y. *Capillary electrophoresis: Principles, practice and applications*; Elsevier: Amsterdam, Netherlands, 1993; pp 14-17.

Lucy, C. A.; Underhill, R. A. *Anal. Chem.* **1996**, *68*, 300-305.

Martell, A. E.; Smith, R. M. *Critical Stability Constants*, Volume 2; Plenum Press: New York, 1975.

Martell, A. E.; Smith, R. M. *Critical Stability Constants*, Volume 3; Plenum Press: New York, 1977.

Mikkers, F. E. P.; Everaerts, F. M.; Verheggen, Th. P. E. M. *J. Chromatogr.* **1979**, 169, 1-10.

Moor, T. S.; Winmill, T. F. *J. Chem. Soc.* **1912**, *101*, 1635.

Mukerjee, P.; Mysels, K. J. *Critical Micelle Concentration of Aqueous Surfactant Systems*, NSRDS-NBS 36; US Government Printing Office: Washington, D.C., 1970.

Nashabeh, W.; Rassi, Z. E. *J. Chromatogr.* **1990**, *514*, 57-64.

Nielen, M. W. F. *J. Chromatogr.* **1991**, 588, 321-326.

Offord, R. E. *Nature* **1966**, *211*, 591-593.

Perrin, D. D. *Dissociation Constants of Organic Bases In Aqueous Solution*; Butterworths: London, 1965; p 51.

Perrin, D. D.; Dempsey, B.; Serjeant, E. P. *pK_a Prediction for Organic Acids and Bases*; Chapman and Hall: New York, 1981.

Perrin, F. *J. Phys. Radium* **1936**, *7*, 1.

Perrin, F. *J. Phys. Radium* **1934**, *5*, 497.

Pitts, E. *Proc. Roy. Soc.* **1953**, A.217, 43.

Pitts, E.; Tabor, B. E.; Daly, J. *Trans. Faraday Soc.* **1970**, 66, 693.

Rice, C. L.; Whitehead, R. *J. Phys. Chem.* **1965**, *69*, 4017-4024.

Robinson, R. A.; Stokes, R. H. *Electrolyte Solutions*, 2nd Ed.; Butterworth Scientific Publications: London, 1959.

Rowe, R. C.; Wren, S. A. C.; McKillop, A. G. *Electrophoresis* **1994**, *15*, 635.

Salimi-Moosavi, H.; Cassidy, R. M. *Anal. Chem.* **1995**, *67*, 1067-1073.

Sepaniak, M. J.; Powell, A. C.; Swaile, D. F.; Cole, R. O. In *Capillary Electrophoresis*; Grossman, P. D., Colburn, J. C., Eds.; Academic Press, Inc.: San Diego, CA, 1992; pp136-189.

Smith, S. C.; Khaledi, M. G. *Anal. Chem.* **1993**, *65*, 193-198.

Spernol, A. *J. Phys. Chem.* **1956**, *60*, 703.

Stokes, G. *Tran. Cambridge Phil. Soc.* **1856**, *9*, 5.

Tavares, M. F. M.; Colombara, R.; Massaro, S. *J. Chromatogr. A* **1997**, 772, 171-178.

The Merck Index, Eleventh Edition; Budavari, S., Ed. MERCK & CO., Inc.: Rahway, NJ, 1989; pp-167.

Thermo; *Crystal 1000 CE Conductivity Detector Users Manual*, Version 1.1; Boston, MA, 1994.

Tiselius, A.; Svensson, H. *Trans. Faraday Soc.* **1940**, 36, 16-22.

Tsuda, T. *J. High Resolut. Chromatogr. Chromatogr. Commun.* **1987**, *10*, 622.

Van Orman, B. B.; Liversidge, G. G.; McIntyre, G. L.; Olefirowicz; Ewing, A. G. *J. Microcolumn Sep.* **1990**, *2*, 176-180.

Wilke, C. R.; Chang, P. *AIChE J.* **1955**, *1*, 264-270.

Williams, B. A.; Vigh, Gy. *Anal. Chem.* **1996**, 68, 1174-1180.

WindowChem Software™ Inc.; *Molecular Modeling Pro™*, Revision 1.2; Fairfield, CA, 1994.

Yeung, K. K.-C.; Lucy, C. A. *Anal. Chem.* **1977**, *69*,3435.

Yeung, K. K.-C.; Lucy, C. A. *J. Chromatogr. A* In Press.

IMAGE EVALUATION
TEST TARGET (QA-3)

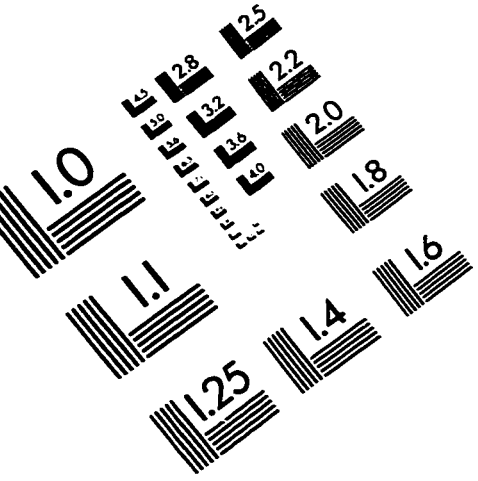

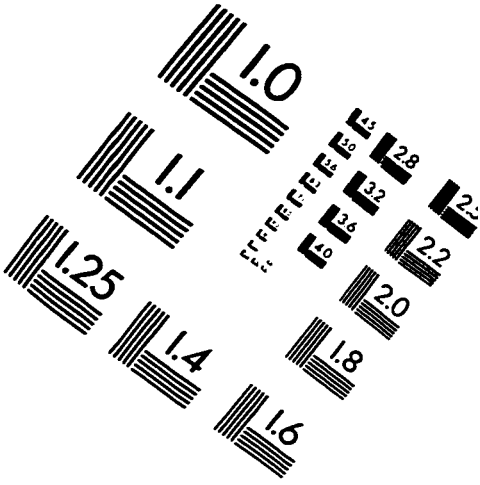

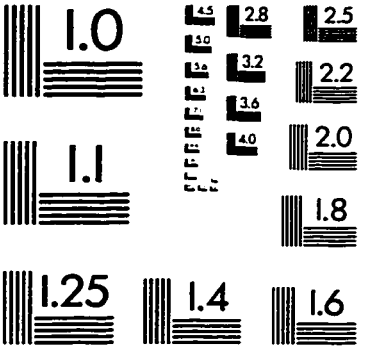

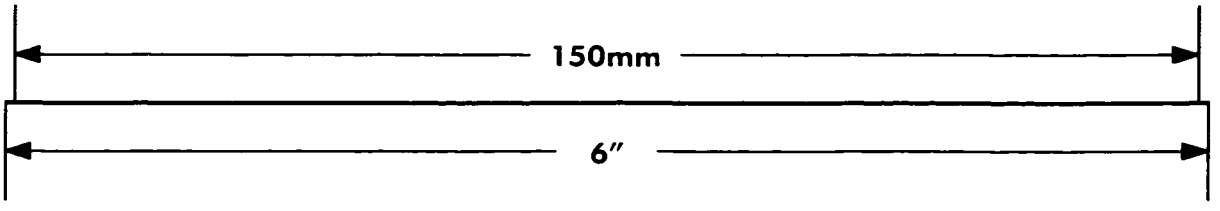

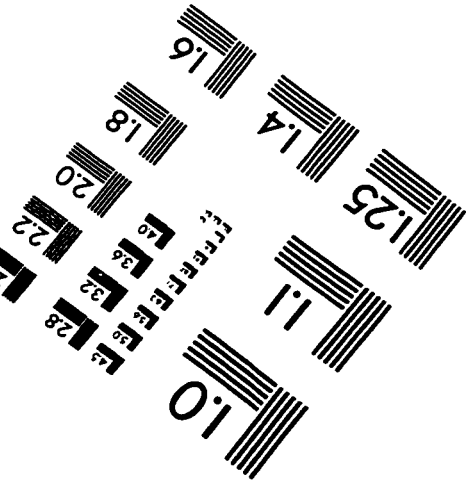

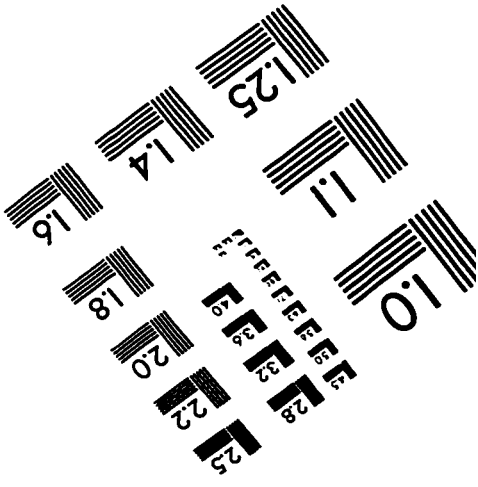

APPLIED IMAGE, Inc
1653 East Main Street
Rochester, NY 14609 USA
Phone: 716/482-0300
Fax: 716/288-5989